30849

NATIONAL LIBRARY
OTTAWA

BIBLIOTHÈQUE NATIONALE
OTTAWA

CANADA

NAME OF AUTHOR...MR. KAROL EDWARD SZKLARZ....

TITLE OF THESIS...EXOELECTRON EMISSION FROM...
AN ALUMINUM ALLOY DURING...
AND AFTER PLASTIC DEFORMATION

UNIVERSITY...U. of A.........................

DEGREE FOR WHICH THESIS WAS PRESENTED...M.Sc..............

YEAR THIS DEGREE GRANTED...1976.......................

Permission is hereby granted to THE NATIONAL LIBRARY OF CANADA to microfilm this thesis and to lend or sell copies of the film.

The author reserves other publication rights, and neither the thesis nor extensive extracts from it may be printed or otherwise reproduced without the author's written permission.

(Signed)...K. E. Szklarz...

PERMANENT ADDRESS:

76 FLINT CRES.
ST. ALBERT
ALBERTA

DATED...Aug. 13........1976

NL-91 (10-68)

INFORMATION TO USERS

THIS DISSERTATION HAS BEEN MICROFILMED EXACTLY AS RECEIVED

This copy was produced from a microfiche copy of the original document. The quality of the copy is heavily dependent upon the quality of the original thesis submitted for microfilming. Every effort has been made to ensure the highest quality of reproduction possible.

PLEASE NOTE: Some pages may have indistinct print. Filmed as received.

Canadian Theses Division
Cataloguing Branch
National Library of Canada
Ottawa, Canada K1A 0N4

AVIS AUX USAGERS

LA THESE A ETE MICROFILMEE TELLE QUE NOUS L'AVONS RECUE

Cette copie a été faite à partir d'une microfiche du document original. La qualité de la copie dépend grandement de la qualité de la thèse soumise pour le microfilmage. Nous avons tout fait pour assurer une qualité supérieure de reproduction.

NOTA BENE: La qualité d'impression de certaines pages peut laisser à désirer. Microfilmee telle que nous l'avons reçue.

Division des thèses canadiennes
Direction du catalogage
Bibliothèque nationale du Canada
Ottawa, Canada K1A 0N4

THE UNIVERSITY OF ALBERTA

EXOELECTRON EMISSION FROM AN ALUMINUM ALLOY DURING AND AFTER PLASTIC DEFORMATION

by

Ⓒ KAROL EDWARD SZKLARZ

A THESIS
SUBMITTED TO THE FACULTY OF GRADUATE STUDIES AND RESEARCH
IN PARTIAL FULFILMENT OF THE REQUIREMENTS FOR THE DEGREE
OF MASTER OF SCIENCE

IN

METALLURGY
DEPARTMENT OF MINERAL ENGINEERING

EDMONTON, Alberta
FALL, 1976

THE UNIVERSITY OF ALBERTA

FACULTY OF GRADUATE STUDIES AND RESEARCH

The undersigned certify that they have read, and recommend to the Faculty of Graduate Studies and Research, for acceptance, a thesis entitled "EXOELECTRON EMISSION FROM AN ALUMINUM ALLOY DURING AND AFTER PLASTIC DEFORMATION", submitted by Karol Edward Szklarz, in partial fulfilment of the requirements for the degree of Master of Science in Metallurgy.

Michael L Wayman . . . .
Supervisor

. . . .

. . . .

Date July 16, 1976.

To Marie

ABSTRACT

A Geiger-Müller flow counter was constructed and operated to effectively detect exoelectrons from a 6063 aluminum alloy. The optically stimulated exoelectron emission rate was recorded during and after plastic deformation.

By properly heat treating the age-hardening 6063 alloy, the microstructures, slip modes and consequent exoelectron emission of the alloy specimens were changed in a systematic manner. A finer slip mode resulted in higher rate of increase of exoelectron emission during tensile strain. This correlation of emission rate with specimen slip mode allowed the suggestion of a mechanism for exoelectron emission during plastic deformation.

It is suggested that upon plastic deformation, slip steps form and break through the metal oxide, exposing dislocation ends, that is, dislocation lines intersecting the exposed metal surface, which form localized exoemission centers. The exoelectron emission rate from these centers then decays with time.

ACKNOWLEDGMENTS

The author is indebted to Dr. M. L. Wayman for providing guidance and encouragement over the span of my graduate studies.

My thanks to Dr. F. H. Vitovec for his advice and comments on problems encountered in this research. I would also like to extend my appreciation to Mr. T. Forman, Mr. G. Chaisson, Mr. B. Konzuk, Mr. G. Cameron, and Ms. M. Johnston for their able technical assistance.

This work was supported by an International Nickel Company of Canada Graduate Research Fellowship in Engineering and Science and by the National Research Council of Canada.

TABLE OF CONTENTS

Chapter Page

I INTRODUCTION 1

II EXOELECTRON EMISSION FROM METALS . . 4

Historical Background 4

Emission Following Abrasion of Metals 10

Emission From Quenched Metals . . 15

Emission From Plastically Deformed Metals 17

Emission From Fatigued Metals . . 24

Summary 28

III EXPERIMENTAL 30

Major Test Equipment 30

Selection of Detection Systems 30

Geiger-Müller Flow Counter . . 31

Electronics 35

Testing Procedure 37

Specimen Preparation 37

Tensile Tests 39

Slip Mode Determination 42

Fatigue Tests 42

TABLE OF CONTENTS (Continued)

Chapter Page

IV RESULTS AND DISCUSSION 44

Detection Systems Performance . . 44

Emission During Tensile Tests . . 47

Slip Mode Correlation 51

Decay After Tensile Tests 54

Suggested Mechanism For OSEE During Tensile Deformation . . . 58

Fatigue Tests 61

V CONCLUSIONS 63

VI FUTURE WORK 65

***

TABLES 66

FIGURES 70

PHOTOGRAPHIC PLATES 106

REFERENCES 114

LIST OF TABLES

Table	Description	Page
1	Chemical Composition of Alloy	66
2	Heat Treatments of Aluminum Alloy	67
3	Summary of Experimental Tests	68
4	Results of Tensile Tests	69

LIST OF FIGURES

Figure		Page
1.	Simplified Schematic Band Model For Luminescence and EEE From Solids	70
2.	Geiger-Müller Flow Counter	71
3.	Pulse-height versus Applied Voltage Curves, Illustrating Ionization, Proportional and Geiger-Müller Regions (taken from [61]).	72
4.	Block Diagram of a System For Single Particle Counting	73
5.	Specimen Configurations	74
6.	Plateaus for G-M Flow Counter	75
7.	SPEC. A30 (T4)	76
8.	SPEC. A38 (T6(450))	77
9.	SPEC. A39 (T6(450Q))	78
10.	SPEC. A40 (T4*)	79
11.	SPEC. A41 (T6(450Q))	80
12.	SPEC. A43 (T4)	81
13.	SPEC. A45 (T6(450Q)	82
14.	SPEC. B1 (T4)	83
15.	SPEC. B2 (T4)	84
16.	SPEC. B3 (T6(450Q)	85
17.	SPEC. B4 (T6(450Q)	86
18.	SPEC. B5 (T6(450))	87
19.	SPEC. B7 (T6)	88
20.	SPEC. B8 (T6)	89

LIST OF FIGURES (Continued)

Figure Page

21. SPEC. B9 (T6(450Q) 90
22. SPEC. B10 (T4) 91
23. SPEC. B11 (T6(450)) 92
24. SPEC. B12 (T4) 93
25. SPEC. B13 (T4) 94
26. SPEC. B14 (T6(450Q) 95
27. SPEC. B15 (T6(450) 96
28. SPEC. B16 (T6 97
29. SPEC. B17 T4L 98
30. SPEC. B18 T4S 99
31. GROUP 1 SPECIMENS 100
32. GROUP 2 SPECIMENS 101
33. GROUP 3 SPECIMENS 102
34. GROUP 4 SPECIMENS 103
35. B11 (T6(450) DECAY 104
36. B10 (T4) DECAY 105

LIST OF PHOTOGRAPHIC PLATES

Plate	Description	Page
1	Specimen Configuration II and its appropriate specimen holder.	106
2	Specimen Configuration III and its appropriate specimen holder.	107
3	Specimens of Configurations II and III mounted in their specimen holders, revealing the test areas.	108
4	S[illegible] close-up of G-M flow counter in [illegible]st position. The specimen is c[illegible]ed to the counter tube and mounted in the Instrom grips. This plate shows the illuminated quartz port, the accelerating grid (through the port) and its voltage sources, and the assorted electrical connections and gas tubing required for operation of the counter.	109
5	An overall, rear view of the testing system. This plate shows the Instron testing frame, the Philips electronics, and the light source.	110
6	Slip structure of a T4 specimen, showing distinct, massive planar slip, x 250.	111
7	Slip structure of a T6 specimen, showing indistinct, fine, wavy slip, x 250.	112
8	Slip structure of a T6(450) specimen, showing an intermediate slip (between T4 and T6) which is less indistinct and wavy than T6, x 250.	113

I. INTRODUCTION

When a solid undergoes a structural change, such as is encountered during plastic deformation, irradiation, or a phase change, the solid surface may emit negative charge carriers in the form of slow electrons (a few electron-volts). After termination of the structural change, the emission rate decays with time. This emission phenomenon was named exoelectron emission (EEE) by Kramer [1] in 1950. Photo-emission and thermo-emission of electrons occur from many substances upon structural change and excitation by visible light and thermal stimulation, respectively. These phenomena, called optically stimulated exoemission (OSEE) and thermo-stimulated exoemission (TSEE), differ from the normal photoelectric effect, which is observed only with sufficiently short wavelength light, and the normal thermionic emission, which is observed only at sufficiently high temperatures. The OSEE and TSEE also decay with time.

The ability to study the structural changes in metals, especially commercial materials, is of great importance. Structural damage in commercial metals may result in failure. Also, structural changes are necessary for both the fabrication and the development of useful properties in metals. The EEE effect, since it occurs because of structural changes in the metal or its surface layer, can be related to deformation processes, including fatigue, in the metal. Also, methods for increasing the service life of the components of machines and structures require knowledge of the physicochemical condition and structure of the metal surfaces as well as their reactions with external influences. There is a general paucity of simple, effective methods of studying the physical condition of surfaces. Exoelectron emission is a promising method for this type of investigation.

It is generally believed that in many cases the emitted electrons are released from defects at the surface of the solid. The electrons are liberated from the defects by the stimulation energy (light or heat) and reach the conduction band. If sufficiently energetic, the electrons may overcome the work function and escape through the crystal surface. Exoelectron emission, then, is characterized by the fact that single particles are detected.

Although the mechanism of EEE is not fully understood, careful studies can lead to much empirical knowledge which could result ultimately in applications to the study of materials. To this end, a Geiger-Müller (G-M) flow counter was constructed as a highly sensitive single particle detector. Since aluminum is known to have a pronounced OSEE effect, studies were carried out on a commercially available 6063 aluminum alloy. This alloy is an age-hardening alloy and therefore its microstructure may be greatly altered by various heat treatments. Test specimens were strained in tension and the mechanical (deformation) behavior correlated with the EEE.

It is not the primary intention of this work to develop a definitive model for EEE, but rather to observe the effect of microstructure (slip mode) on the process. It is then possible to speculate about the emission mechanism; however, the long-term aim is to use EEE as an aid to prediction of mechanical properties, specifically fatigue behavior. This thesis is a preliminary step toward that goal.

II. EXOELECTRON EMISSION FROM METALS

Excellent review articles on exoelectron emission from metals have been published by Grunberg [2] in 1958 and Brotzen [3] in 1967. This section will firstly present the chronological development of EEE ideas up to 1958. This will be followed by discussion of EEE during various forms of metal deformation.

Historical Background

Exoelectron emission has been observed directly or indirectly for over 130 years. Vitovec [4] refers to the work of Moser [5], published in 1842. Moser found that cold-worked or abraded metals affected light sensitive materials, such as photographic emulsions, in the dark. The action of freshly disturbed surfaces on photographic emulsions partly caused by EEE, is called the "Russel effect" [6] and will not be considered further. Oberhöfer [7] refers to early work by Elster and Geitel (1896) and Klaphecke (1931) dealing with emission stimulated by means of illumination and by the application of heat, respectively.

Scharmann states in his historical review [8] that many physicists have detected exoelectrons without realizing it. Curie observed in 1899 [9] a decaying radioactivity of materials brought near radium. Rutherford [10] also observed this behavior with thorium compounds. When the Geiger-Müller counter, which was highly sensitive to low-level radiation, came into use, electron emission was often discovered within these tubes. Newly constructed tubes often had to be 'aged' to reduce the internal background counting level. In 1941, L. C. van Atta et al. [11] found a high background level in the counting rate of their Geiger tubes when studying nuclear excitation processes with X-rays. Previously, in 1935, Tanaka [12] measured slow-decay curves of aluminum, silver, copper and nickel foils irradiated with 300 KeV electrons. Shortly afterward, Lewis and Burcham [13] observed that abraded or scratched specimens of aluminum, copper, brass and nickel when introduced into a Geiger-Müller counter triggered off a large number of pulses.

The first comprehensive reports of a delayed electron emission phenomenon was published by Kramer [1] in 1950. From his findings Kramer drew attention to the fact that this phenomenon afforded a means of investigating metal surfaces. His work consisted of experiments in which metals were subjected to various treatments and then examined with a point counter. The metal specimens formed part of the counter cathode. It was found that deformed metal surfaces emitted negative charge carriers at an intensity level greater than that expected for thermionic emission. This emission decayed with time. From experiments on Wood's metal, Kramer assumed that the transformation of metals from the amorphous to the crystalline state caused an emission of electrons. As solidification is an exo-thermal process, he named the electrons "exoelectrons". Although the phenomenon is now known to be structure dependent, the term "exoelectron emission" is still used, as well as the name "Kramer effect", honouring Kramer's contributions in the field.

In 1956, Bathow and Gobrecht [14] overcame the difficulties caused by exposing the surface of a specimen to the air or to the counting gas in a counter. They enclosed the specimen in a vacuum chamber and electron-optically focused the emission current into a counter through an electron transparent window. This showed that the origin of the emission cannot be ascribed to instrumental causes, such as the bombardment of the specimen surface by positive ions or metastable atomic or molecular particles. Tests in high vacuum also revealed that EEE is related to the presence of surface films or to the interaction between gas molecules and the metal surface. The possibility that an interaction of the metal surface with oxygen (chemisorption) was the cause of emission, had been discussed by Haxel, Houtermans and Seeger [15]. Tests on aluminum, zinc and other metals showed that oxygen and a surface film was necessary for emission. Seeger [16], for instance, had clearly shown that thermal emission from aluminum, upon stimulation with ultra-violet light, was associated with the presence of an oxide film.

Photo-electric emission from abraded metal surfaces was also studied in the mid-1950's. It was found that abrasion appeared to shift the photo-electric threshold to longer wavelengths by several hundred angstroms; this shift receded with time. This is the OSEE effect which coincides with changes in the work function at the metal surface. For aluminum, Grunberg and Wright [17] [18] attributed the effect to the creation of color centers in the aluminum-oxide surface layer. They specifically considered F'-centers — oxygen vacancies at which two electrons were trapped. The emission takes place through photo-excitation of these centers, which give up their energy to nearby shallow surface centers (unspecified) from which electrons are emitted. During deformation the vacancies could be formed mechanically in the oxide layer in anion-cation pairs. Also, the decay of the emission was accelerated by increased oxygen pressure. Seidl [19] suggested that the electron traps were created by absorbed oxygen. Grunberg and Wright also studied exoelectron emission during deformation of aluminum under photo-stimulation. During plastic deformation they found that intensity I increased approximately as

$$I = A(\ell - \ell_o)^n ,$$

where ℓ is the amount of deformation and ℓ_o is the initial degree of deformation at which an increase of emission is observed. A and n are constants, n being close to 2 or 3.

Kramer [20] and Bohun [21] found a similarity between optical luminescence and exoelectron emission in insulating crystals. With this information, Hanle [22] made an attempt to explain the EEE mechanism on the basis of a comprehensive band model. This explanation which is in general still accepted, can be considered in simple terms to involve the absorption of energy, and the consequent release of exoelectrons from the surface lattice imperfections. The energy absorption, the "excitation process", causes electrons to move from the valence band to the conduction band as shown in Fig. 1. The various processes in Fig. 1 are explained as follows:

1. By energy absorption, electrons are lifted from the valence band into the conduction band.
2. After the electrons remain there for a short time,
3. the electrons drop into traps which may be located within the solid (volume traps) or at its surface (surface traps). The energetic position of the

traps, "trap depth", is characteristic of the material considered.

4. By putting more energy into the solid (stimulation) the electrons can be liberated from the traps by lifting them into the conduction band.
5. If the electrons return by the emission of light ($h\nu$) to the valence band by way of 'acceptors' luminescence or thermo-luminescence occurs.
6. Exoelectron emission occurs if the electrons leave the surface of the solid, overcoming the work function.

The intensity of the exoelectron emission is related to the number of trapped electrons and therefore to the excitation energy. Proportionality is expected as long as the available traps are not exhausted. This provides interesting applications in radiation dosimetry (see e.g. Oberhofer [7]).

Müller [23] also in 1956, demonstrated the importance of lattice defects by the observation of cuprous oxide films. Specimens whose X-ray pattern revealed a strongly disturbed lattice were more sensitive to exoemission after X-radiation than films with a nearly perfect structure.

Thus by 1958, exoelectron emission had been the subject of numerous investigations, but its mechanism remained unknown. Since then, there has been further intensive work which is reviewed below by topic, rather than chronologically, thereby facilitating a better understanding of the current state of knowledge.

Emission Following Abrasion of Metals

Vacuum studies of EEE by Lohff [24] indicated that internal processes taking place in metal specimens, in the absence of oxidation, affected subsequent emission rates. Aluminum samples were abraded at low oxygen pressures and the emission was allowed to decay for a period. Evacuating the system caused the emission rate to drop. Restoration of the original oxygen pressure raised the emission but to a lower level than at evacuation. This means that emission-controlling processes occur even when emission is suppressed by high vacuum.

After studying the OSEE decay from abraded beryllium, calcium, aluminium and magnesium at various temperatures, Ku and Pimbley [25] suggested a mechanism for the emission in which lattice vacancies are generated in the metal by abrasion. The vacancies diffuse to the surface and become sites for adsorption or oxidation. When the sum of the energy of the vacancy released plus the energy of photo stimulation exceeds the photo-electric work function of the metal, emission of an electron takes place. Subsequently Pimbley and Francis [26] used this model to obtain an emission rate decay equation of the type:

$$I = Ae^{-K_1 t} + Be^{-K_2 t} ,$$

where I is emission rate (intensity), t is time, A and B are constants and K_1 and K_2 are decay constants which vary with temperature, T, as

$$K_i = K_i^o e^{-E/kT} .$$

The activation energy, E = 0.24 eV, was found to be the same for the first and second decay constants. The emission rate was taken to be proportional to the vacancy flux across the metal surface, but the activation energy obtained did not correlate with that for vacancy diffusion in aluminum [27].

Ramsey and Garlick [28] abraded aluminum specimens at 10^{-3} Torr and 195°K. Immediately after abrasion the OSEE rapidly rose, peaked and then decayed although the emission rate was much smaller than that at room temperature. At lower pressures, the emission was hardly affected but at higher temperatures, the decay was suppressed. These results were explained by an oxidation model proposed by Cabrera [29]. According to this model, chemisorption is presumed to take immediately after abrasion, starting at preferential nucleation sites. The oxide film contains many defects, especially vacancies, which speed up the diffusion of metal ions and thus oxide growth. Electrons from the metal can be trapped at vacancies about 1 eV below the oxide conduction band. These electrons may then be removed by light absorption at photo energies lower than the metal photo-electric threshold.

Elliott and O'Neill [30] recently showed that the time to reach maximum emission after abrasion rose with the approximate time for the formation of a monolayer of adsorbed gas. In Poland, Lewowoski [31] showed that the moisture content of the counter gas affected the EEE process, with high moisture content causing more rapid decay of emission. Also recently, Momose [32] sandblasted Ni and Cu specimens with SiC particles and then aged the specimens in wet or dry air. He then heated the specimens and obtained emission "glow curves" (emission rate versus temperature increase). The glow curves exhibited a peak which coincided with the temperature of dehydration for the appropriate metal oxides. Furthermore the peak was greater in wet air than in dry air. Prior ageing in these atmospheres caused an increase in the maximum emission to some saturation value. These results were explained as being due to the "slow interaction of water vapour with the freshly deformed metal surface".

Exoelectron emission from the surface of abraded or filed aluminum excited by ultrasonic vibration was studied by Langenecker and Ray [33]. The effect of ultrasonic vibration was to increase the EEE. The same increase of emission could be obtained by the application of thermal energy, which was four orders higher than the ultrasonic energy. This result was explained by the fact that sound passing through a crystal lattice is hardly absorbed by atoms away from dislocations. Heat, however, is dispersed among all the atoms of the sample. The authors believed that this selective effect of ultrasonic vibration on dislocations forms active emission centers where the dislocations emerge at the surface.

A recent article by Craciun [34] has made some important observations on EEE decay after abrasion of aluminum and magnesium samples. Craciun reported a "spontaneous regeneration" of EEE rate in abraded aluminum and magnesium following removal of one or more of the working parameters of the detection system. A conventional open window Geiger-Müller counter was used to detect emission under photo or thermal stimulation conditions. The working parameters included the effects of illumination, temperature, external accelerating field, and counter voltage.

Craciun believed that positive counter gas ions, diffusing to the cathode, produced an electric double layer at the emitting specimen surface. This produced an electric field superimposed upon the external field accelerating the electrons and thus enhanced exoemission of electrons. The ion layer increased until a dynamic equilibrium was established between the ions arriving at the sample surface and the ions neutralized at the sample surface. The centers of EEE were considered as capture centers (traps) for electrons. The time-dependent decay of the EEE would then be a depopulation of these traps.

The metals investigated had metal oxides (Al_2O_3 and MgO) that exhibit n-type semiconductor properties. Therefore, metal-semicondictor junctions existing at the sample emitting surface could cause an intense electric field which would hinder electron passage through the metal-oxide interface. However, electrons of sufficiently high energy and velocity are known to be able to "tunnel" through junction barriers. Those electrons may be captured by defects (traps) in the oxide layer, thus providing emitting centers.

It must be noted, however, that EEE is also observed in vacuum, so Craciun's explanation cannot be the entire story. In general, the abrasion of metals provides a simple way to study EEE decay, however, the extent of deformation and the type of defects produced cannot be quantitatively controlled.

Emission From Quenched Metals

Relatively few papers have been published on exoemission from quenched metals. Scharmann and Seibert [35] discovered that the threshold wavelength for photoelectric emission from aluminum at 10^{-5} Torr is raised not only by mechanical working but also by quenching. Ageing of the specimens at this pressure caused the threshold wavelength to return to shorter wavelengths. Such results could be explained by defect migration in the aluminum.

Claytor, Gragg, and Brotzen [35] also used aluminum in quenching experiments. The aluminum disks and wires tested emitted exoelectrons only after quenching from temperatures below 450°C. The energy of formation of the defect causing the exoemission was found to be 1.8 eV. This, however, is an appreciably higher energy than required for vacancy formation in aluminum.

It has been long known that at elevated temperatures point defects are found in considerable concentrations. Kurov and Sidorova [37] quenched 0.2 mm. thick aluminum specimens from various temperatures. Their results substantiated the results of Claytor et al. [36] with higher quench temperatures emitting fewer exoelectrons. Kurov and Sidorova, however, used their data to confirm a relationship between the vacancy concentration in aluminum and the EEE. The quenching experiments were conducted in conjunction with plastic deformation tests. Upon deformation of a sample the vacancy concentration and dislocation density increased; however, after deformation ceased, the vacancy concentration gradually returned to its original level while the dislocation density remained almost the same. The dislocations, then, can act as sinks for the vacancies. Although quenching from a higher temperature increases the vacancy concentration, the quench also causes thermal stresses within the sample which, in turn, produce dislocations. The higher the quenching temperature, the greater the number of dislocations produced, which result in a greater vacancy absorption, thereby reducing the EEE. This result is interesting and surprising as it is known the vacancy concentration of metals does go up with temperature and quenching should preserve many of the vacancies.

Emission From Plastically Deformed Metals

With specimens subjected to mechanical testing, as opposed to abrasion, the degree of plastic deformation can be controlled and quantitatively measured. During the late 1950's and throughout the 1960's, many workers attempted to obtain correlations between information from deformation processes and EEE. Basically, three types of mechanisms for EEE were proposed, involving dislocation - surface interactions, vacancies in surface oxide layers and cracks in surface oxide layers.

In 1960, Meleka and Barr [38] showed that when a zinc single crystal, covered with a highly photo sensitive stripping emulsion, was plastically deformed, the slip lines of the zinc appeared on the developed emulsion. Although this was an example of the Russel effect, Meleka and Barr hypothesized that the regions where dislocations intersect the crystal surface act as emission sites for exoelectrons.

Serious attempts to correlate the mechanically induced changes in poly-crystalline aluminum with OSEE were conducted in the late 1950's by Von Voss and Brotzen [39] and Claytor and Brotzen [40]. These workers used a Geiger-Müller counter as their electron detector. This permitted control of strain, strain rate, stress and temperature. Tests at room temperature [39] showed that the emission rate during tensile straining and subsequent decay depended strongly on the strain history of the specimen. Therefore they concluded that OSEE was structure sensitive. Deformation of aluminum at low temperatures [40] and subsequent annealing produced an emission "glow curves". From both series of tests, Brotzen concluded that:

a) point defects, i.e. vacancies, are created in the Al crystals during plastic deformation,

b) these defects, depending on the temperature, migrate towards sinks, including the surface,

c) some of the point defects succeed in locating themselves in the oxide layer, creating discrete energy levels in the forbidden energy band, and

d) these are the original sites from which OSEE or TSEE occurs.

Since the vacancies in the oxide layer continue to diffuse, the emission decays. A diffusion equation for point defects was solved, yielding the rate of arrival of defects at the surface oxide layer and consequently a rather complex equation for decay of emission.

Sujak, in Poland, directed an important series of experiments during the 1960's. He showed that the decay of OSEE from polycrystalline aluminum after bending [41] followed the form described by Pimbley and Francis [27] for decay after abrasion. During this bending deformation, the rise in the OSEE rate was approximately proportional to the third power of strain, according to

$$I = A(\varepsilon-\varepsilon_o)^3$$

where A is a constant, ε is strain and ε_o is the initial strain. Sujak justified this form on the basis of lattice vacancy formation and lattice dislocation movement. A following paper [42] showed that, for aluminum, a definite amount of tensile strain, ε_o, had to be applied before OSEE could be detected.

When varying thicknesses of oxide on the aluminum were produced electrolytically a maximum in ε_o was found to occur at an oxide thickness of 1 μm. Sujak concluded that the rupture of the oxide layer during plastic deformation was important and proposed that the cracks formed had to achieve a certain opening displacement before OSEE occurred. Gieroszynski, Mader, and Sujak [43] also investigated the effect of moisture content on aluminum specimens of varying oxide thicknesses. They found the rise in ε_o with increasing oxide thickness less pronounced when the moisture content of the atmosphere rose.

Sujak and co-workers also conducted measurements of EEE in vacuum [44] using an electron multiplier. These tests confirmed their previous results with the Geiger-Müller counter. Sujak and Gieroszynski [45] showed an interdependence of OSEE from aluminum with oxide thickness, frequency and intensity of the stimulating light, and applied accelerating field. Higher frequency and/or intensity of stimulating light decreased ε_o. These workers therefore put forward a mechanism [46] for EEE which considered the formation of cracks in the oxide layer as a result of plastic deformation. It was thought that a strong electric field would lie across cracks in the oxide and oppose the escape of electrons from a underlying emitting layer. This layer was considered a semiconducting, transitional metal-oxide interface containing emitting centers formed by the influx of lattice defects from the metal. Electrons emitted by the layer would not always be able to leave the cracks and therefore could set up a space charge that varied with time and affected the kinetics of the emission process. It must be stated that this mechanism has not met general acceptance as there has been no evidence supporting large electric fields (10^7 V cm^{-1}) within oxide cracks.

In vacuum, aluminum with a thick oxide layer (>50nm) can emit exoelectrons without photostimulation [47]. Two maxima are present at small deformation values.

Arnott and Ramsey [48], investigating EEE under these conditions, found two different types of EEE, one of which was a pressure dependent OSEE for oxide thicknesses greater than 45 nm. They concluded that the OSEE from aluminum deformed in tension resulted from the lowering of the work function due to the adsorption of oxygen and water molecules on fresh Al exposed by slip breaking through the oxide film. Above oxide thicknesses of about 45 nm, the second type of EEE was observed without light stimulation and was characterized microscopically by the absence of visible slip and the formation and propagation of cracks in the oxide.

Beginning in the late 1960's, a large number of articles on EEE have appeared in the U.S.S.R. An early article by Mints and Kortov [49] showed that electron emission during metal deformation was caused by formation of a large number of defects at the metal surface. The authors considered that the emission centers are the points at which dislocations emerge at the metal surface. In areas containing dislocations, there are changes in the interatomic distances, causing a change in the energy distribution of the electron states. This may result in a local change of the metal's work function. When the surfaces of weakly oxidizing gold and stainless steel were mechanically ground at approximately 10^{-5} Torr, emission occurred which was almost insensitive to pressure. Aluminum and copper were tested in the same way the EEE increased with increasing pressure. Therefore EEE from metal surfaces is not entirely due to oxidation. To show the effect of defect mobility on EEE, nickel and manganese austenitic steels were used. (The defect mobility in iron-nickel alloys is higher than in iron-manganese alloys.) The "time to maximum emission" dependence on the degree of deformation for both austenites agreed well with the mobility of defects in these austenites.

In a later article, Melekhin, Kortov and Mints [50] showed that two-dimensional defects of the twin boundary and stacking fault type are capable of forming centers on the surface of metals and thus emit exoelectrons.

Magnesium has also been a favorite metal in which to produce EEE. Gel'man and Roikh [51] investigated the time dependence of OSEE, surface potential, and oxide thickness in deformed and undeformed magnesium. They concluded that the OSEE from the magnesium surface is governed by the surface potential, the thickness and the formation rate of the oxide. The deformation of the magnesium is then not the reason for OSEE, but affects the emission kinetics by changing the nature of the oxidation processes. The OSEE kinetics seem to be governed firstly by the changes in surface potential when the oxide is thin. As the oxide thickens, its effect on the OSEE increases. The exoelectrons were detected by an interesting air-filled proportional counter with a hemispherical cathode and a tear-drop-shaped anode wire.

In a later report Gel'man and Fainshtein [52] studied the two stages of OSEE in the oxidation of magnesium. The authors hypothesized a relation between the thickness L of the surface oxide film and the wavelength λ_- of the emitted electrons which appear at the metal-oxide interface. For $L < \lambda$, the OSEE was thought to be an oxidation-stimulated photoelectric effect from the metal. The energy of the electrons escaping from the metal is greater than the energy of the electrons detected by an amount corresponding to the potential drop across the surface film. The first stage of OSEE continues until the oxide and adsorbed film reach a total thickness greater than 30 Å. For $L > \lambda$, the OSEE enters a second stage, in which scattering and capture of electrons by film defects become important. Exoelectrons are then liberated from local levels associated with oxide defects and adsorbed molecules.

Recently, Shkil'ko and Kresnin [53] stretched magnesium ribbons in a vacuum chamber and examined both the OSEE and the dark EEE. They concluded that EEE, after deformation, was due to the migration of vacancies from the bulk metal to the metal surface.

Therefore it is evident that both the oxide layer and the formation of bulk defects in a plastically deformed metal contribute to EEE; the dominant mechanism for EEE being unknown.

Emission From Fatigued Metals

Ever since Kramer's original experiments [1], the possibility of using EEE to study fatigued metals has been considered. As EEE emanates from the metal surfaces, it contains information regarding the structure changes in the surface of a metal in the process of deformation. There are two levels of observation in the study of EEE from fatigued metals:

1. Emission is obtained from a large surface area, measuring total fatigue damage. This is an easier observation than
2. emission from a movable small area (approximately 100 μm^2) which measures localized fatigue damage.

Until recently only the first method was used and this gave EEE rate during the fatigue life of a specimen and the number of cycles to start emission.

Mints and Kortov [49] carried out cyclic loading on pure copper, aluminum and gold, after deformation by grinding and micro impact. The authors found that upon cyclic loading, the internal friction level of the specimens increased then remained constant. With this deformation, the EEE also increased to saturation indicating a correlation between EEE and defect mobility. In a later paper, Mints et al. [54] found a correlation between EEE and the degree of deformation, surface relief and fatigue strengthening during cycles of alternating stress. The EEE was regarded as an electrical effect which is the result of storing of deformation energy in a metal. This assumption was supported by studies of the amplitude-dependent internal friction, which may characterize the dissipation of energy during stress cycles.

In 1972, Hoenig et al. [55] published an important article on the possibility of applying EEE to specific types of non-destructive evaluation. The authors showed that EEE occurs during the initiation and growth of cracks. Metal specimens, notably aluminum, were fatigued to a certain percentage of their fatigue life. During fatigue a complex structure of vacancies and dislocations develop near the specimen surface. Most of these defects would be sessile at room temperature but upon heating a significant fraction of these defects (vacancies) would be expected to diffuse to the surface. The resultant EEE would be used as a measure of the fatigue damage to the specimen. The heating would be to a temperature far below that at which metallurgical changes could occur (90° C for aluminum). The authors obtained increased EEE with increases in percentage of fatigue life, thus showing a promising potential for non-destructive evaluation of metals (at least aluminum). They also succeeded in showing that the area of maximum fatigue damage was also the region with maximum EEE.

The study of small regions on a fatigued surface has only been reported very recently. Beginning in 1972, Baxter has published a number of articles examining small regions of fatigued surfaces. He constructed an apparatus capable of mechanically scanning a 15 μm ultra violet spot across a fatigued specimen surface [56]. The development and accumulation of fatigue damage, and the associated changes in surface topography, are very localized phenomena. The technique of scanning the surface with a small spot of stimulating radiation provides more detailed results in contrast with earlier investigations where the entire surface was illuminated. Tests on aluminum and steel demonstrate that fatigue damage produces OSEE after less than 1% of the fatigue life. The localized emission increases throughout the fatigue life, with failure ocurring in the region of most intense emission. The regions of intense localized emission correspond to the location where fatigue cracks develop and propagate. Further studies [57] substantiated these results and produced the interesting observation that small tensile strains caused emission while similarly small compressive strains did not. Baxter believes that OSEE is an enhanced photo electric effect. The cracking of brittle oxide layers is considered the important factor in producing EEE. Indeed, for brittle surface coatings, it has been theoretically predicted that cracks should develop in tension at a lower strain level than in compression [58]. The exoelectrons are presumably emitted from microcracks in the oxide.

Baxter has also succeeded in obtaining a visual display of fatigue damage by means of OSEE [59]. This was made possible by the use of direct electron optical imaging of the exoelectrons, as in a photoemission microscope. Baxter showed conclusively that OSEE resulting from fatigue deformation of a metal originates completely from the slip lines on the surface and concluded that exoelectrons are emitted only where the surface oxide is locally ruptured during the formation of a slip step. Finally, Baxter [60] showed that the intensity of localized OSEE in steel is a measure of the accumulated surface damage. The development of persistent slip bands produces microcracks in the surface oxide. The growth of these bands and the formation and propagation of fatique cracks increases the area of fresh metal surface from which OSEE occurs. Baxter used the EEE increase as a crude calibration for the prediction of the remaining fatigue life. This is certainly one of the most interesting applications of EEE phenomena.

Summary

The evidence compiled in the literature seems to indicate that EEE phenomena, at least for strongly oxidizing metals, is directly connected to the oxide or adsorbed surface layer on the metal. The mechanism of emission from these surface layers, however, seems to be in doubt. The various mechanisms suggested fall into two basic types, where:

1. the surface layer controls the EEE, and
2. the defects in the metal control the EEE. In the

In the first type of mechanism:

1. the growth of the surface layer by oxidation or adsorption provides some of the stimulation for EEE, or
2. some electrons in the metal tunnel through the metal oxide interface and are trapped at discrete energy levels within the oxide, later to be readmitted, or
3. large electric fields could form within oxide cracks and cause EEE from the underlying metal-oxide

interface.

In the second type of mechanism:

1. point defects migrate from the metal into the oxide layer and create electron traps within this layer, or
2. a dislocation-vacancy mechanism exists whereby dislocations absorb vacancies and form EEE centers where they intersect the metal surface.

Most probably more than one of the various mechanisms are involved, with the dominant mechanism being determined by the particular specimen and experimental conditions.

Most of the research to-date has been conducted on pure metals with little attention being given to alloys. Experiments on alloys allow the researcher to control by heat treatment the metallurgical structure and thus parameters such as deformation behaviour and slip mode, without changing specimen composition or the oxide characteristics. The present work is an attempt to correlate EEE with deformation characteristics in an aluminum alloy under tensile and fatigue loading.

III. EXPERIMENTAL

Major Test Equipment

Selection of Detection System

The first experimental objective was the selection and construction of a convenient, sensitive electron detection system. There are two basic types of exoelectrons detection systems:

1. the traditional single particle counters, such as open point counters, Geiger-Müller (G-M) counters and open electron multipliers, and
2. the more recent current measuring devices containing FETs and capable of measuring as little as 10^{-15} A.

Kramer [1] began his work with an open point counter operating in air at atmospheric pressure. An open point counter consists of a pointed anode wire surrounded by a cylindrical cathode which is open at one end so that the anode wire can be adjacent to the sample. These counters are simple, easy to construct and inexpensive but they have severe limitations. They require high anode voltages, have a very small plateau region and resolving capacity, and are very temperature sensitive.

G-M counters offer high sensitivity, good resolution and good stability, however, the exposure of the specimen to the counting gas is required in order that low energy electrons can be detected.

Open electron multipliers with Cu-Be dynodes have highly desirable characteristics, but low energy electrons are not efficient in inducing secondary electron emission. Furthermore, these devices require high vacuum or ultra-high vacuum for operation and are costly and complicated systems.

All the above detectors can permit in-situ optical and thermal stimulation and temperature control of the specimen. The major problem in studying EEE has been the small emission currents (10^{-9} to 10^{-13} A) and low electron energy (about 1 eV). However, the advent of the FET and the operational amplifier has made it possible to measure currents of 10^{-15} A. Thus a small voltage applied to an anode grid will permit detection of the exoemission current even in ambient air [55].

In the present case, as a highly sensitive current measuring device was not available the first type of system, a G-M flow counter was chosen, designed and constructed.

Geiger-Müller Flow Counter

The design of the counting tube was modified from one by Von Voss and Brotzen [39]. The body of the counter see Fig. 2, was a 2 in. i.d. 6061 aluminum alloy tube, 10 in. long. The specimen mounting surface was a 2 in. wide channel in the reinforced center of the tube. The open counter window was a hole of 1 in. diameter in the center of the channel. This channel maintained the (flat) specimen in the correct position. For specimens of less than 2 in. width, a teflon specimen holder was inserted into the channel. Each specimen holder had a channel and an open window suitable for a particular specimen configuration as shown in plates 1, 2 and 3. The specimen, then, was open to the counting gas of the counter. To allow the impingement of visible or ultraviolet light on the specimen surface, a 3/4 in. sealed quartz-glass port was installed directly opposite the counter window. This port also allowed visual observation of the specimen surface during a test.

A .003 in. tungsten wire, stretched along the long axis of the tube, served as the counter anode. The ends of the counter were made of teflon, sealed with silicone vacuum grease and firmly clamped in place by aluminum rings. These endpieces allowed for insulated electrical and sealed gas flow feed-throughs. As well as supporting the anode wire, the endpieces also supported a 1 in. i.d. cylindrical grid, of 22 mesh copper, which was concentric with the anode wire. By applying a small positive potential to the grid, an external accelerating voltage could be applied between the specimen and the grid.

The counter gas used was 1% methane in helium, the methane serving as the quenching agent.

The operation of the counter is as follows. When an electron is emitted from the specimen surface, it is accelerated, by the large electric field within the counting tube, toward the anode wire. Upon reaching a certain energy this electron begins ionizing the counting gas. If the anode voltage is within the G-M region as shown in Fig. 3, ionization of the helium molecules avalanches through the counter tube. This causes a single pulse which can be counted. During the migration of the positive ions to the cathode, the helium ions with an ionization potential of 24.48 volts collide with methane molecules with an ionization potential of 12.6 volts. Because of the difference in the ionization potentials, the charge is transferred to the methane molecules. Therefore, only methane ions reach the cathode where they are neutralized[1]. The energy released when this occurs goes into dissociating methane molecules rather than producing further ionization [61]. Since the methane does not recombine in the counter, it would be depleted, therefore a slow flow of counter gas was provided through the tube to maintain a constant supply of methane molecules for dissociation. This flow also allowed the counter to operate at a slight positive pressure inhibiting air from entering the counter tube. The gas flow was monitored by bubbling the discharge through a water filled flask.

---

[1] There are two mechanisms by which an electron can be emitted as a result of neutralization: the energy difference between the ionization potential of the ion and the work function of the cathode may be radiated as a proton which may release a photo-electron; or the energy difference may be used directly in a radiationless liberation of an electron from the cathode.

For each test, a specimen, in a specimen holder, was clamped between an aluminum plate and the specimen mounting surface of the counter. The top clamping surface was faced with 1/16 in. teflon to reduce sliding friction. An O - ring between the teflon specimen holder and the counter specimen mounting surface and generous amounts of silicon vacuum grease about the specimen, prevented air from entering the counter tube. The counter tube could be suspended from the frame of any tensile or fatigue testing machine.

The limitations on the specimen dimensions imposed by the counter are listed below:

1. A flat specimen is necessary.
2. A 3 in. length of the specimen is in contact with the specimen mounting surface on the counter.

3. The maximum specimen width is 2 in., and
4. the maximum test area i.e. the size of the counter window is 1 in. in diameter.

Electronics

The electronic equipment necessary to process the information from a single particle detector, such as the G-M flow counter, is shown in block diagram Fig. 4. The detector may be of any type which is capable of pulse-type operation. The output of the detector appears as a pulse of current at the input of the pre-amplifier. The pre-amplifier produces some gain of the signal (up to 100 times) and it transforms the voltage which is developed across the small capacity at the input of the pre-amplifier into an approximately equal voltage across the high capacity of an output cable. The over-all gain of the system, pre-amplifier and linear amplifier combined, depends on the size of the detector output pulses but gains as low as 10 are possible for G-M tubes. An oscilloscope may be used to observe the size and shape of the pulses.

The discriminator passes only those pulses with a height (voltage) exceeding a certain minimum. The action of the discriminator makes it possible to reject smaller (noise) pulses while counting the larger pulses. The output pulses from the discriminator are of a standard height and usually of a constant width. These pulses go into a scaler which can divide the rate of occurrence of the pulses down to one which can be followed by a register. The value of this register may be printed out for analysis. These measurements can be converted to an average counting rate by dividing the total counts by the time of counting. Alternatively the counting rate may be directly obtained by an electronic determination of the rate of arrival of the pulses. Such a system, called a counting-rate meter, permits a continuous output through a chart recorder.

Two separate electronic systems were employed for the project considered. The first consisted of:

1. High Voltage D.C. Power Supply model 408A by John Fluke Mfg. Co.,
2. Linear Amplifier model 348 by Franklin Electronics Inc.,
3. Log-Linear Count Rate Meter model N-731 by Hamner Electronics Co., and
4. Honeywell Electronik 15 Chart Recorder by Honeywell Controls Ltd.

The second system was a Philips circuit panel combination model PW 1370/00 which included:

1. a HV supply-amplifier/analyser - ratemeter model PW 4620,
2. counter-timer-printercontrol model PW 4630,
3. a flat bed recorder model PM 8003, and
4. a Victor printer model PW 4202/03.

Testing Procedure

Specimen Preparation

It has been known for some time that, with simultaneous plastic deformation and illumination, aluminum shows a pronounced OSEE effect. Most previous work, however, has been carried out using relatively pure aluminum. In this project, two batches of a polycrystalline commercial aluminum alloy were obtained in the form of 1/8 in. x 1 in. strip. These two batches were stated to be of the 60XX series but a chemical analysis carried out by atomic absorption methods (using Pye Unicam SP 1950 Atomic Absorption Spectrophotometer) yielded the results given in Table 1. Both batches meet composition specifications for alloy 6063 [62].

The specimens were machined from the appropriate strip in the hardened (as received) condition, allowing for easier and more efficient machining. The constraints of the G-M counter and the testing system resulted in the use of three different specimen configurations as described in Fig. 5. Plates 1, 2, and 3 show the various specimen configurations and their appropriate specimen holders, revealing both sides and the specimen test area. Configuration III, an alternate configuration for the MTS Testing System, was not used in this project.

The tested specimens were numbered consecutively in each batch, therefore, B12 is the twelfth 'run' of the second batch. The specimen preparation techniques were as listed below:

1. Specimens A1 to A29 are the as-received alloy, hand polished to 400 grit and aged two days at room temperature or left unpolished. These were used for the preliminary runs to become familiar with the apparatus and the OSEE effect, and to standardize detector conditions, and calibrate. All 29 specimens were configuration I.
2. Specimens A30 to A37 were heat treated, polished by a buffing wheel and then aged two days at room temperature. Buffing improved the finish of the specimen test area. These specimens were configuration I while specimens A38 onwards were Configuration II.

3. Specimens A38 to A45 were heat treated, polished by a buffing wheel and aged two days at -17°C. Holding at -17°C, eliminated the possibility of age hardening during the holding period.
4. Specimens B1 to B17 were first buffed, then heat treated and tested immediately (within 1/2 day). Any holding of the specimens was done at -17°C.
5. Specimen B18 was first buffed, heat treated as B17, buffed again, then briefly heat treated to remove effects of buffing and then tested immediately.

The various heat treatments carried out on the specimens are given in Table 2. The reasons for these specific heat-treatment and surface preparation conditions will be discussed later. According to the standard convention [63] T4 means solution heat treated and T6 means solution heat treated and artificially aged.

Tensile Tests

Tensile tests were carried out using an Instron model TTD Universal Testing Machine, which was calibrated as follows. Firstly, the Instron cross-head rate and chart speed were found to be accurate to within 1%. Secondly, the plastic strain rate on a dummy specimen was measured and determined to be within 5% of the Instron cross-head rate. This was done by producing strain (obtained from a strain gauge) versus time curves.

Tensile testing produced controlled plastic deformation of the specimens and thus OSEE. Before each test the specimen was lightly wiped with a Kimwipe paper tissue to remove any moisture from the test area. Alcohol was not used to remove moisture due to the possibility of surface film formation. The specimen was sealed within the suspended counter and a high gas flow rate was used to flush out the counter tube for 1/2 an hour. Thereafter the gas flow rate was maintained at about one bubble per second.

The protruding specimen ends were clamped in the Instron grips prior to straining as shown in plate 4. The counter was thereby rigidly fixed within the testing frame so that the specimen test area could be illuminated through the quartz port by a variable incandescent light source. The voltage and current were applied to the light source from a stabilized d.c. power supply to prevent light intensity variations. The light intensity was constant within a group of specimen tests but varied between groups and was designated as either high or low intensity. No effort was made to register light intensities or frequencies. Plate 5 shows the light source illuminating the specimen test area.

A low impedance d.c. source was required to apply the external accelerating voltage to the internal grid, therefore, standard batteries of 67½ V and 135 V were used. The grid voltage determines the counter characteristics as will be shown in 'Detection System Performance'. A radioactive pitchblende source was used as a standard with which the counter anode voltage could be set within the G-M operating region and the detection system calibrated for proper operation. The background count rate was then monitored for 15 minutes to ensure stability.

The rate of deformation (strain) of the specimen was controlled by selecting an Instron cross-head rate of either .01 or .02 in./min.. With the first set of electronics, a load versus time chart recording was synchronized with an emission count rate versus time chart recording. The second (Philips) set of electronics also allowed, in addition, the printing out of a 10 second emission count every 20 seconds.

The tension tests were carried out until fracture of the specimen. In some cases, the decay of the OSEE after fracture was also recorded for as long as 50 hours. Table 3 contains a summary of the experimental conditions pertaining to all the tensile tests conducted during this research. Both electronic systems were calibrated by pulse generators, resulting in correction curves for record count rates. The raw data was then

1. corrected for recorded count rate errors,
2. corrected for counts lost by the G-M counter (see Detection System Performance) and
3. plotted as in emission rate versus plastic strain.

Slip Mode Determination

Regular configuration II specimens were heat treated to T4, T6 and T6(450) conditions. These specimens were then polished to a 1 micron diamond finish holding at -17°C between polishing stages. A good metallurgical finish is necessary to optically image slip bands. These polished specimens were each strained in tension to 16% plastic strain corresponding to slightly less than the ultimate tensile strain of the least ductile specimen (T6). Micrographs were then taken of the surface slip structure at 250 X using a Zeiss Ultraphot III Metallograph using Nomarski Interference Contrast.

Fatigue Tests

Fatigue tests, of a qualitative nature only, were carried out on T4 specimens using the Instron system. Low frequency, short life fatigue tests were performed due to testing system and time limitations. To obtain a sensitive OSEE response from the specimen test area very high illumination intensities were used. Also at this time, an air heater/blower was used to thermally stimulate the specimens at some percentage of their fatigue life. The heater produced 250°C at the blower tip but the test area was likely at 100° to 150°C. TSEE/OSEE time curves were obtained.

IV. RESULTS AND DISCUSSION

Detection System Performance

In order to adequately operate the detection system it was first necessary to determine the performance characteristics of the G-M flow counter. There were two important considerations, the G-M region for the counter anode voltage and the resolving power of the counter. A change in the external accelerating grid voltage effectively shifted the G-M plateau of the counter. Plateaus for the two grid voltages used, 67½ V and 135 V, are shown in Fig. 6. The anode voltages employed in the tests were chosen to be 30 volts over the threshold voltage of the G-M plateau.

The response rate of the G-M flow counter was limited by the deionization time of the tube. The dead time of a detector, τ, is the minimum time interval between two countable pulses. The loss in counting rate due to the dead time was estimated in the following manner from conventional counting statistics. A G-M tube cannot detect an electron unless its arrival is preceded by an interval τ during which no particle passes through the G-M tube. We assume that electrons pass into the G-M tube at an average count rate N_o counts per second.

The probability of having an interval τ during which no electron arrives is

$$W_o = \exp(-N_o\tau) \ . \qquad (1)$$

The probability of one or more electron passing into the G-M tube in this interval τ is

$$W_1 = 1 - \exp(-N_o\tau) \ . \qquad (2)$$

The number of electrons not counted is

$$N_o - N_c = N_o[1 - \exp(-N_o\tau)] \ , \qquad (3)$$

where N_c is the observed count rate. Thus

$$N_c = N_o \exp(-N_o\tau) \ . \qquad (4)$$

The exponential term is expanded so that

$$N_c = N_o/[1 + N_o\tau + \frac{(N_o\tau)^2}{2} + \cdots] \ , \qquad (5)$$

and if the count rate is small, i.e. $N_o\tau<<1$,

$$N_c = N_o/[1 + N_o\tau] \ . \qquad (6)$$

Looking at it another way, for a given N_c the time fraction during which the counter is insensitive is $N_o\tau$. If N_o is the rate of arrival of electrons then $N_oN_c\tau$ electrons will pass uncounted. Therefore,

$$N_o = N_c + N_oN_c\tau \ , \qquad (7)$$

or

$$N_c = N_o/[1 + N_o\tau] \ . \tag{8}$$

which corresponds to equation (6).

The dead time for G-M counters with sensitive amplifiers is approximately 10^{-4} sec. [61]. The τ varies with count rate, sensitivity of amplifier, dimensions and form of G-M counter. The particular G-M flow counter and the electronics used in this study were very sensitive so that τ was taken as 10^{-4} sec.; this assumption was supported by subsequent counter performance characteristics. To satisfy the condition $N_o\tau \ll 1$, only count rates below $N_o < 10^3$ counts/sec., or $N_o\tau < 0.1$ were employed. The count rate of 10^3 counts/sec. was arbitrarily denoted as 'counter saturation' since above this the dead time becomes very long and thus significantly affects the G-M counter performance.

All emission rate data was adjusted by

$$N_o = N_c/[1 - N_c\tau] \ , \tag{9}$$

but the results were considered valid only to the 'counter saturation'. The deviations at saturation of the counter rate may be seen in Fig.'s 14 to 20 and 23 to 30.

Other factors affecting system performance included discrimination of the counter signals and the time constant used in obtaining the count rate. Since the pulses from a G-M counter are all equal in height (voltage), the discrimination of the signal may be set quite high. High time constants of 4 sec. were used to minimize statistical fluctuations in the count rate.

Emission During Tensile Tests

The OSEE rates during tensile straining of specimens A30 to B18 are given in Fig.'s 7 to 30. These graphs show how the natural logarithm of OSEE rate, ℓn I, increases with the engineering plastic strain, e, and will be referred to as the 'OSEE growth'. The OSEE growth can be quantitatively considered only up to the ultimate tensile strength (UTS) of the specimen. This is because the OSEE is known to be strain rate dependent [39], and after the UTS, necking causes localized plastic strain and therefore a much higher strain rate.

It can be seen that the form of all the OSEE growth curves can be approximated as

$$\ell n\, I = K(e-e_o) + \ell n\, A \,, \tag{10}$$

or

$$I = A \exp[K(e-e_o)] \,. \tag{11}$$

where K and A are constants and e_o is the engineering plastic strain at initial emission. This form is quite different from the previous forms reported [64] [41],

$$I = A(\varepsilon-\varepsilon_o)^n , \tag{12}$$

where A is a constant, n is 2 or 3, ε is strain (variously defined) and ε_o is the strain at initial emission. Equation (12) has been explained such that n is controlled by the type of defect operating, being taken as 3 if dislocation motion and vacancy formation are simultaneously occurring [64]. The same argument cannot be used to explain the equation (11) determined in the present case.

For the purposes of comparing the behavior of different specimens, various OSEE parameters, as measured from the growth curves, are given in Table 4. These include: the average background count rate, A; the slope of the growth curve (the growth constant) before UTS, K; the plastic strain at initial emission, e_o; the growth constant after UTS, M; and the plastic strain at UTS. As the oxide thickness of the specimens was not rigidly controlled, the e_o varied greatly among the tests and thus could not be used for comparison purposes. The growth constants, K and M, however, should not be dependent on the initial oxide thickness but rather on the OSEE mechanism as influenced by the intensity and frequency of illumination and by the strain rate. The growth constants, K and M, were determined by a least squares method below and above the UTS, respectively. All data points used were below the counter saturation (10^3 cps). In addition, the M values were calculated using only the first few points following UTS since strain rate changes rapidly as fracture is approached.

Specimen groups 1 and 3 (Table 4) (lower intensity illumination) have lower K values than groups 2 and 4 (higher intensity illumination). This is expected on the basis of previous work and is due to a shift to longer threshold wavelengths of the photo-electric effect.

In general, when M values were calculated, they were distinctly different from K values. Normally, the M value for a specimen was considerably larger than the K value but, on occasion, a test would reveal a much lower M value. This erratic behavior can be attributed, in part, to the testing arrangement. The window in the specimen holder must illuminate a constant test region since the OSEE is proportional to the size of the test area. However, after UTS the region of maximum strain rate is localized and may even fall partially outside the illuminated area. The increase in strain rate at UTS is likely responsible for other differences between K and M.

In addition to the change in slope, there is in many cases a drop in emission in the vicinity of the UTS (see e.g. Fig. 14). This is likely due to the transition to a small region of localized deformation (and therefore OSEE) as necking begins. For these reasons only the K values will be considered in the remainder of this discussion.

The main thrust of this project is the correlation of OSEE growth behavior with the various heat treatments (and resulting microstructures) of the 6063 aluminum alloy. The comparisons are made within a group of tests where all conditions (strain rate, light intensity, counter conditions) were held constant. Fig. 31 compares the growth curves, as given by equation (11), of group 1 specimens. In this and the subsequent three figures, it must be noted that the positions of the curves depend on the background level and the thickness of the oxide (through e_o) and only the slopes (K) are significantly grouped. The K values of the curves fall into two regions:

1. T4, and
2. T6(450) and T6(450Q) with the higher values.

The one exception is A41 which is T4 but falls within the T6(450) and T6(450Q) curves. This specimen, however, had an ageing time of 1½ weeks at room temperature which was much longer than the other T4 specimens. This anomalous result is explained below. Fig. 32 shows the growth curves of group 2 specimens and the K values fall into three regions:

1. T4
2. T6(450) and T6(450Q) at higher values, and
3. T6 at the highest values.

Fig. 33 shows that group 3 specimens behave as do group 1; Fig. 34 shows that group 4 behaves like group 2.

These consistent results clearly show that different heat treatments, and thus microstructures of the same aluminum alloy, produce different OSEE growth rates upon plastic deformation. Specifically T4 gave lowest K values, T6 highest and T6 450 and 450Q intermediate values. Some insight into these results may be obtained by considering the differences in slip mode caused by the various microstructures.

Slip Mode Correlation

1. The T4 treatment (solution heat treated) causes the formation of very few precipitates and, since solute atoms are retained in solution, the Stacking Fault Energy (SFE) is low. There are thus few precipitate obstacles to dislocation motion and a planar slip mode occurs upon plastic deformation. Plate 6 shows a typical T4 specimen with distinct, massive planar slip. This correlates with the lowest observed K values.

2. The T6 treatment forms a great many small, finely dispersed precipitates which act as effective obstacles to dislocation motion. This causes indistinct, very fine, wavy slip (plate 7) and a corresponding high K value.
3. The T6(450) and T6(450Q) treatments form a few very large precipitates which offer obstacles to dislocation motion but leave clear paths between the particles for dislocations to move. The slip mode (plate 8) is wavy but not as wavy as T6. Correspondingly, the K values are intermediate between those for T4 and T6.

This explains the anomalous A41 specimen with its increased natural (room temperature) ageing, as mentioned above. This ageing produces precipitate obstacles to dislocations, which increases the K value.

The over-ageing temperature of 450°C was chosen to reveal the effect of quenched-in defects on the OSEE. Quenching from above 450°C causes no subsequent EEE in aluminum [36] [37] but the aluminum should have many quenched-in point defects. If EEE is dependent on point defect movement, then the K values obtained should be different for quenched T6(450Q) and air cooled (T6(450) specimens. The observed K values for T6(450) and T6(450Q), however, were very similar. This then indicates that point defects are not important in producing EEE, however, no firm conclusion can be drawn without further work.

The excellent correlation of slip structure with K values shows that the type of slip band formation is definitely related to the OSEE during plastic deformation of the specimen. It is suggested that the OSEE rise is governed by dislocations intersecting the surface, in slip bands, that is, slip bands creatin[illegible]ed sites from which electrons are emitted. Speci[illegible] the results can be interpreted as a correlation of [illegible] rate with the density of dislocation lines intersecting the aluminum surface. For example, fine, wavy slip (many dislocation lines intersecting the surface) produces the highest K values while, on the other hand, coarse, planar slip (few dislocation lines intersecting the surface) produces the lowest K values. It should also be noted that the OSEE rate does *not* correlate with the yield strength or UTS of the specimens, since the T6 overaged heat treatments had the lowest strength while the T6 had the highest.

Since consideration of the OSEE decay behavior is germane to the explanation of these effects, further discussion will be deferred until the decay has been considered.

Decay After Tensile Tests

After termination of straining, the OSEE was observed to decay as a function of time. It is suggested that this is related to the oxide layer which forms on the clean surface exposed by slip or fracture. It is instructive to consider Craciun's [34] mathematical representation of the decay which is based on the idea that electrons 'tunnel' through the oxide-metal interface and are trapped within the oxide, to be emitted later when stimulated by light. The decay is due to the traps being emptied, with the assistance of optical stimulation, faster than they are refilled with electrons from the metal. This is believed to be the case after the cessation of plastic deformation.

Let n_o be the number of electron traps of a given type per unit volume in the oxide where n of them are occupied by electrons at time t.

If v_1 and V_2 are the rates of filling and emptying (emission) of the electron traps, respectively, then

$$v_1 = P(n_o-n) \quad , \tag{13}$$

and

$$v_2 = kn \tag{14}$$

where P is the filling factor and k is the emission factor. The rate of change in the number of occupied traps is therefore given by

$$\frac{dn}{dt} = v_1 - v_2 \, , \tag{15}$$

or,

$$\frac{dn}{dt} + (P + k)n = Pn_o \tag{16}$$

The solution to this first order differential equation is

$$n = \frac{Pn_o + C \exp[-(P + k)t]}{P + k} \, . \tag{17}$$

To determine C, the boundary condition t = 0 is applied: At $t = 0$, let $(n)_{t=0} = f\, n_o$, $0 < f < 1$, i.e. a fraction f of the traps are filled. Then

$$C = f\, n_o(P+k) - Pn_o \tag{18}$$

and, from (17)

$$n = \frac{Pn_o + (fn_o(P+k) - Pn_o)\exp[-(P+k)t]}{P + k} \, . \tag{19}$$

Let the recorded OSEE rate be

$$\frac{dN}{dt} = akn = \frac{akPn_o + ak[fn_o(P+k) - Pn_o]\exp[-(P+k)t]}{P + k} \, , \tag{20}$$

where a is a constant relating the output from the detection system to the emission rate of electrons from the traps.

at $t = 0$ and $t = \infty$, equation (20) becomes, respectively

$$\frac{dN}{dt}_{t=0} = akfn_o \tag{21}$$

and,

$$\frac{dN}{dt}_{t=\infty} = \frac{P}{P+k} n_o ak \tag{22}$$

Now since $P<<1$, equation (22) is approximately zero (emission rate falls to zero at infinite time), thus the first term in equation (20) can be neglected, leaving it in the form

$$\frac{dN}{dt} \sim A \exp(-\lambda t) \tag{23}$$

where

$$A = \frac{ak[fn_o(P+k)-Pn_o]}{P+k} \tag{24}$$

and

$$\lambda = P + k \tag{25}$$

As there are likely to be a number m of different types of electron i, and since the equation (23) applies to only one type, then for the material as a whole

$$\frac{dN}{dt}_{total} = \sum_{i=1}^{m} A_i \exp(-\lambda_i t) . \tag{26}$$

It must be noted that the above treatment ignores the progressive thickening of the oxide.

Some representative results of decay observations are given in Fig. 35 for short term (< 200 min.) decay and in Fig. 36 for long term decay (< 3000 min.). The decay curves are clearly of the form given by equation (24). This leads to the conclusion that OSEE decay is controlled by traps in the oxide in the manner proposed by Craciun [34] and described quantitatively by equation (24).

During *short term* decay, however, it is possible that electrons may be emitted directly through the oxide layer [52]. Exoelectron energies of up to 3 eV have been observed but the majority are below 1 eV [65]. The wavelength λ of an electron is related to its momentum p by the de Broglie relation.

$$\lambda = \frac{h}{p} = \frac{h}{\sqrt{2m_o E}} \tag{27}$$

where h is Planck's constant, m_o is the rest mass of the electron and E is its kinetic energy. Using the established values for h and m_o, and using ½ eV for E, λ is approximately 1.7 nm. This indicates the order of magnitude of a surface layer that an electron may pass through directly from the metal.

It is known that at room temperature, aluminum forms a coherent oxide of about 2 nm thickness in approximately 1 hour with only very slow oxide growth afterwards [66]. It is suggested, therefore, *that in the short* *term (less than about one hour) decay, the oxide is thin enough that it allows the direct emission of electrons from the aluminum.* Electrons are continuously trapped in the growing oxide but most of the OSEE comes directly from the metal. After about one hour of oxidation there is expected to be a gradual transition to a second, oxide-controlled phase, where electrons from the metal are trapped within the oxide, to be later emitted as explained by Craciun (see also Fig. 1). The *short term* decay kinetics are dominated by the oxide growth kinetics which may also be described by a series of exponentials [67]. The present work then supplies further evidence in support of the relation between the oxide and the long term emission of exoelectrons from aluminum. However, since the tensile tests lasted much less than an hour, it is the *short term* decay behavior which is germane to the OSEE growth during plastic deformation. This discussion, therefore, returns to the emission which occurred during the tensile tests.

Suggested Mechanism For OSEE During Tensile Deformation

For the tensile tests, the oxide layer is such that even the fine, wavy slip of the T6 specimens would break through the oxide. This action results in fresh metal being exposed; because of the oxide layer coarse slip exposes more fresh metal than fine slip. However, the highest K values correlate with fine slip, i.e. with the least amount of freshly exposed metal. It thus appears that a simple model based on oxidation of freshly exposed surface cannot apply in the present case.

The K values, however, do correlate with the density of dislocations intersecting the surface. The density of dislocations intersecting the surface along a slip line is expected to be roughly independent of the coarseness of the slip step, thus the greater the number of slip lines on the surface, the higher the density of intersecting dislocations. It has been suggested by others [33] [28] [49] [50] that the emission could occur from such sites. A reasonable mechanism whereby this might occur is as follows.

At the point at which dislocations emerge at the metal surface, the interatomic distances are distorted causing changes in the energy distribution of the electron states. This may result in a local change of the metal's work function and/or in chemisorption or preferential oxidation. It is suggested that one of these processes is responsible for the enhanced emissions thus explaining the correlation with slip mode.

It appears that all that [illegible] necessary for OSEE is that slip steps break through the oxide surface. This may be seen by examining the results of specimen B17 and B18. The microstructures of these specimen are essentially the same but B17 has a thick oxide while B18 has a very thin oxide. The OSEE growth behavior for the specimens is very similar, indicating slip was able to break through both surfaces.

During plastic deformation a group of slip lines develops rapidly. Slip then ceases in that particular slip band and OSEE occurs, from the emission sites associated with the dislocation ends, while further strain is accommodated by development of new groups of slip lines. With time, then, each slip line undergoes an emission decay process. The overall OSEE observed is the cumulative effect caused by an ever-increasing number of slip lines as tensile straining proceeds. This explains the OSEE as detected by the G-M counter and the correlation of slip mode with the growth constants.

It is also of interest to note that the growth curves commonly exhibited discontinuous jumps as strains proceeded. Serrations were also observed on the load elongation Instron plots, and are presumably due to discontinuous bursts of slip, causing bursts of OSEE. The sensitivity of the strain measuring equipment was insufficient to detect a one to one correspondence between slip bursts and OSEE bursts. It would be of interest to check this with more sensitive equipment.

Fatigue Tests

The exploratory fatigue tests gave interesting results, although they were of a qualitative nature only. Due to the high stress amplitude applied to the specimens, plastic deformation occurred during the first quarter cycle. This produced OSEE as in the tensile tests. The OSEE rate rose quickly to a maximum and then slowly decayed with respect to the number of cycles. On rapid fracture there was a great increase in OSEE rate. These observations are in full agreement with previous reports [49] and are fully consistent with the tensile results.

Heating the specimen after interrupting the fatigue test caused a similar rise, followed by a fall in TSEE/OSEE rate above the level of emission obtained from fatigue. The heat was then removed and the specimen was aged in the counter for 1 day. Upon reheating the specimen the TSEE/OSEE peak returned. This regeneration of the TSEE/OSEE supports the model for emission proposed by Craciun [34]. In other words, the oxide is thick enough to trap electrons from the metal and later emit them. These traps are constantly being occupied and this accounts for the regeneration in TSEE/OSEE.

The heating behavior during decay from plastic deformation indicates that the TSEE is additive to the OSEE. This is a most interesting result and could imply that different types of electron traps are involved in the two processes. Further work in this area would likely be fruitful.

V. CONCLUSIONS

The conclusions derived on observing exoelectron emission from a 6063 aluminum alloy are listed below in point form:

1. A pronounced OSEE effect can be obtained from 6063 aluminum alloy upon plastic deformation and illumination.
2. A G-M flow counter is an effective device for detecting OSEE and TSEE.
3. The OSEE is sensitive to illumination intensity and specimen strain rate.
4. An approximation to OSEE rate versus specimen plastic strain is given by

   $$I = A \exp [K(e-e_0)].$$

5. Various microstructures, which affect dislocation motion, of the same alloy yield distinctly different K values.
6. These K values correlate to the specimen slip structure, that is, the density of dislocation lines intersecting the metal surface, with higher numbers of dislocation lines (finer slip) giving higher K values.
7. To obtain OSEE, the slip steps need only to break through the oxide, since the ends of the dislocations

appear to act as localized OSEE centers.

8. It is suggested that when the oxide which forms on the freshly exposed metal is thin (approximately < 2 nm), the electrons may escape directly through the oxide.

9. OSEE decay following deformation or fracture may be described by the equation

$$I = \sum_{i=1}^{m} A_i \exp(-\lambda_i t) \ .$$

10. It is suggested that for thicker oxides which form during long term decay electrons from the metal are trapped within the oxide but may be later emitted under stimulation.

VI. FUTURE WORK

As EEE is related to the physicochemical condition of a metal surface, there are many possibilities for expanding metallurgical research using this effect. Application of EEE gives the possibility of obtaining information about defects at the surfaces of solids. Efforts can be undertaken to apply EEE to photography, detection of small quantities of substances, analysis of chemical reaction at surfaces, dosimetry, and non-destructive testing. Immediate possibilities for future work, from this research, are:

1. the further investigations of metallurgical variables (such as phase transformations, microstructures etc.) on EEE from many metals;
2. the study of specific types of deformation processes, especially fatigue, with respect to EEE;
3. the similarity and differences of OSEE versus TSEE (some evidence has been obtained in this work that these are additive);
4. the application of OSEE/TSEE to non-destructive testing, monitoring of deformation processes, especially fatigue, such as are encountered in the fabrication or service of metals, and
5. the investigation of Craciun's model under vacuum.

TABLE 1

CHEMICAL COMPOSITION OF ALLOY

ELEMENT	COMPOSITION (wt/0)	
	Batch 1	Batch 2
Mg	0.41	0.41
Si	0.25	0.29
Cu	0.013	0.013
Cr	0.013	0.013
Fe	0.143	0.139
Ni	0.009	0.008
Mn	0.047	0.048
Zn	0.009	0.009
Al	bal.	bal.

TABLE 2

HEAT TREATMENTS OF ALUMINUM ALLOY

Designation [63]	Temperature (°C)	Time at Temperature (If within)	Cooling	Purpose
T4	535	a) A30 → A45 1 hr. in air	cold water quench	solution heat treatment
		b) B1 → B16 ½ hr. in air	"	"
		c) B17 (T4L) 4 hrs. in air	"	"
		d) B18 (T4S) 4 hrs., quench, buff, and 10 min. in air	"	"
T6 (start with) T4	180	all specimens 3 hrs. in air	-	artificial age-hardening (fine dispersion of precipitates)
T6(450) (start with) T4	450	a) A30 → A45 1 hr. in air	air cool	over ageing (coarse dispersion of precipitates)
		b) B1 → B16 ½ hr. in air	"	"
T6(450Q) (start with) T4	450	a) A30 → A45 1 hr. in air	cold water quench	as T6(450) plus higher vacancy concentration
		b) B1 → B16 ½ hr. in air	"	"

TABLE 3

SUMMARY OF EXPERIMENTAL TESTS

Specimen	Specimen Configuration	Specimen Preparation	Heat Treatment	Light Intensity	Grid Voltage (volts)	Cross-heat Rate (in./min.)	Electronics System
A1-A29	I	1	as received preliminary tests				1
A30	I	2	T4	lower	135	.01	1
A31-A37	I	2	heat treated preliminary tests and experimental breakdown due to atmospheric leaks, electronic breakdown, human error etc.				
A38	II	2	T6(450)	lower	135	.01	1
A39	II	2	T6(450Q)	lower	135	.01	1
A40	II	2	T4*	lower	67½	.01	1
A41	II	2	T6(450Q)	lower	67½	.01	1
A42	II	2	experimental breakdown				
A43	II	2	T4	lower	67½	.02	1
A44	II	2	experimental breakdown				
A45	II	2	T6(450Q)	lower	67½	.02	1
B1	II	3	T4	higher	67½	.01	1
B2	II	3	T4	higher	67½	.01	1
B3	II	3	T6(450Q)	higher	67½	.01	1
B4	II	3	T6(450Q)	higher	67½	.01	1
B5	II	3	T6(450)	higher	67½	.01	1
B6	II	3	experimental breakdown				
B7	II	3	T6	higher	67½	.01	1
B8	II	3	T6	higher	67½	.01	2
B9	II	3	T6(450Q)	lower	67½	.01	2
B10	II	3	T4	lower	67½	.01	2
B11	II	3	T6(450)	lower	67½	.01	2
B12	II	3	T4	higher	67½	.01	2
B13	II	3	T4	higher	67½	.01	2
B14	II	3	T6(450Q)	higher	67½	.01	2
B15	II	3	T6(450)	higher	67½	.01	2
B16	II	3	T6	higher	67½	.01	2
B17	II	3	T4L	higher	67½	.01	2
B18	II	4	T4S	higher	67½	.01	2

* aged 1½ weeks at R.T.

TABLE 4

RESULTS OF TENSILE TESTS

Group No.	Specimen No.	Fig. No.	Heat Treatment	Average Background A(counts/sec.)	Growth Constant to UTS,K	Plastic Strain at Initial Emission $e_o(x10^{-2})$	Growth Constant After UTS,M	Plastic Strain at UTS
1	A30	7	T4	3.1	3.18	13.0	-	82.0
1	A38	8	T6(450)	6.5	[illegible]	1.2	7.37	30.1
1	A39	9	T6(450Q)	7.4	4.00	0.4	7.67	30.8
1	A40	10	T4*	4.7	4.67	4.0	4.22	29.2
1	A41	11	T6(450Q)	3.9	4.60	0.7	8.31	25.6
1	A43	12	T4	4.7	3.33	18.0	6.56	38.6
1	A45	13	T6(450Q)	4.0	5.20	0.1	10.02	30.4
2	B1	14	T4	6.4	15.10	0.1	-	34.2
2	B2	15	T4	3.5	23.87	10.2	-	34.6
2	B3	16	T6(450Q)	3.7	28.46	6.3	-	32.8
2	B4	17	T6(450Q)	4.6	31.63	5.2	-	32.8
2	B5	18	T6(450)	5.7	32.75	4.5	-	32.6
2	B7	19	T6	3.2	39.19	6.7	-	16.6
2	B8	20	T6	5.2	48.16	6.3	-	16.4
3	B9	21	T6(450Q)	15.4	13.72	19.0	8.67	31.6
3	B10	22	T4	18.3	7.56	6.6	-	33.3
3	B11	23	T6(450)	9.9	11.58	25.5	16.82	35.4
4	B12	24	T4	7.7	22.99	2.4	-	33.0
4	B13	25	T4	6.1	18.13	4.6	-	34.8
4	B14	26	T6(450Q)	5.7	30.13	5.1	-	31.4
4	B15	27	T6(450)	5.3	25.35	14.4	-	34.4
4	B16	28	T6	5.2	58.19	7.5	-	14.8
4	B17	29	T4L	6.2	17.50	5.5	-	38.8
4	B18	30	T4S	5.6	18.28	5.7	-	39.6

* aged 1½ weeks at R.T.

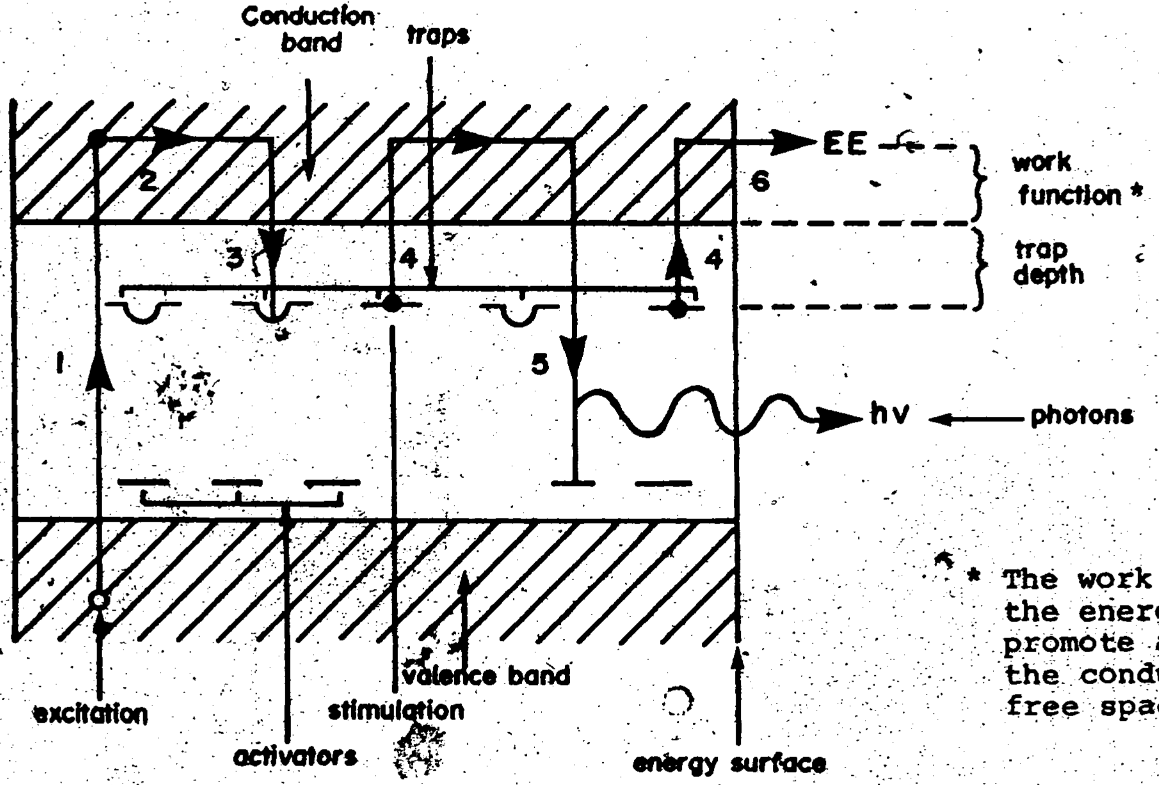
Conduction band
traps
EE
work function *
trap depth
1
2
3
4
4
5
6
hv
photons
excitation
activators
stimulation
valence band
energy surface

* The work function is the energy required to promote an electron from the conduction band to free space.

FIGURE I. SIMPLIFIED SCHEMATIC BAND MODEL FOR LUMINESCENCE AND EEE FROM SOLIDS (TAKEN FROM [7])

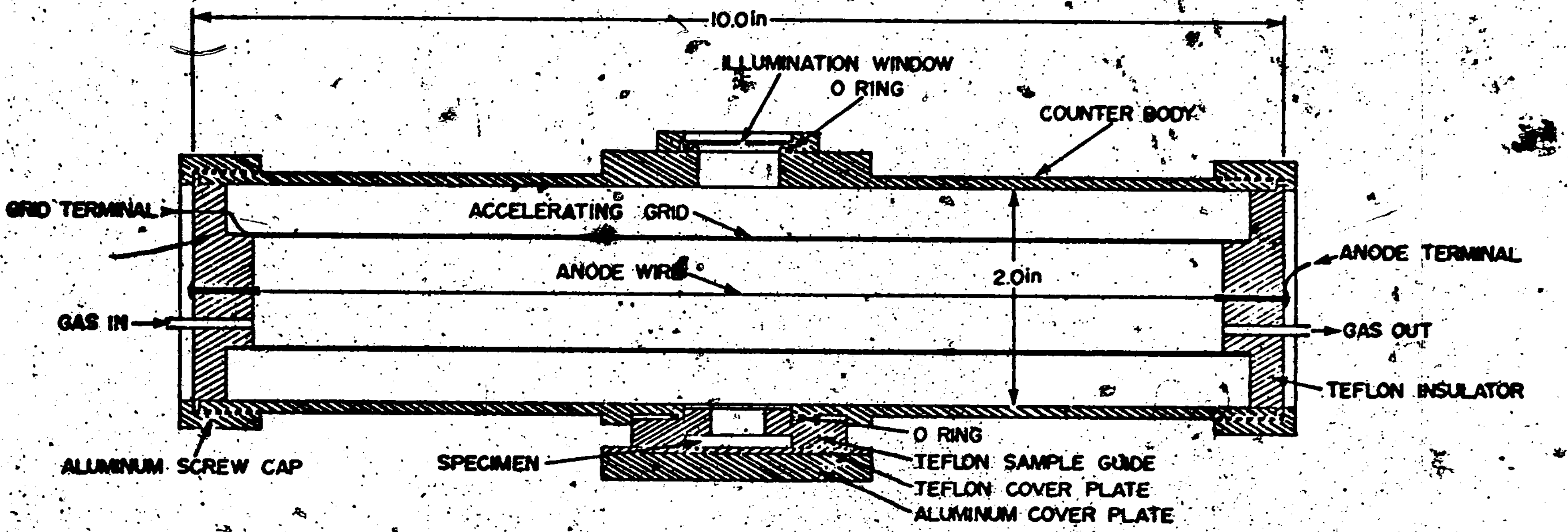
10.0in
ILLUMINATION WINDOW
O RING
COUNTER BODY
GRID TERMINAL
ACCELERATING GRID
ANODE WIRE
2.0in
ANODE TERMINAL
GAS IN
GAS OUT
TEFLON INSULATOR
O RING
ALUMINUM SCREW CAP
SPECIMEN
TEFLON SAMPLE GUIDE
TEFLON COVER PLATE
ALUMINUM COVER PLATE

FIGURE 2. GEIGER-MÜLLER FLOW COUNTER (CROSS SECTION)

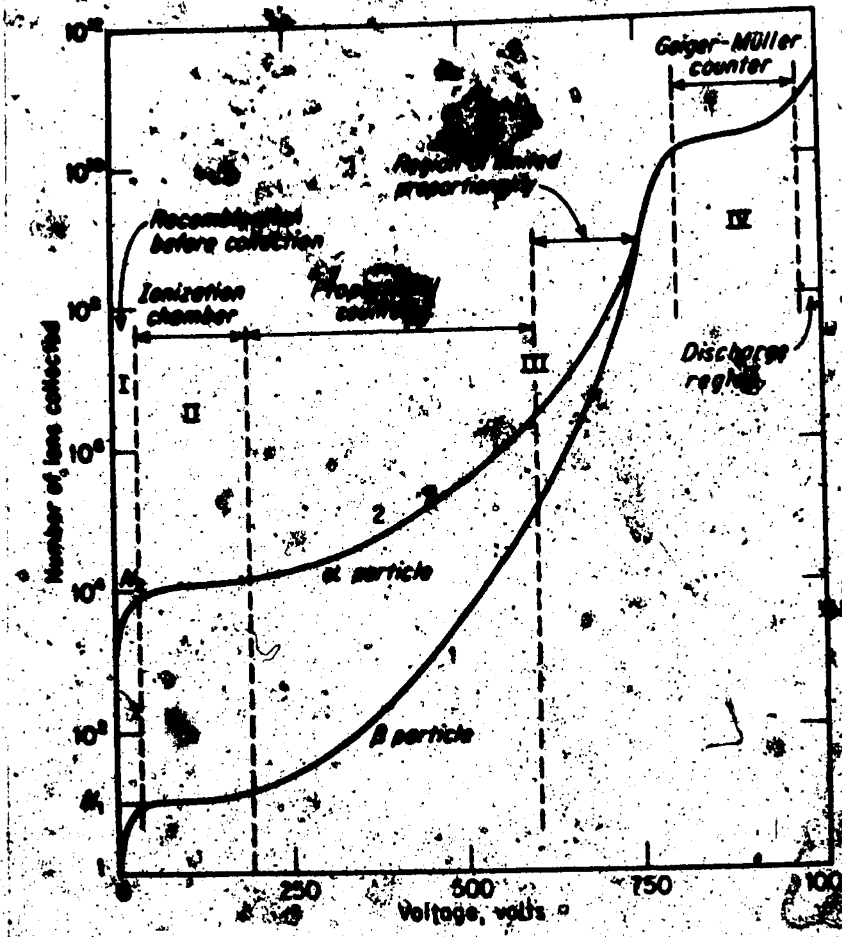

Figure 3 - Pulse-height versus applied voltage curves, illustrating ionization, proportional and Geiger-Müller regions (taken from [61]).

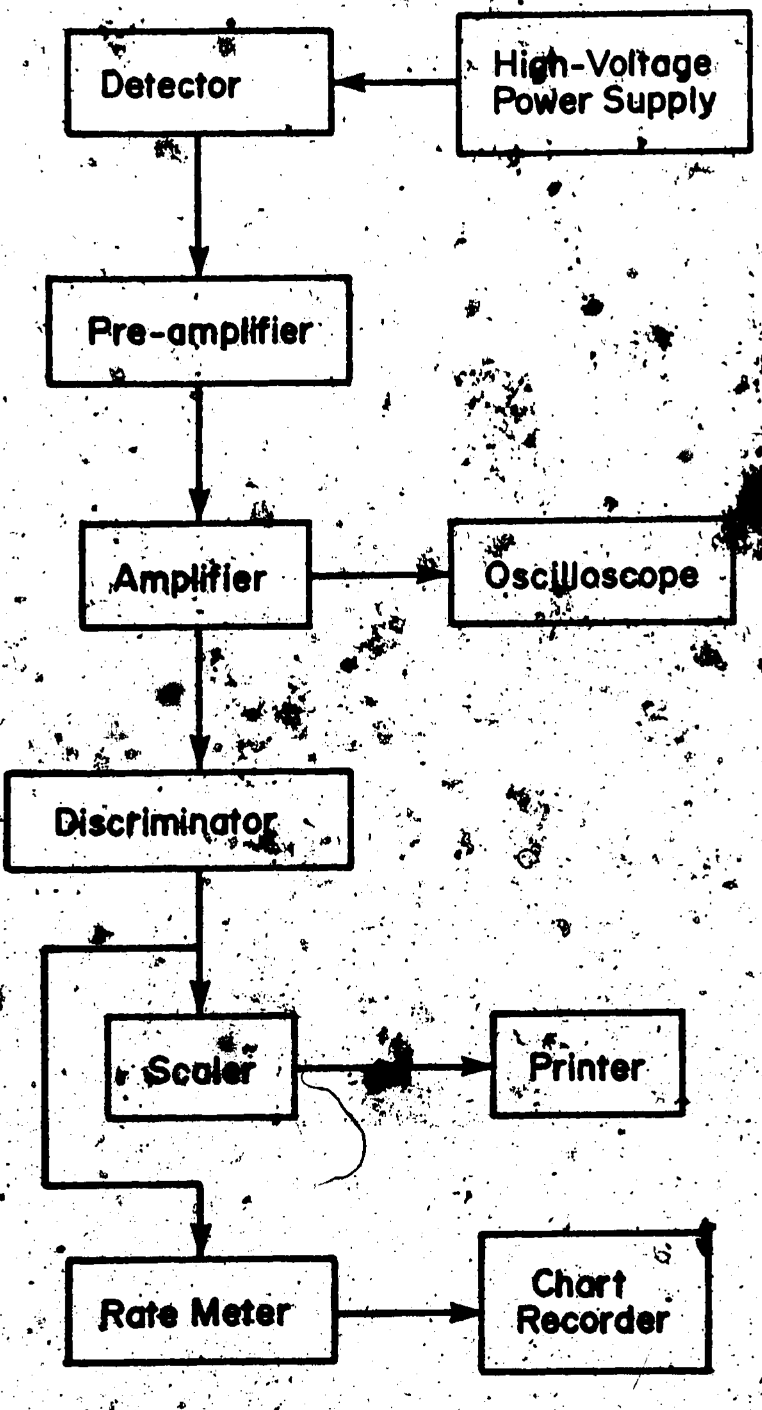
Detector
High-Voltage Power Supply
Pre-amplifier
Amplifier
Oscilloscope
Discriminator
Scaler
Printer
Rate Meter
Chart Recorder

FIGURE 4. BLOCK DIAGRAM OF A SYSTEM FOR SINGLE PARTICLE COUNTING

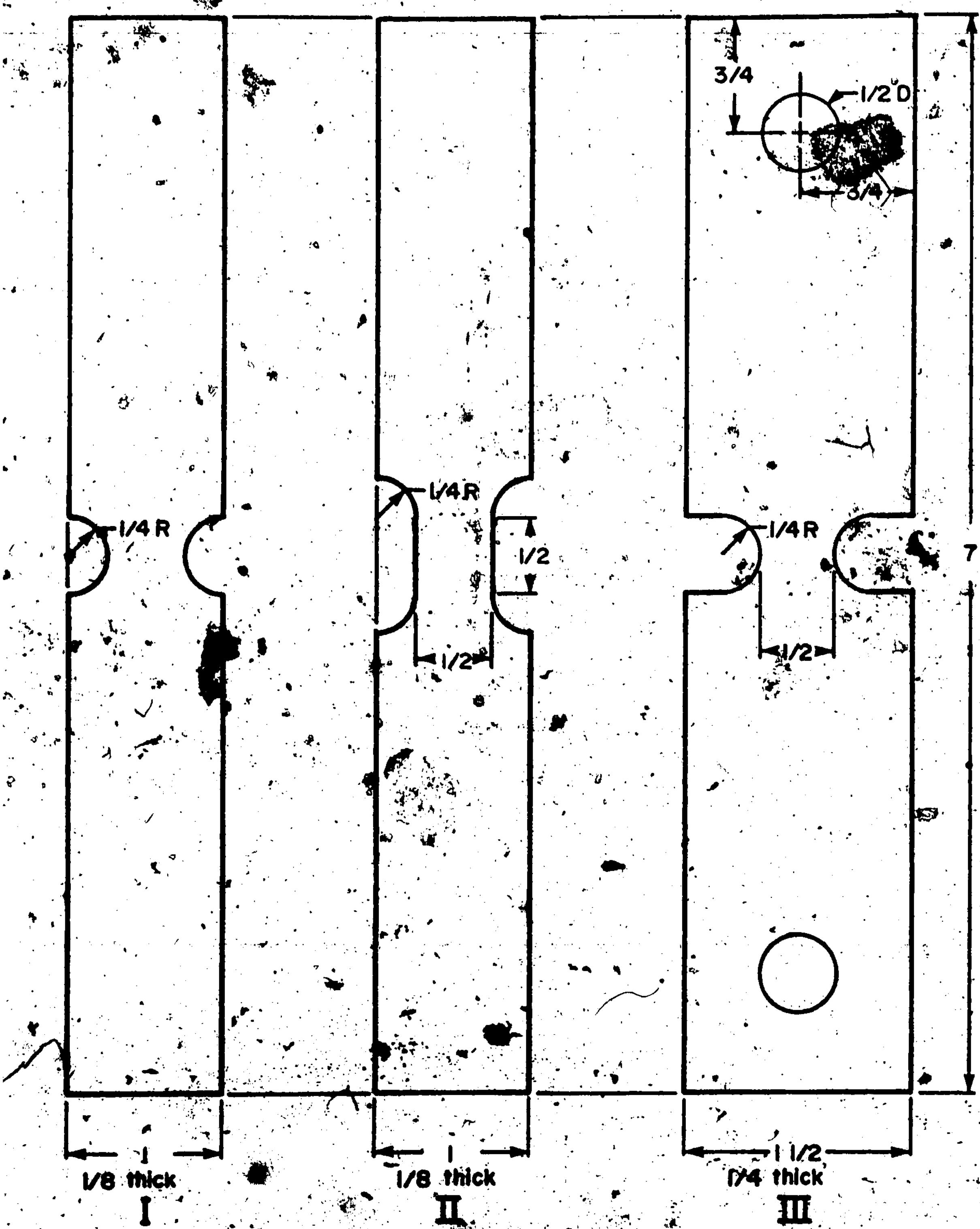
3/4
1/2 D
3/4
1/4 R
1/4 R
1/2
1/2
1/4 R
1/2
7
1
1/8 thick
I
1
1/8 thick
II
1 1/2
1/4 thick
III

NOTE: DIMENSIONS IN INCHES

FIGURE 5. SPECIMEN CONFIGURATIONS

FIGURE 6. PLATEAUS FOR G-M FLOW COUNTER

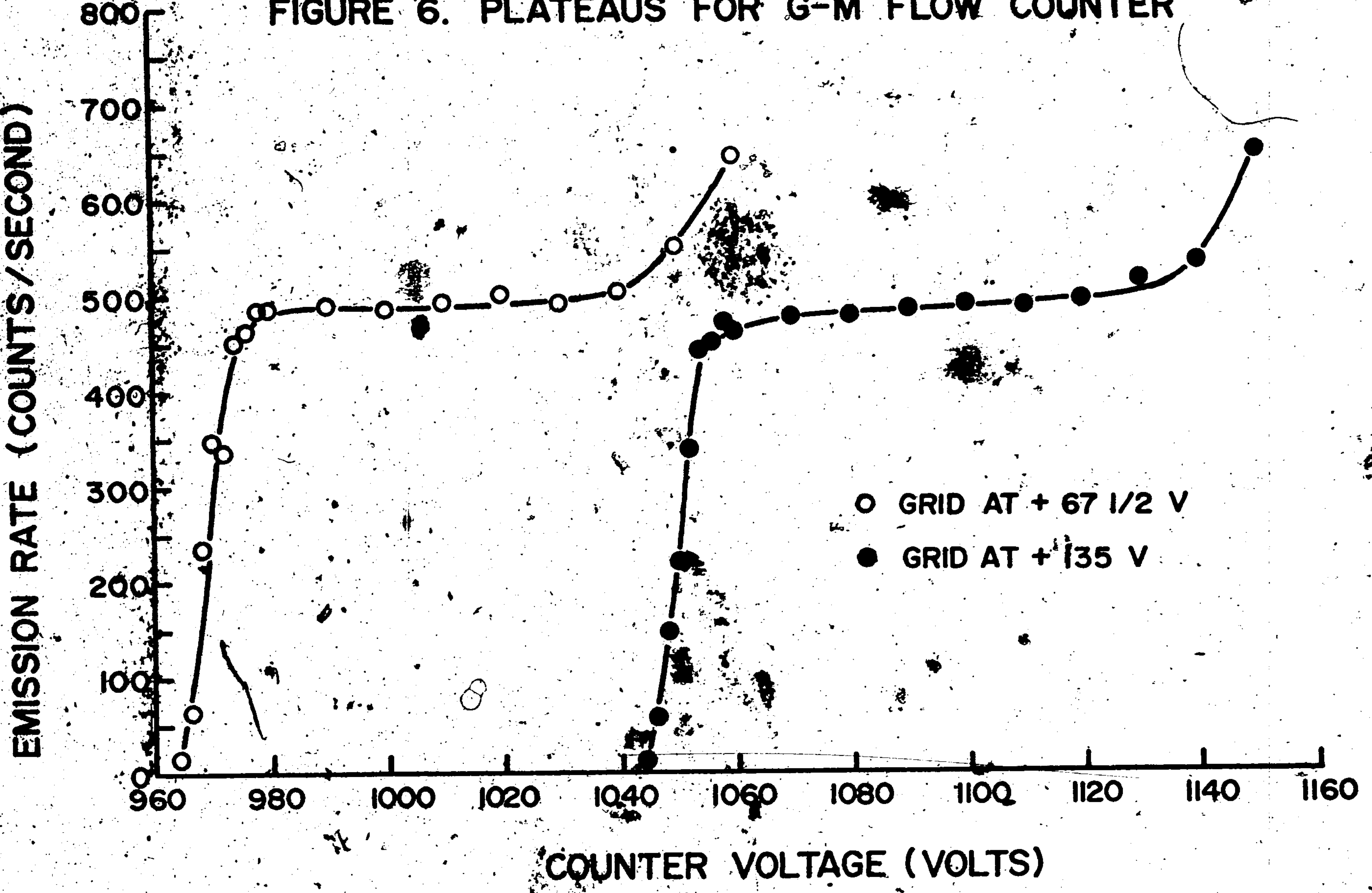

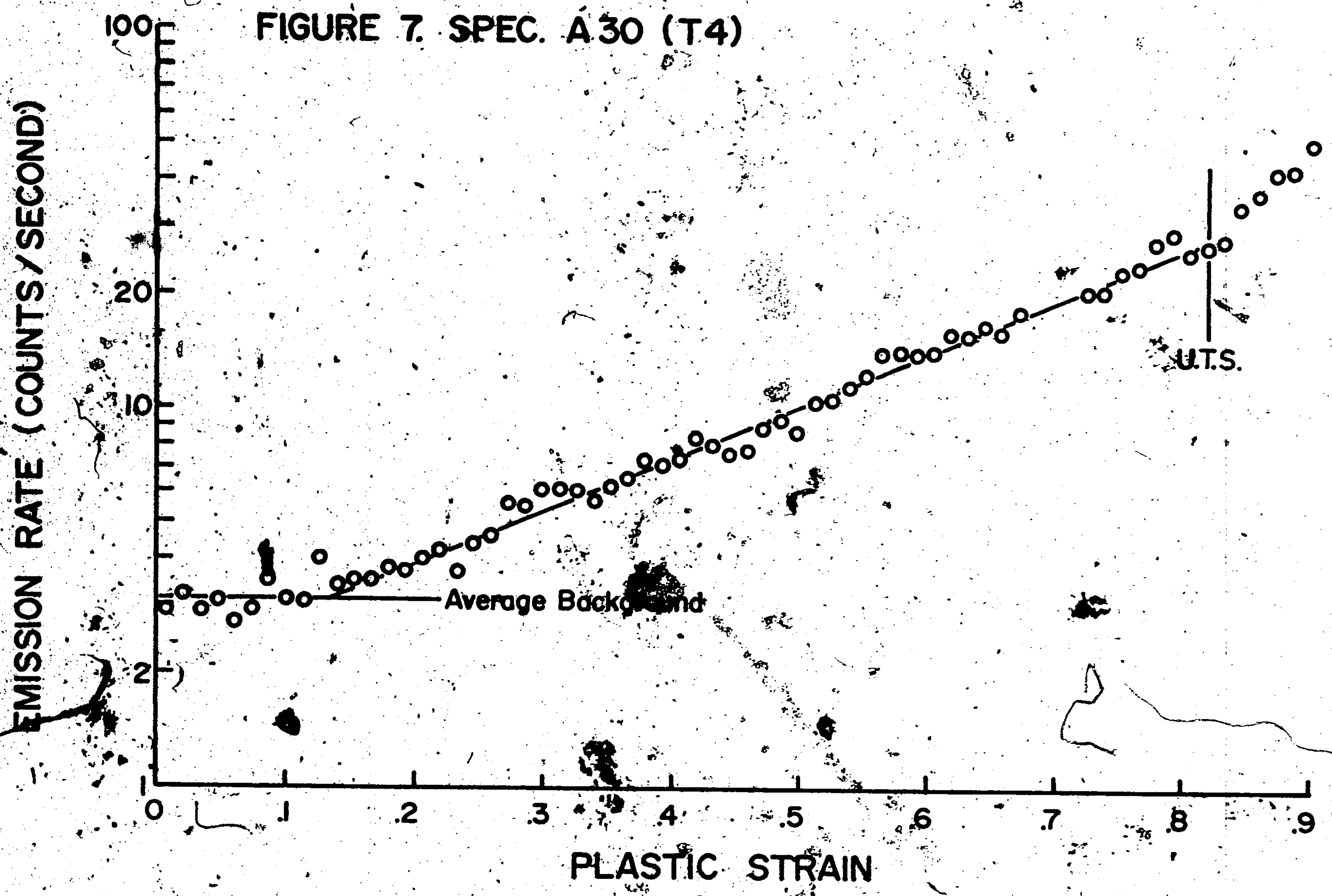

FIGURE 7. SPEC. A30 (T4)

FIGURE 8. SPEC. A38 (T6(450))

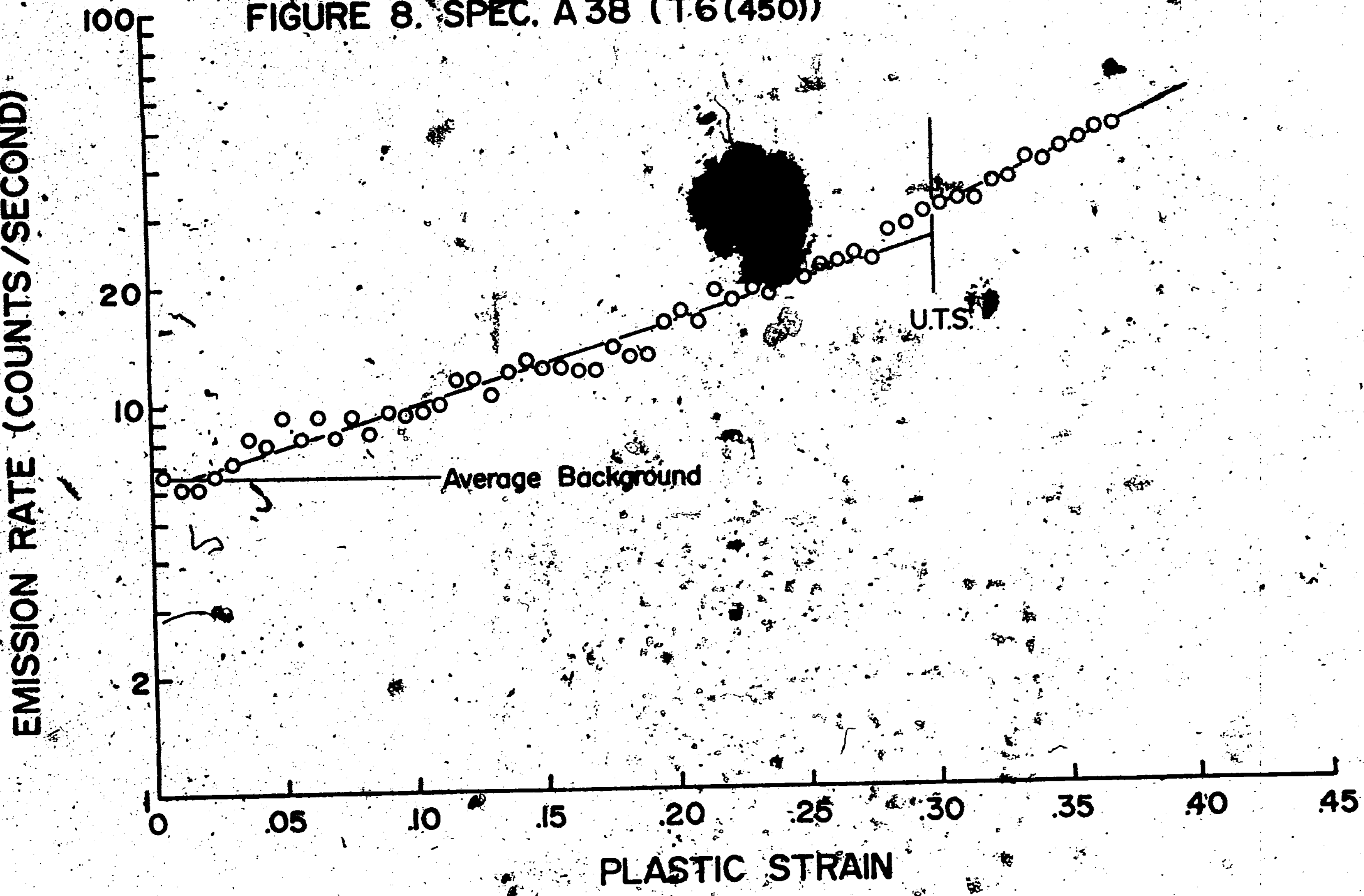

FIGURE 9. SPEC. A39 (T6(450 Q))

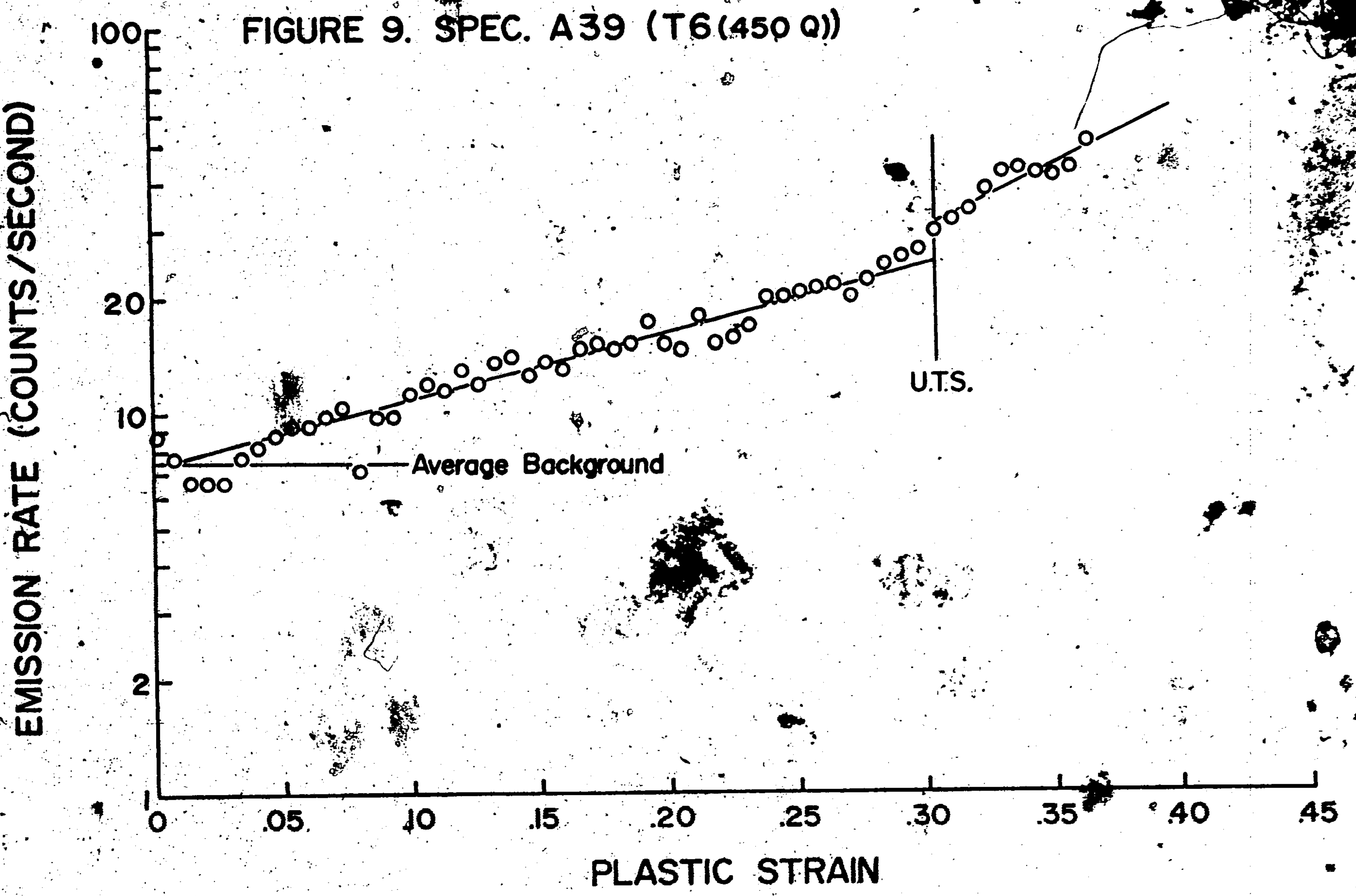

FIGURE 10. SPEC. A40 (T4)

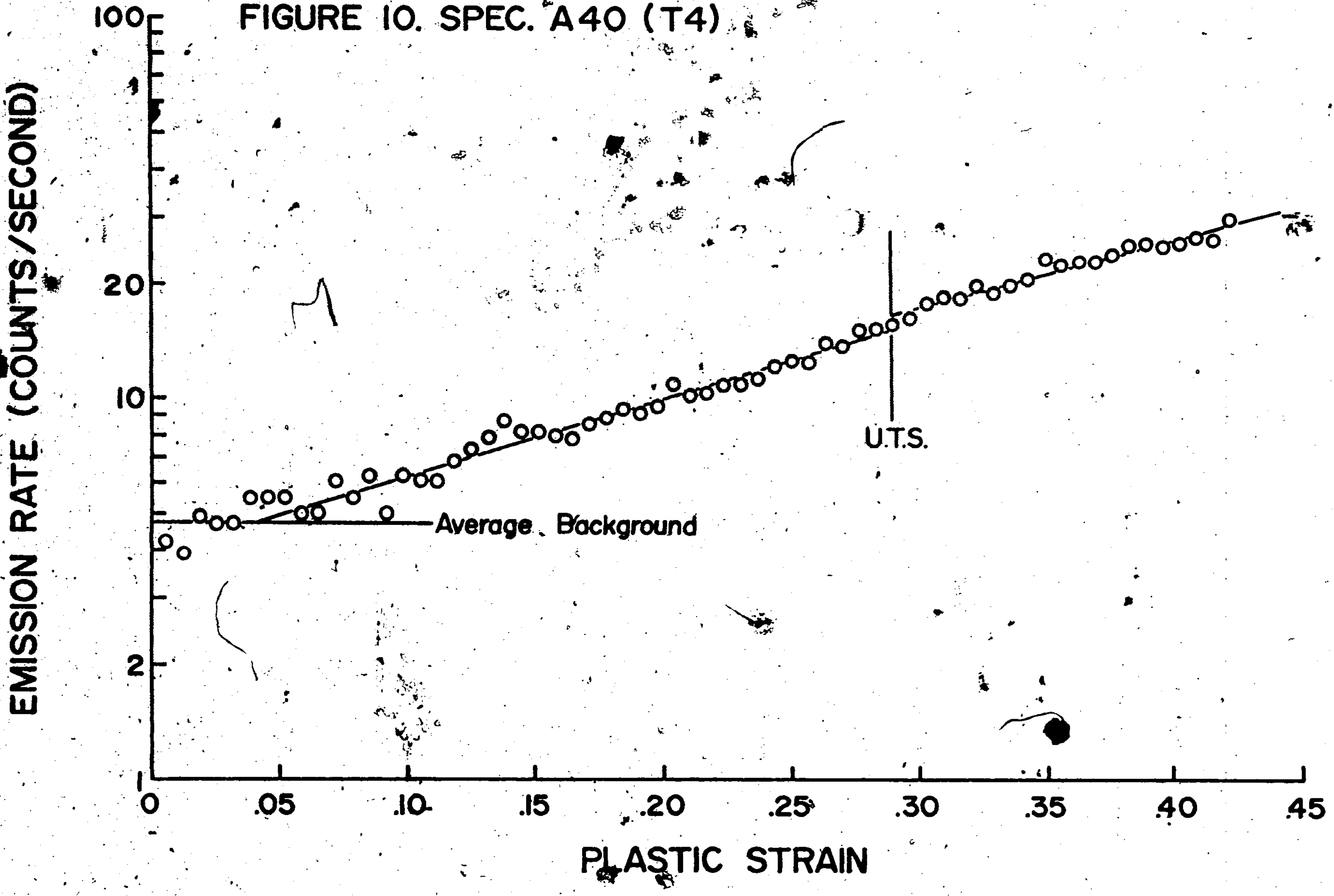

FIGURE 11. SPEC. A41 (T6(450 Q))

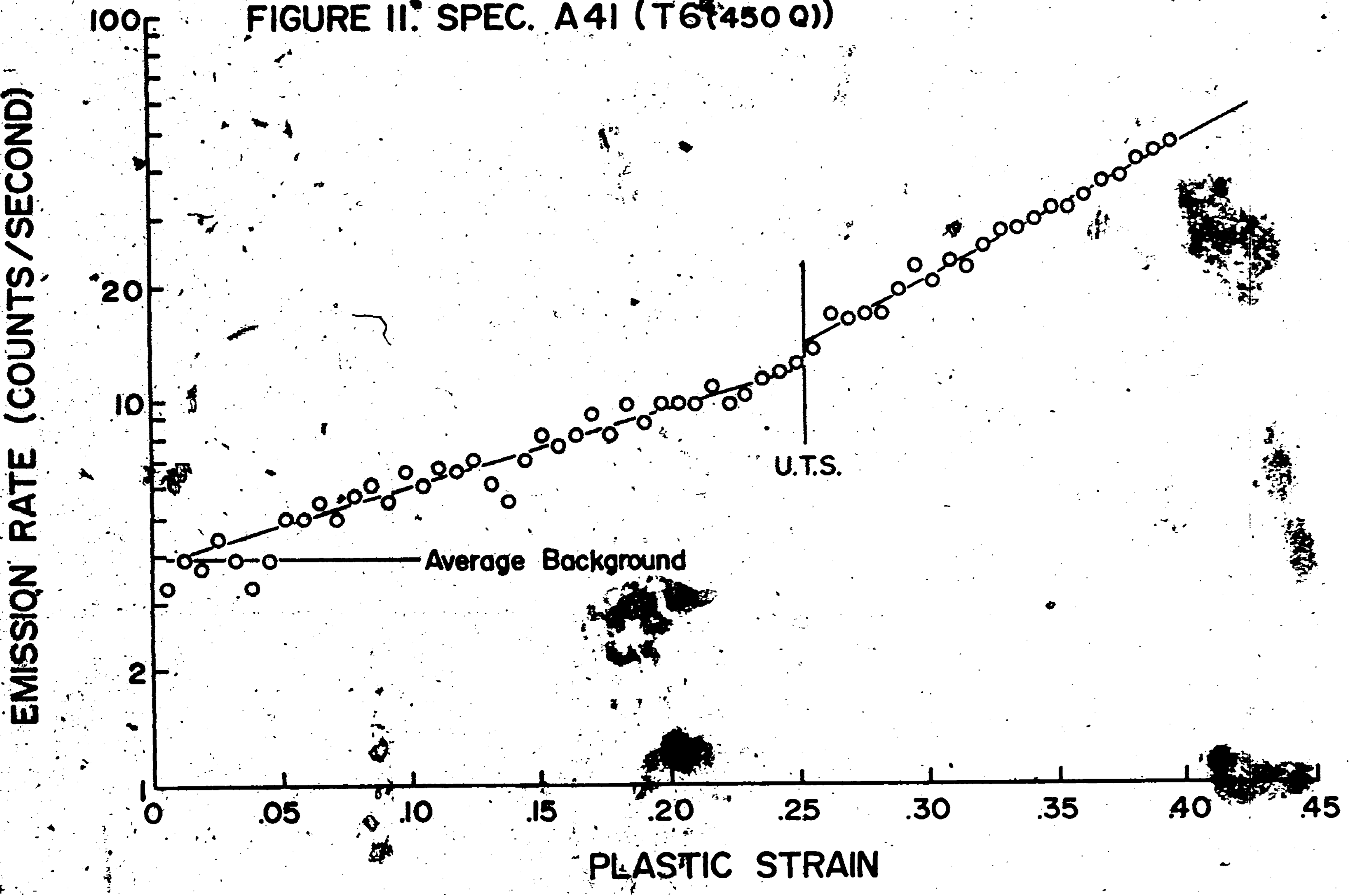

FIGURE 12. SPEC. A43 (T4)

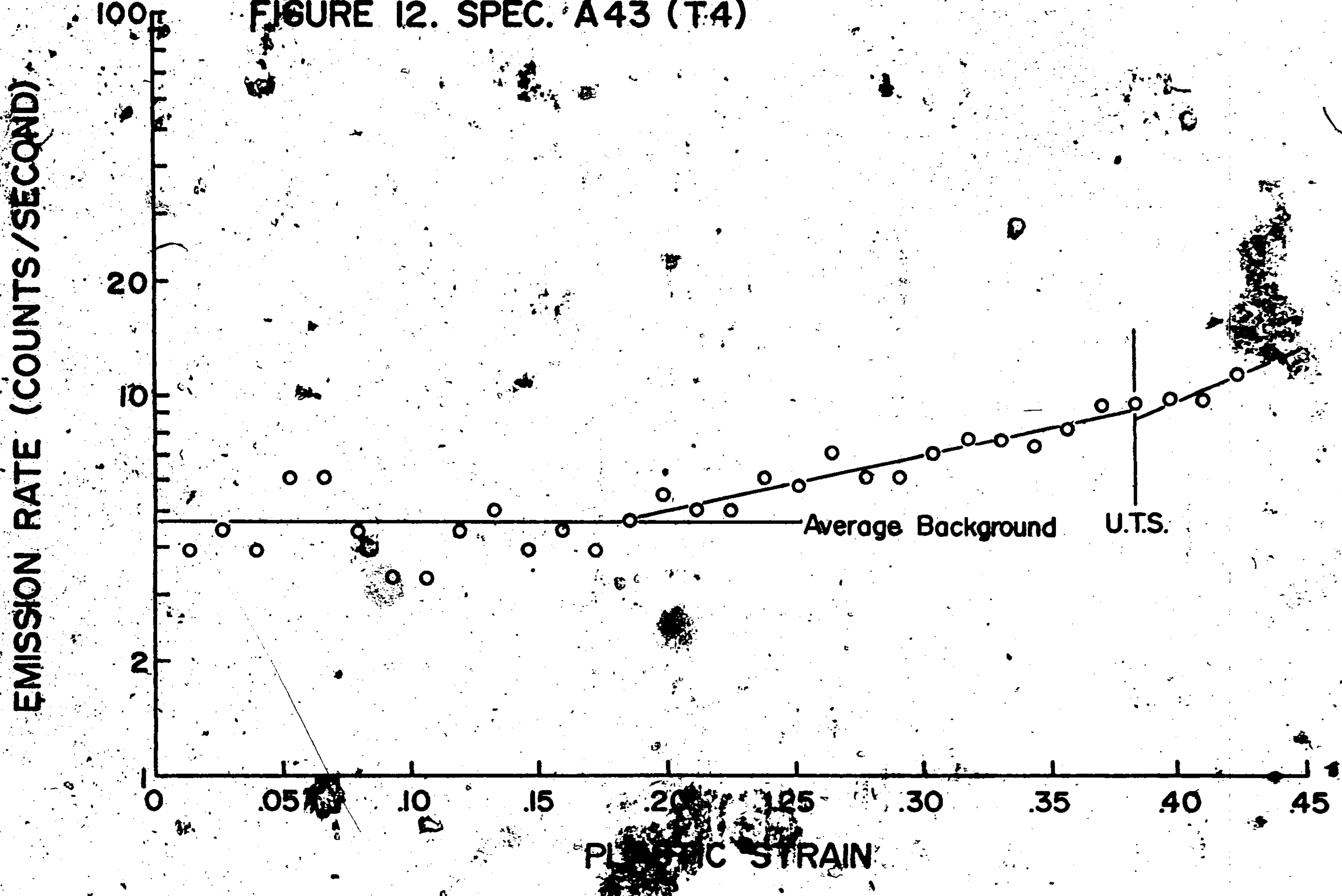

FIGURE 13. SPEC. A45 (T6(450

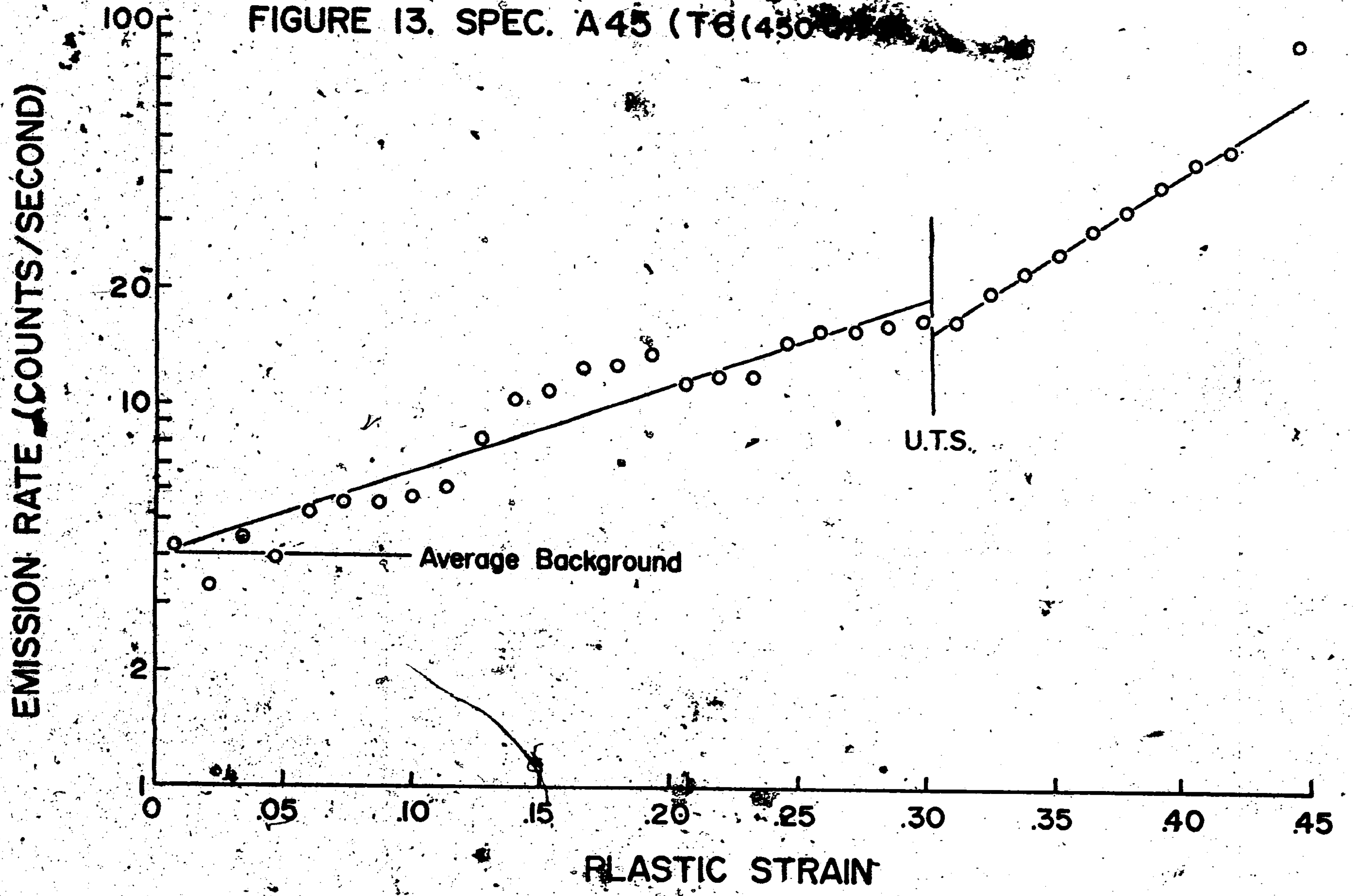

FIGURE 14. SPEC. B1 (T4)

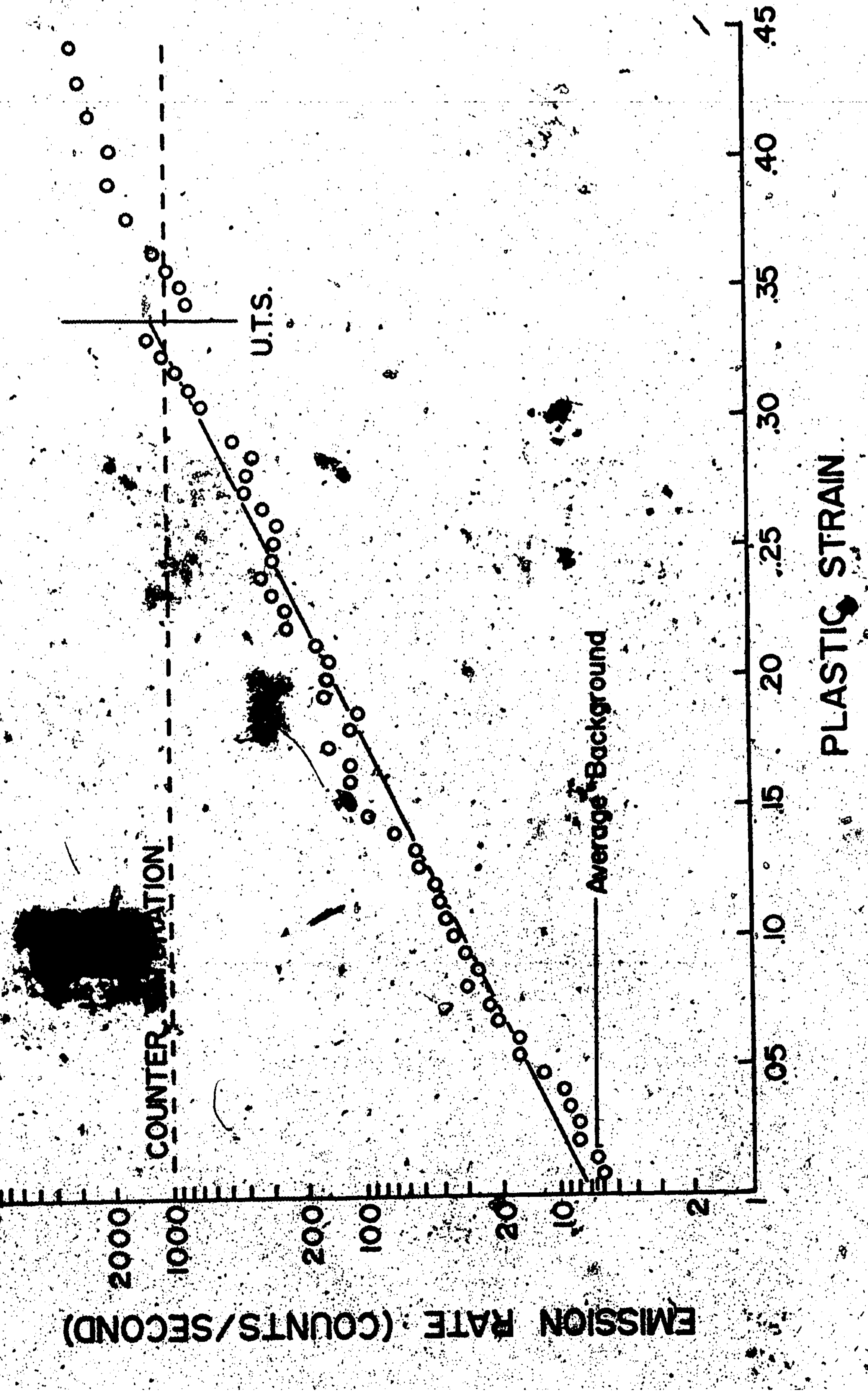

FIGURE 15. SPEC. B2 (T4)

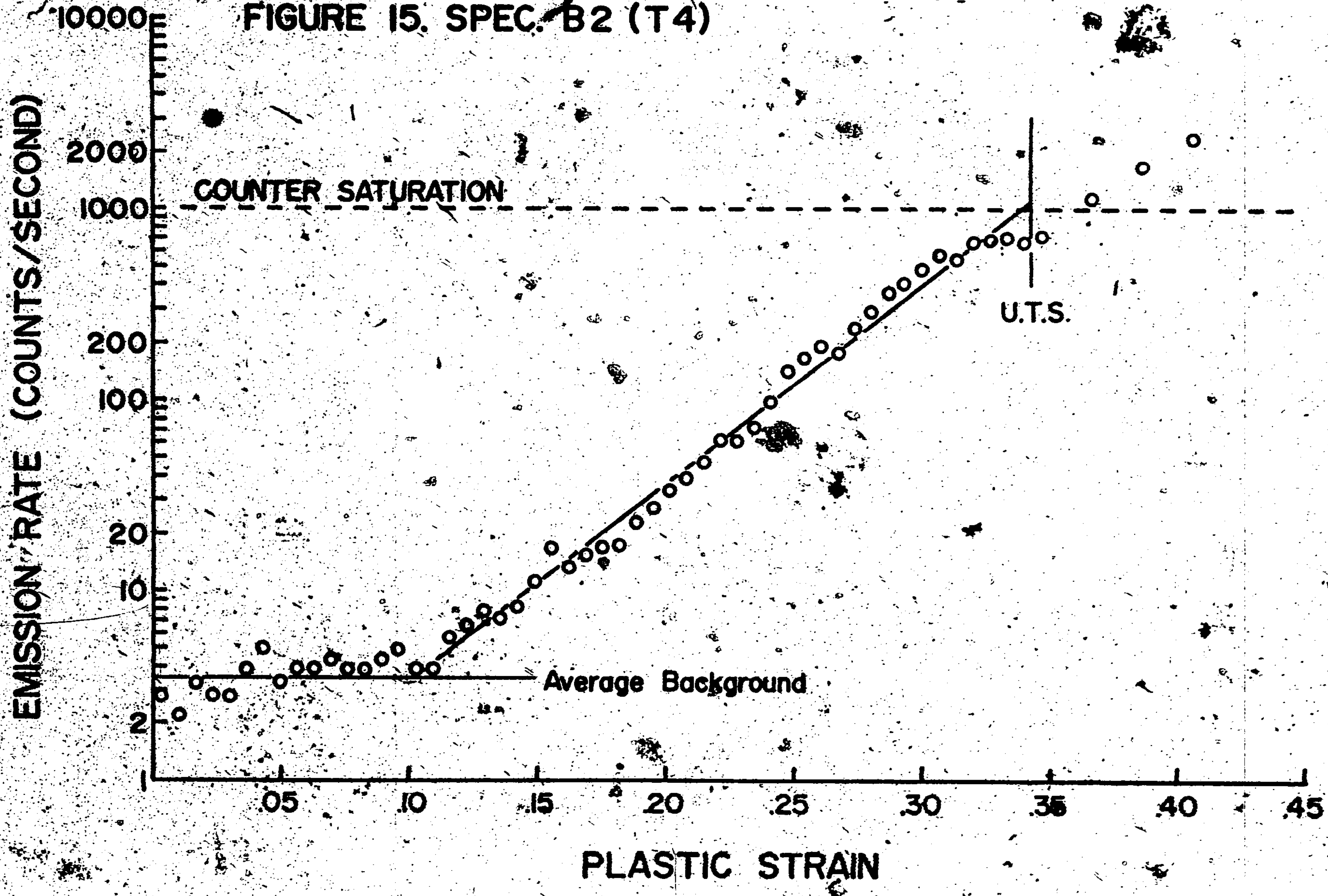

FIGURE 16. SPEC. B3 (T6 (450 Q))

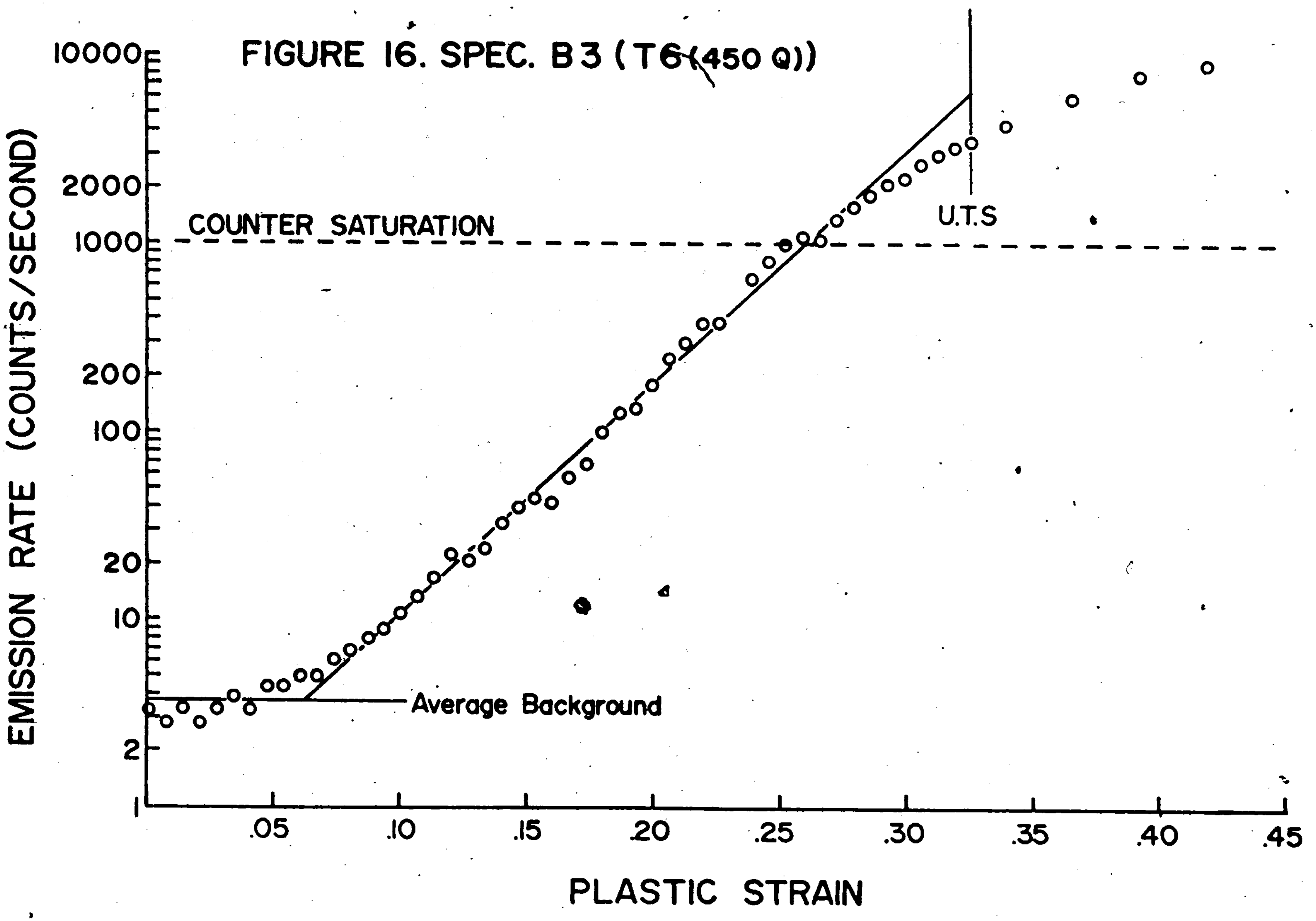

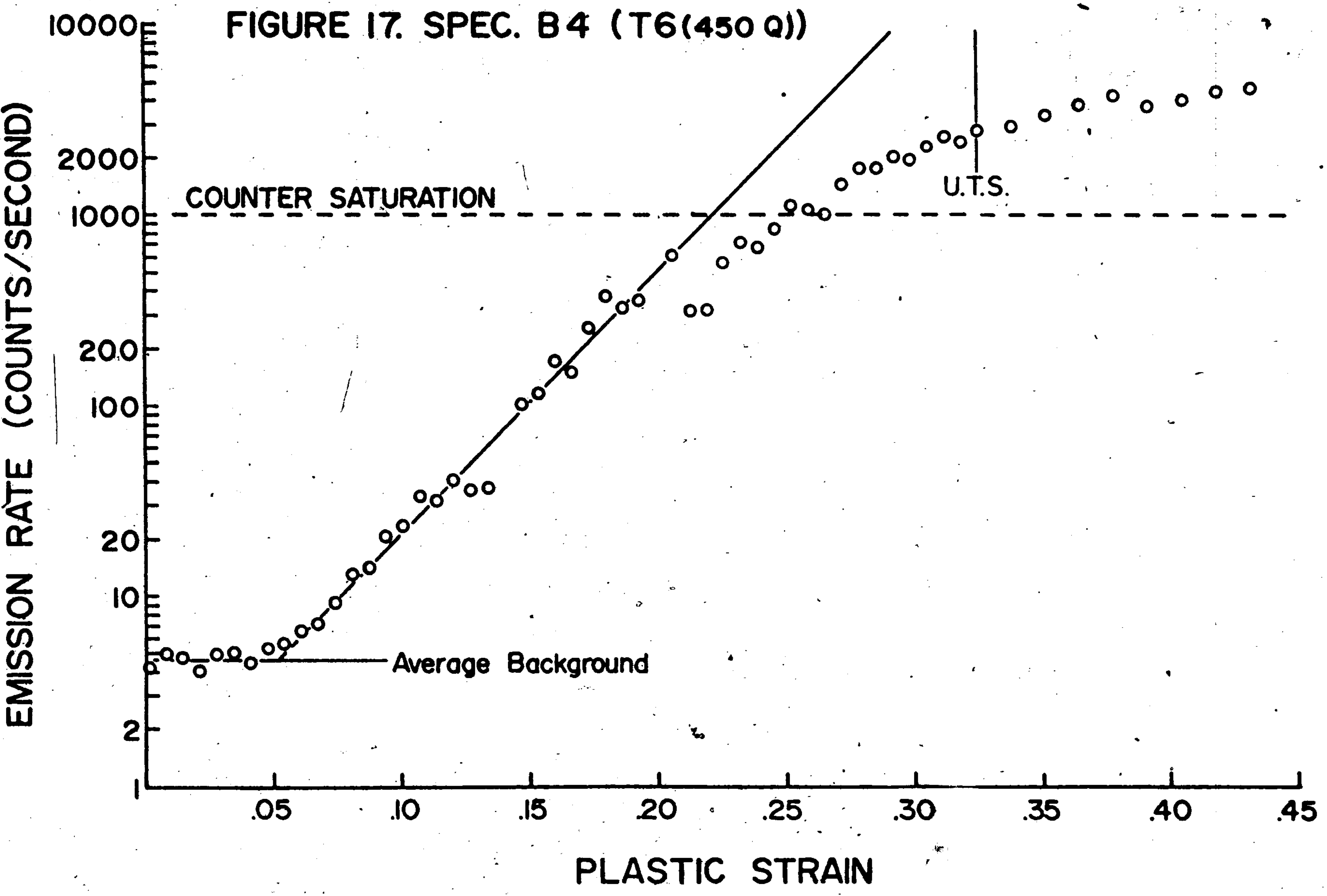

FIGURE 17. SPEC. B4 (T6(450 Q))

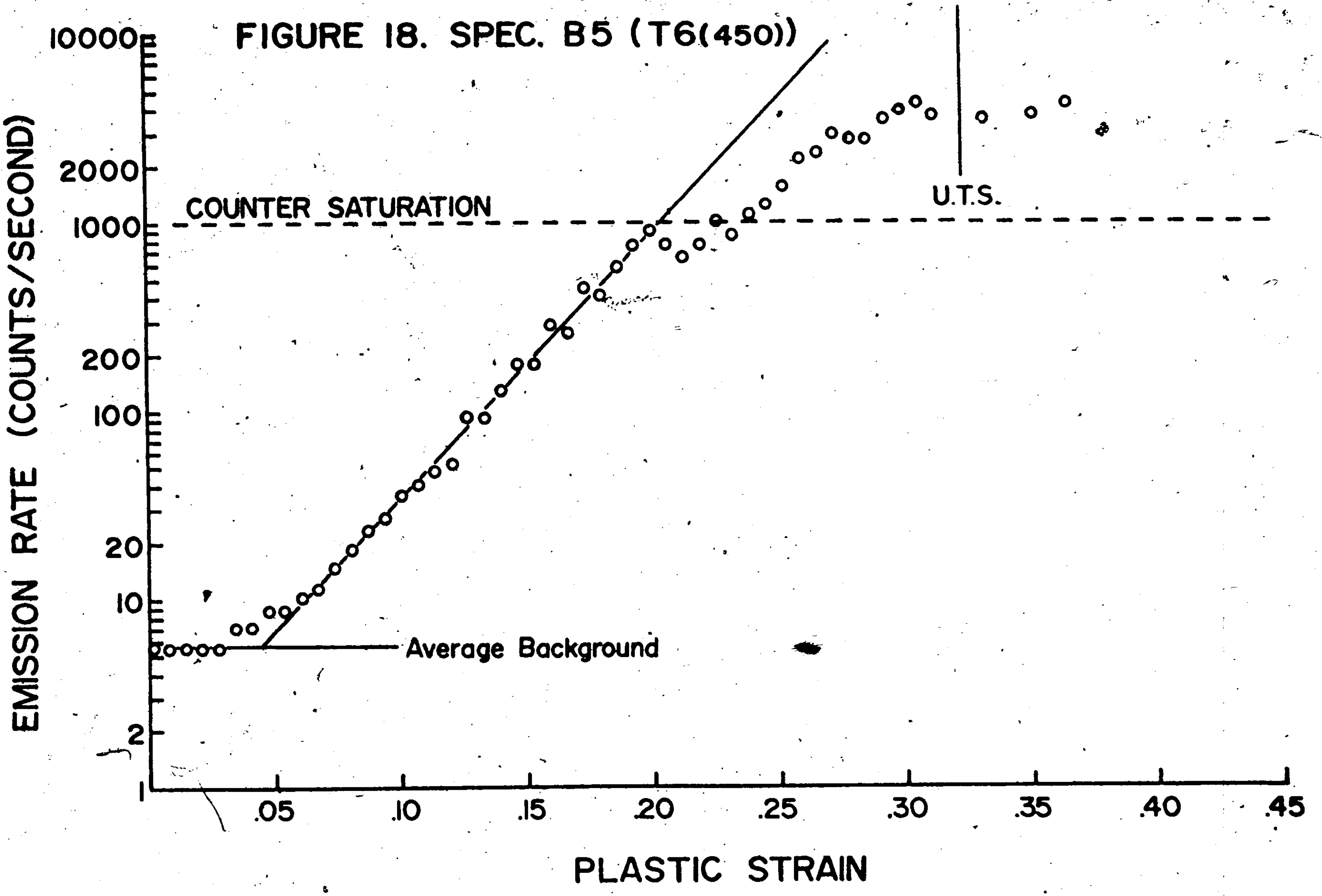

FIGURE 18. SPEC. B5 (T6(450))

FIGURE 19. SPEC. B7 (T6)

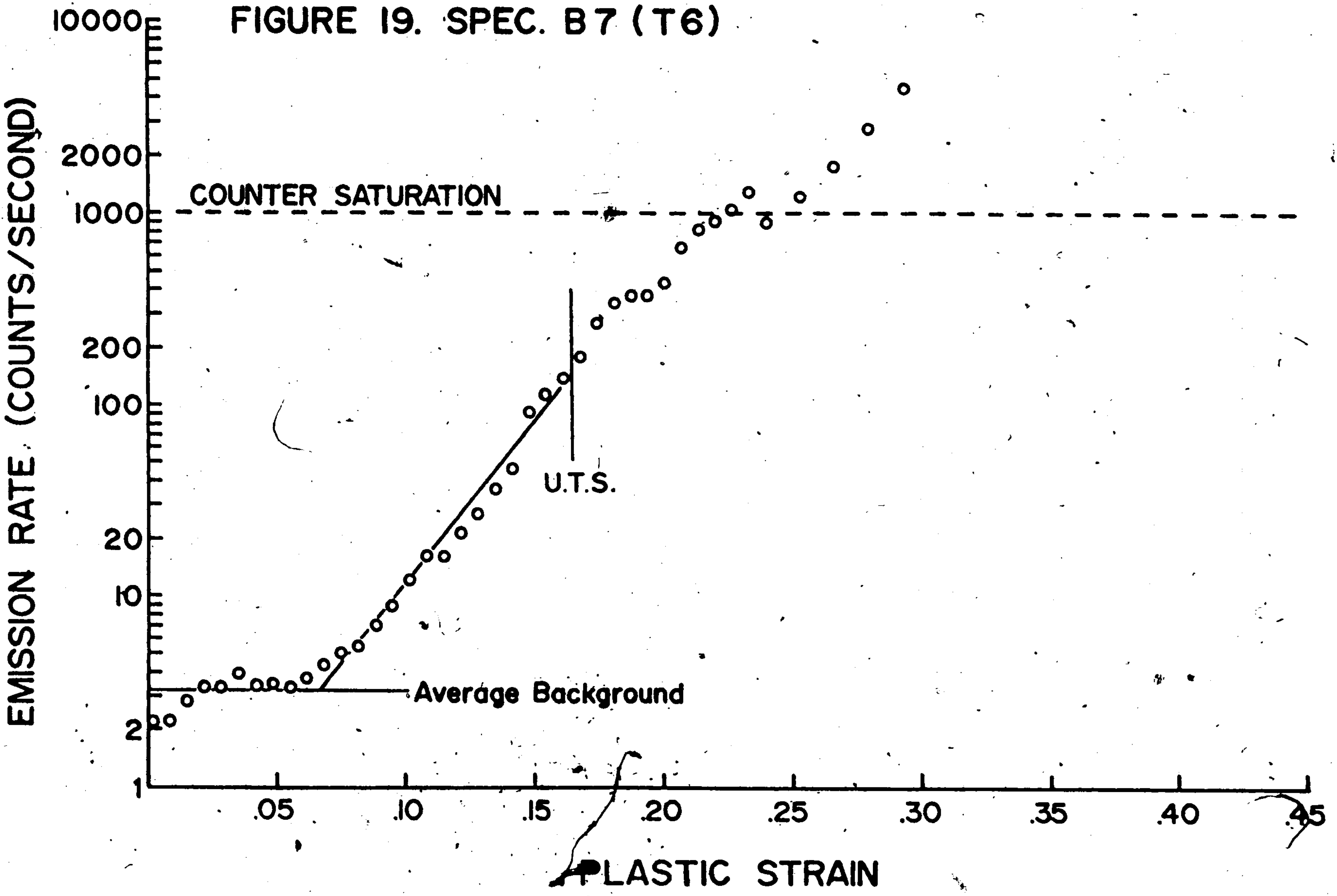

FIGURE 20. SPEC. B8 (T6)

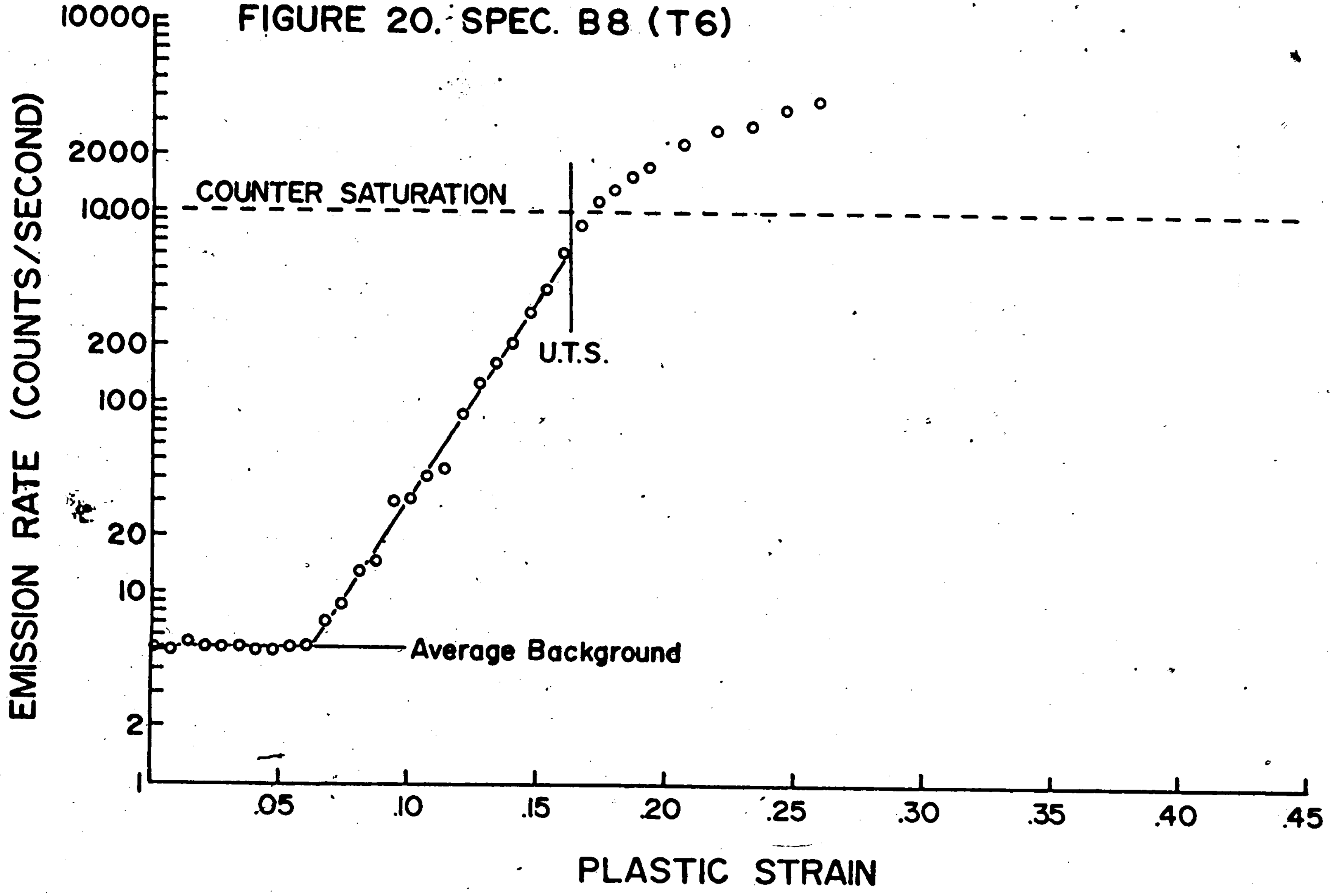

FIGURE 21. SPEC. B9 (T6(450 Q))

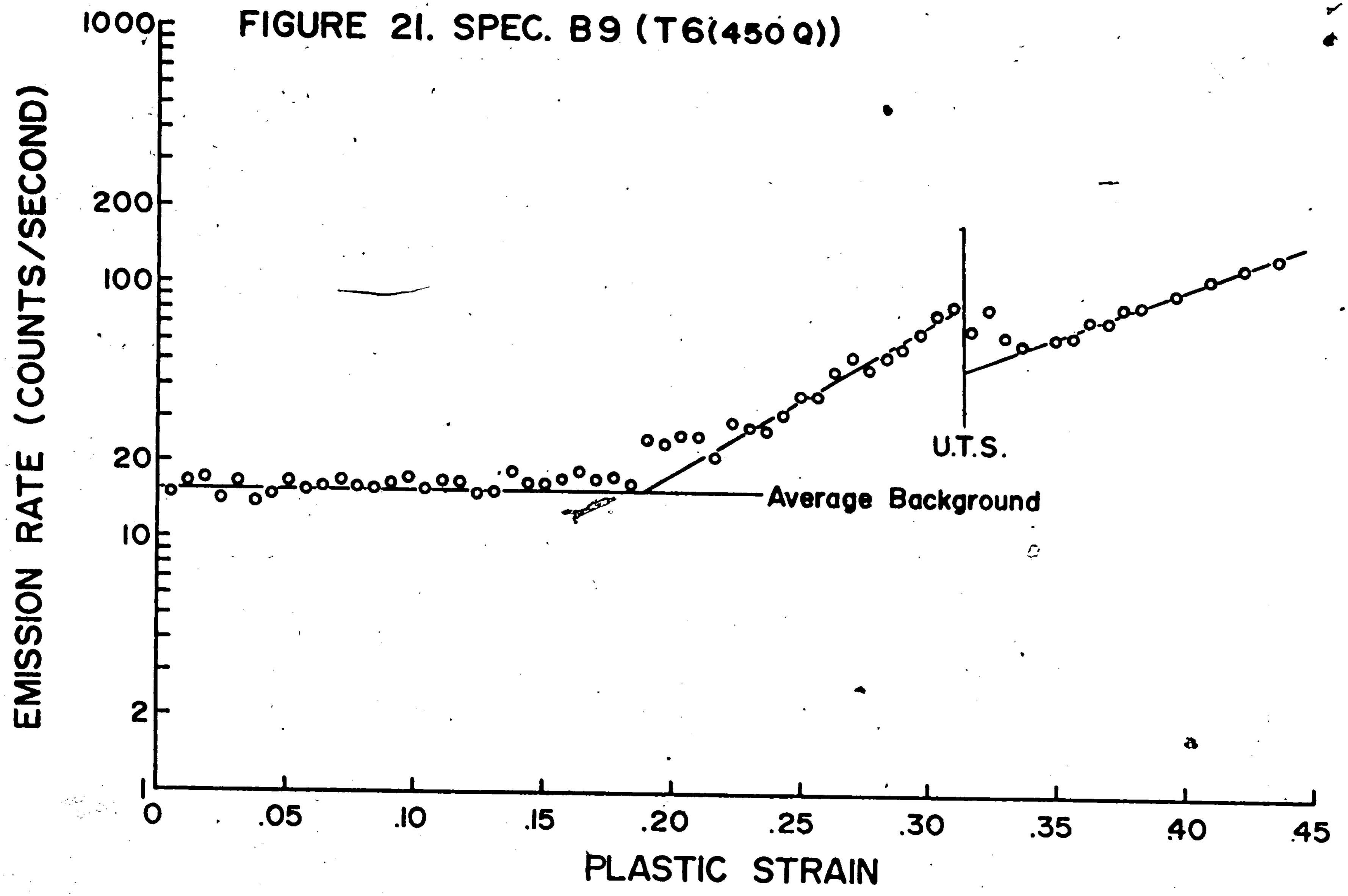

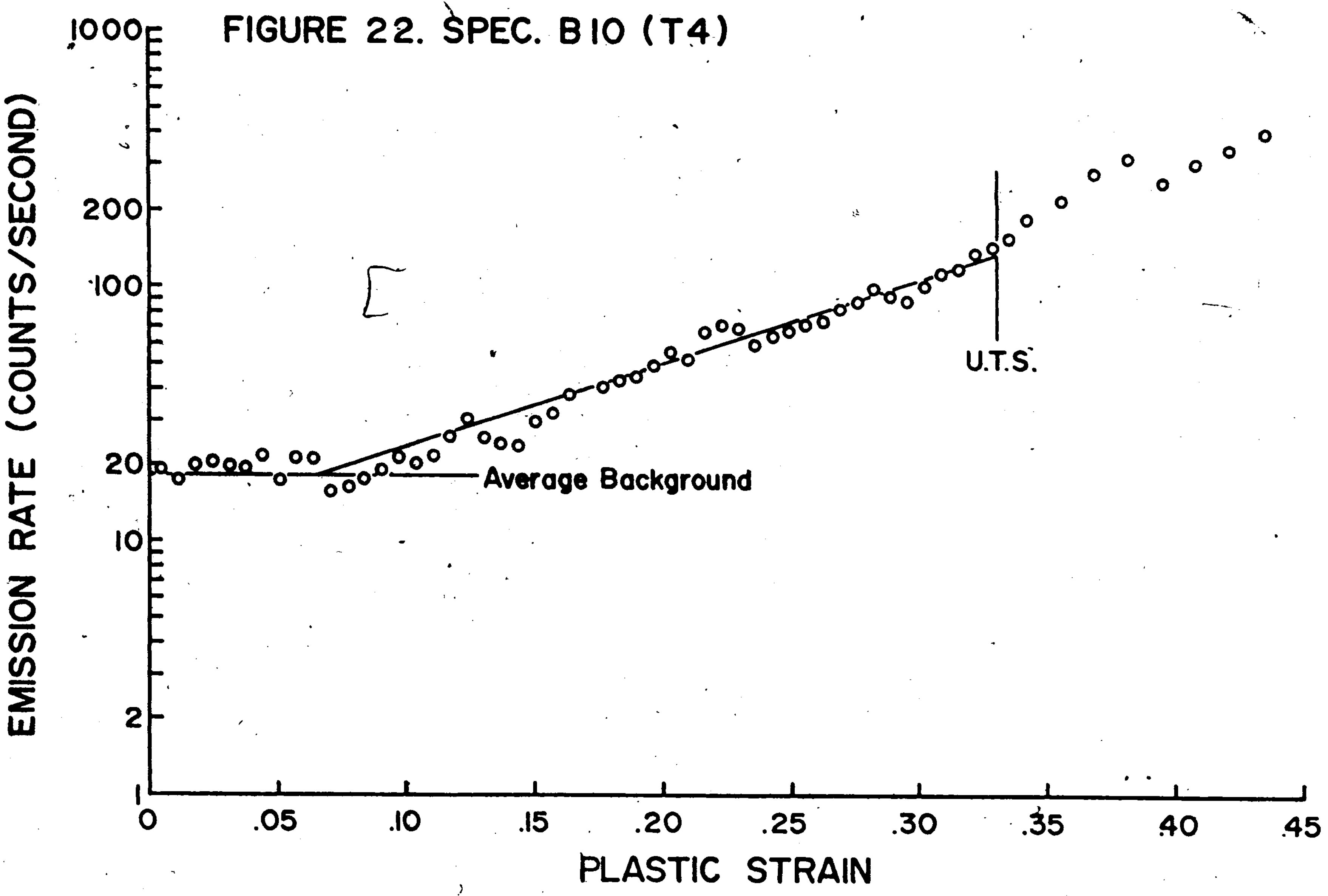

FIGURE 22. SPEC. B10 (T4)

FIGURE 23. SPEC. B11 (T6(450))

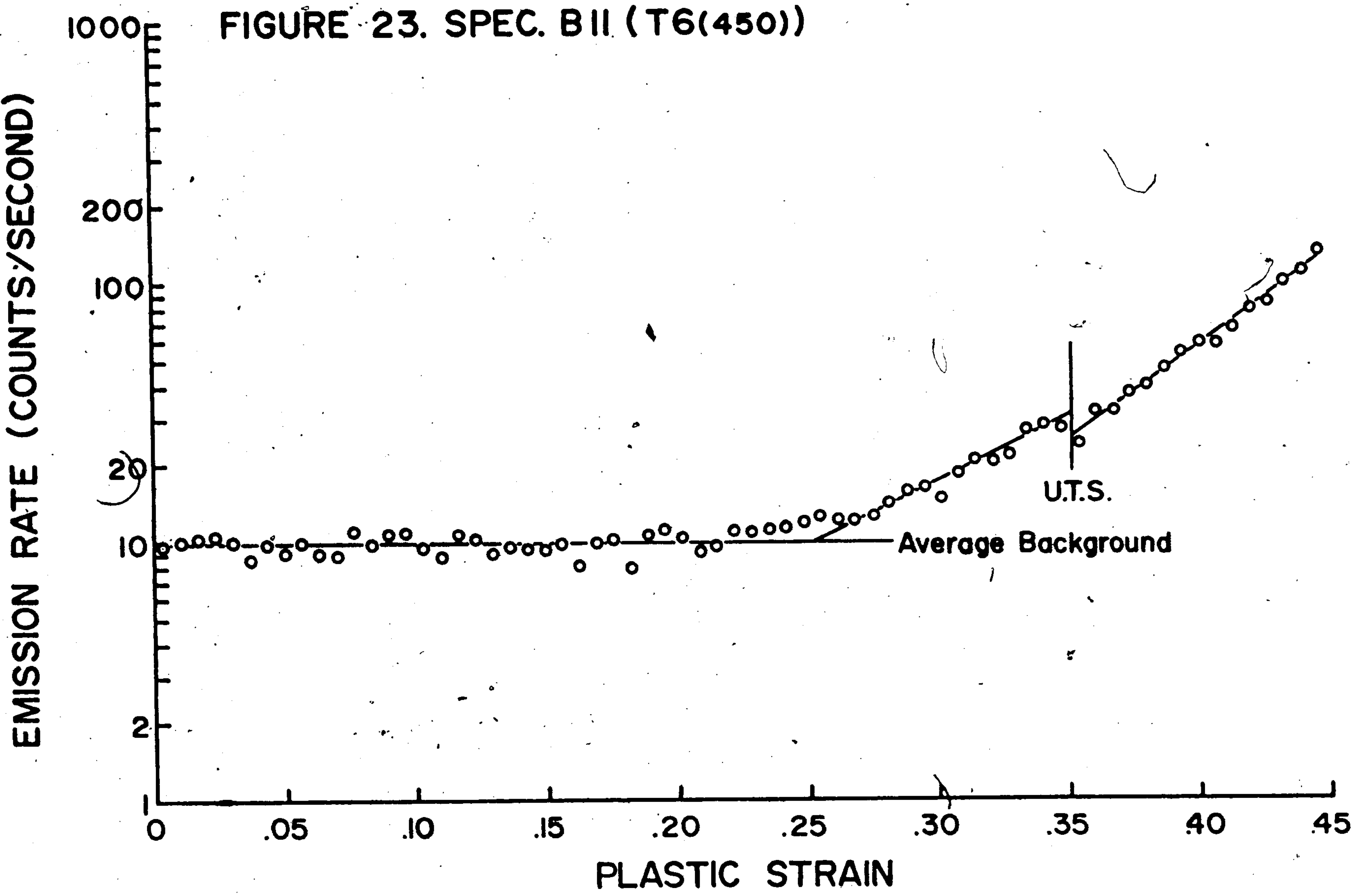

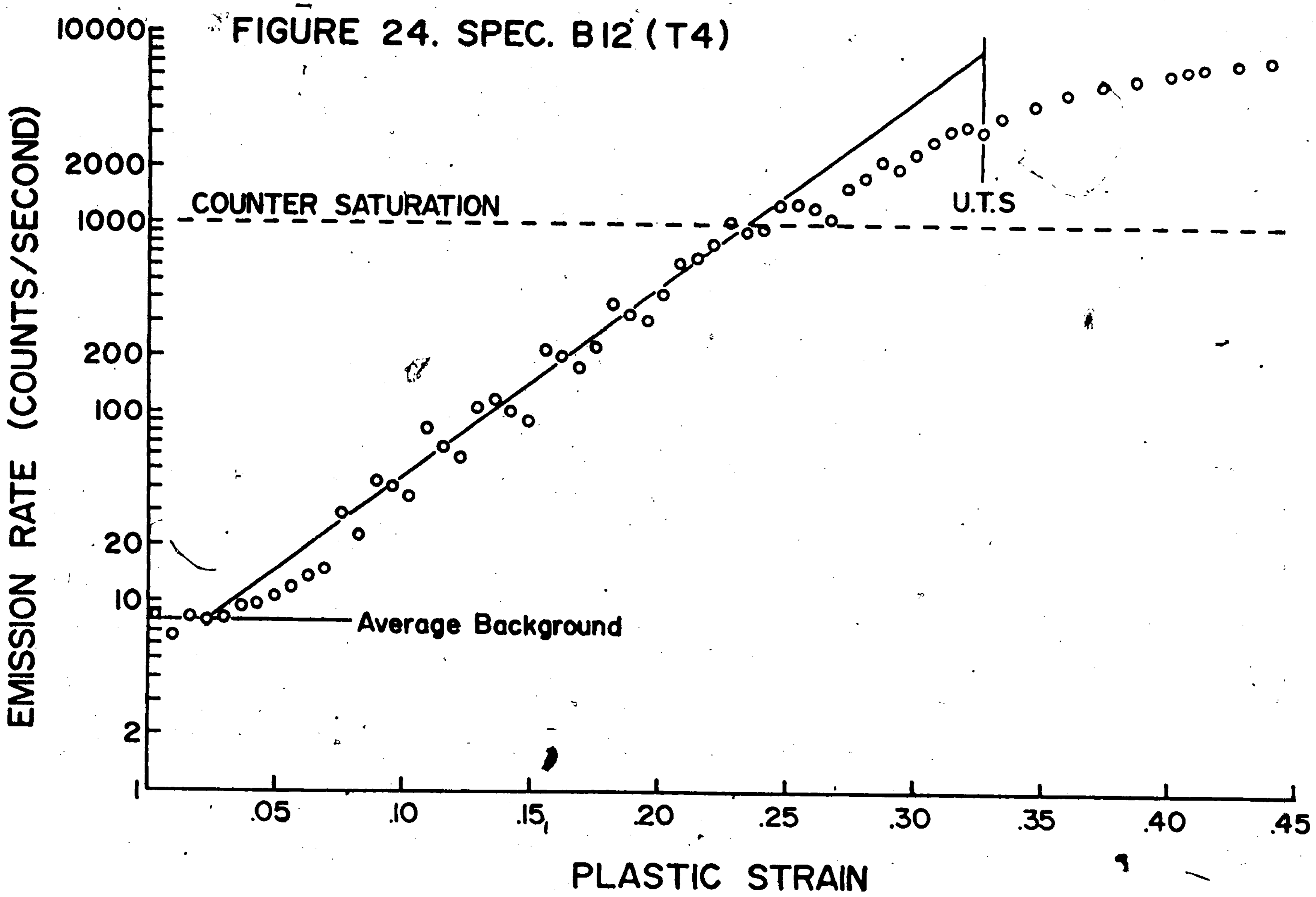

FIGURE 24. SPEC. B12 (T4)

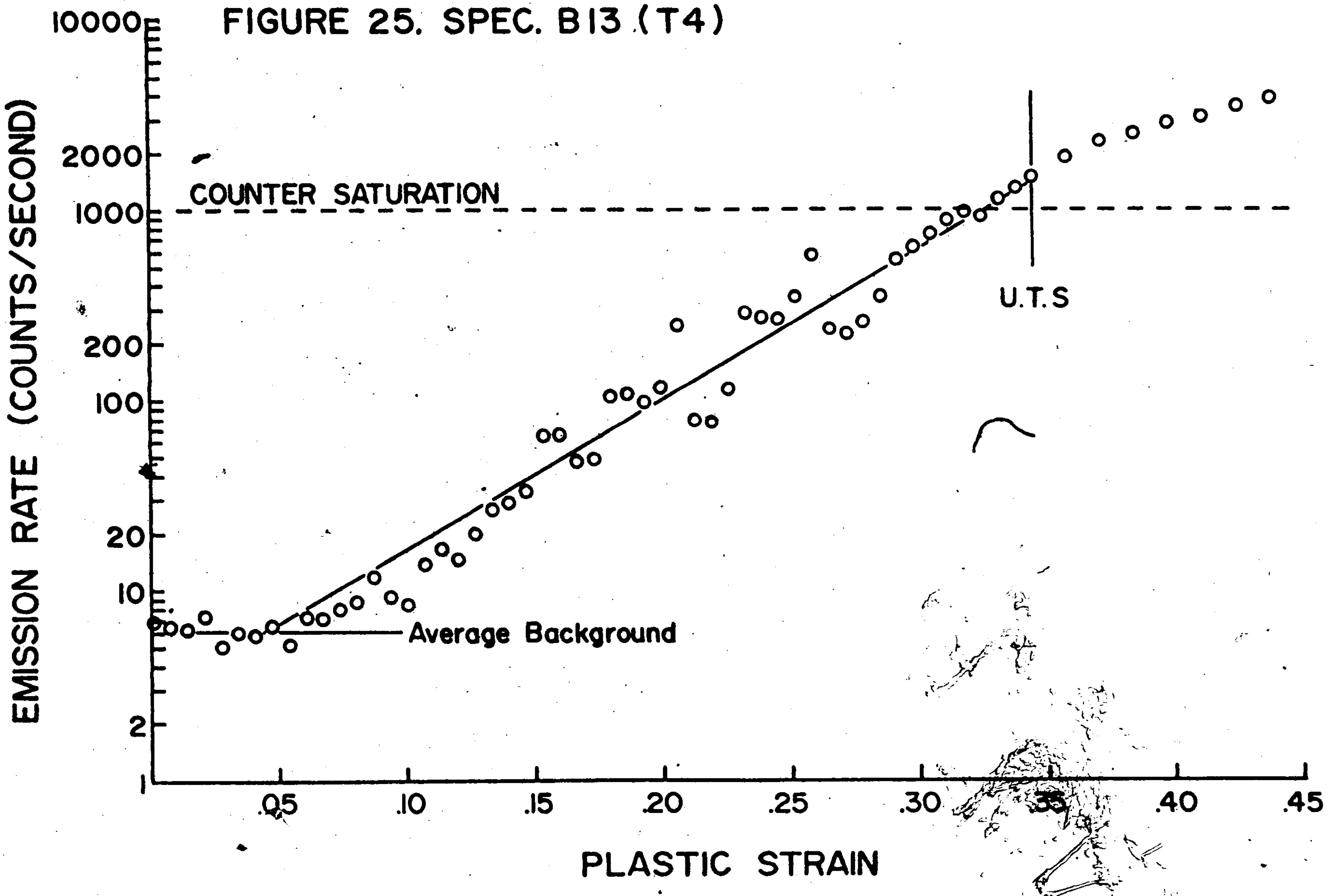

FIGURE 25. SPEC. B13 (T4)

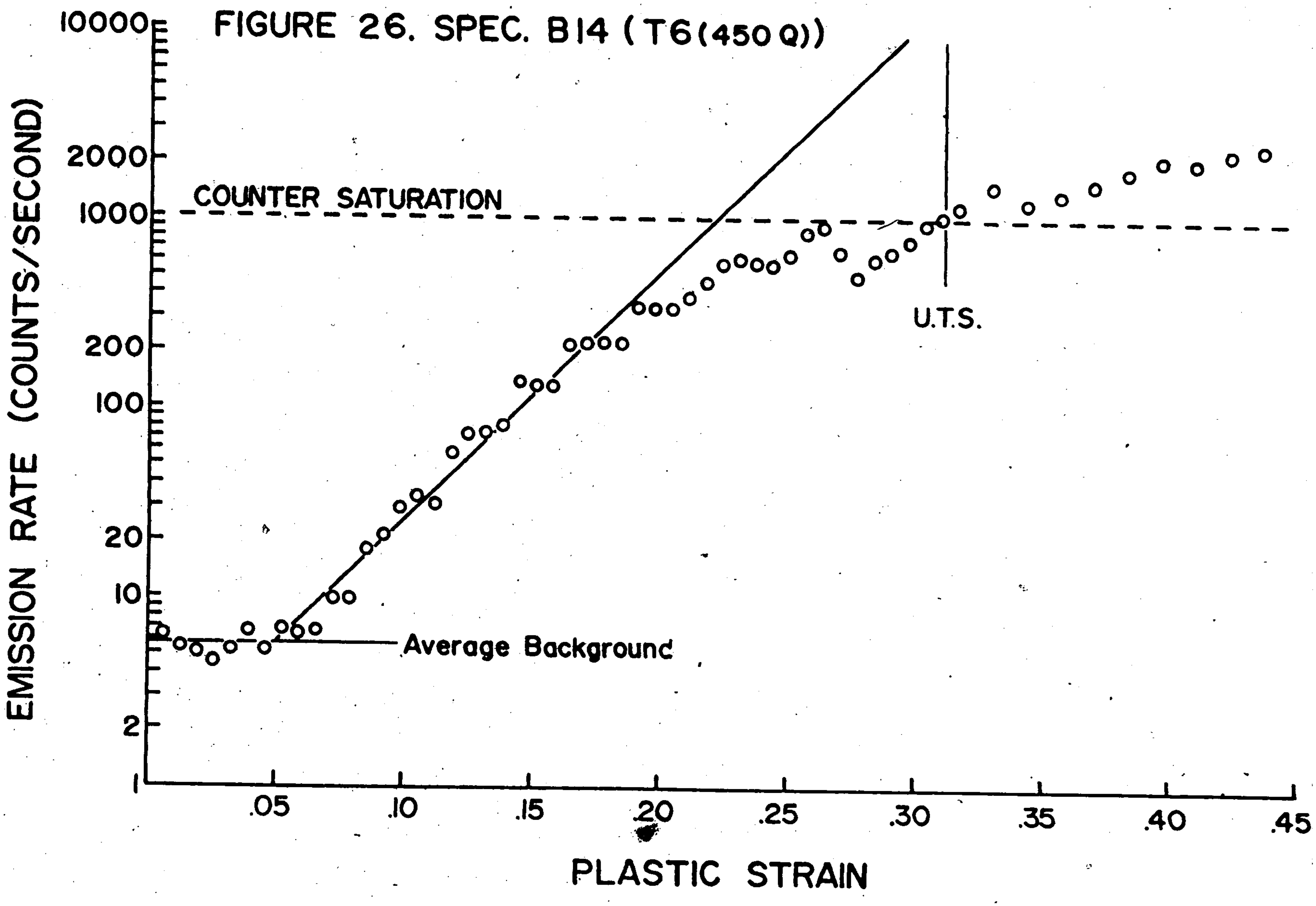

FIGURE 26. SPEC. B14 (T6(450Q))

FIGURE 27. SPEC. B15 (T6(450))

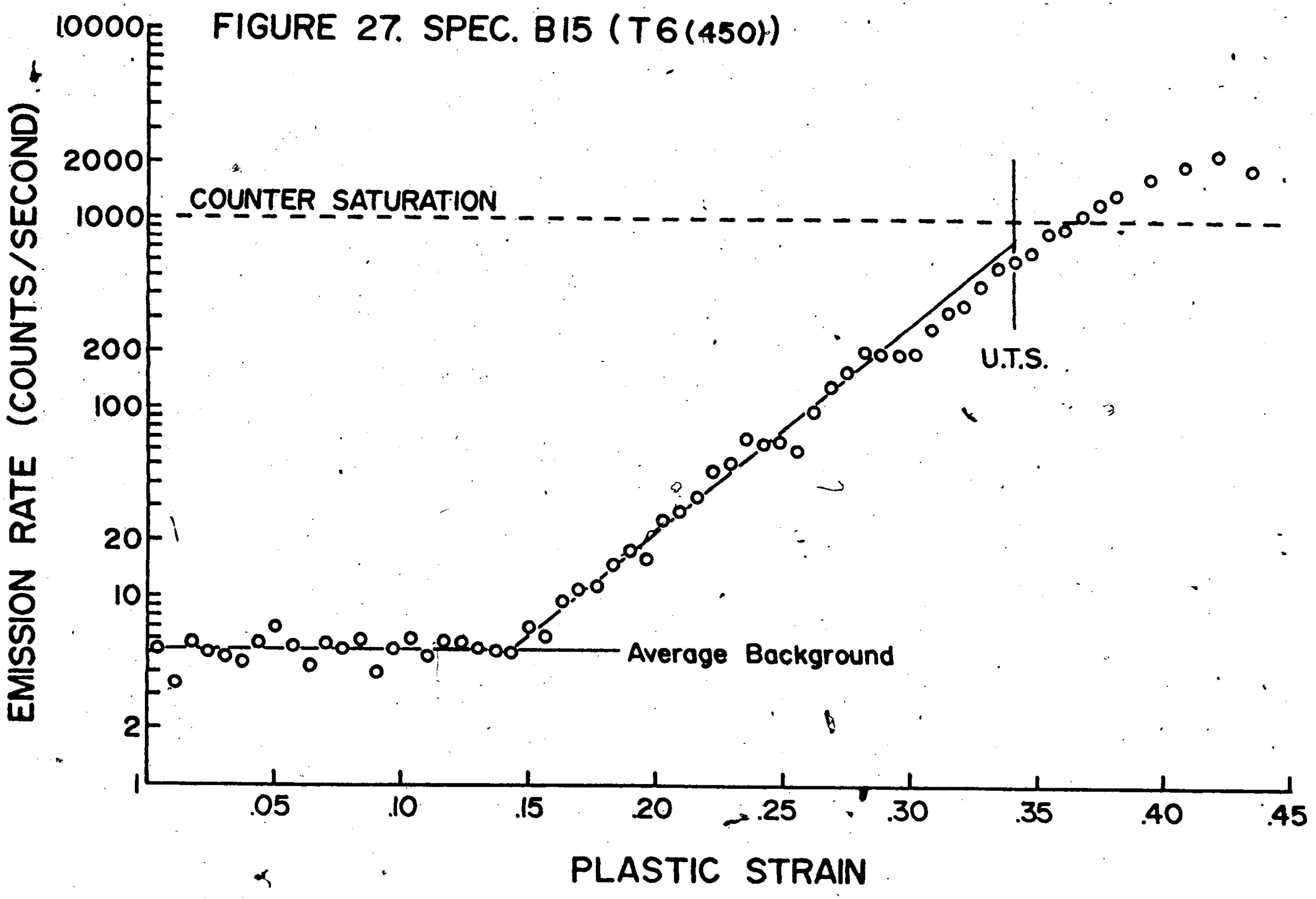

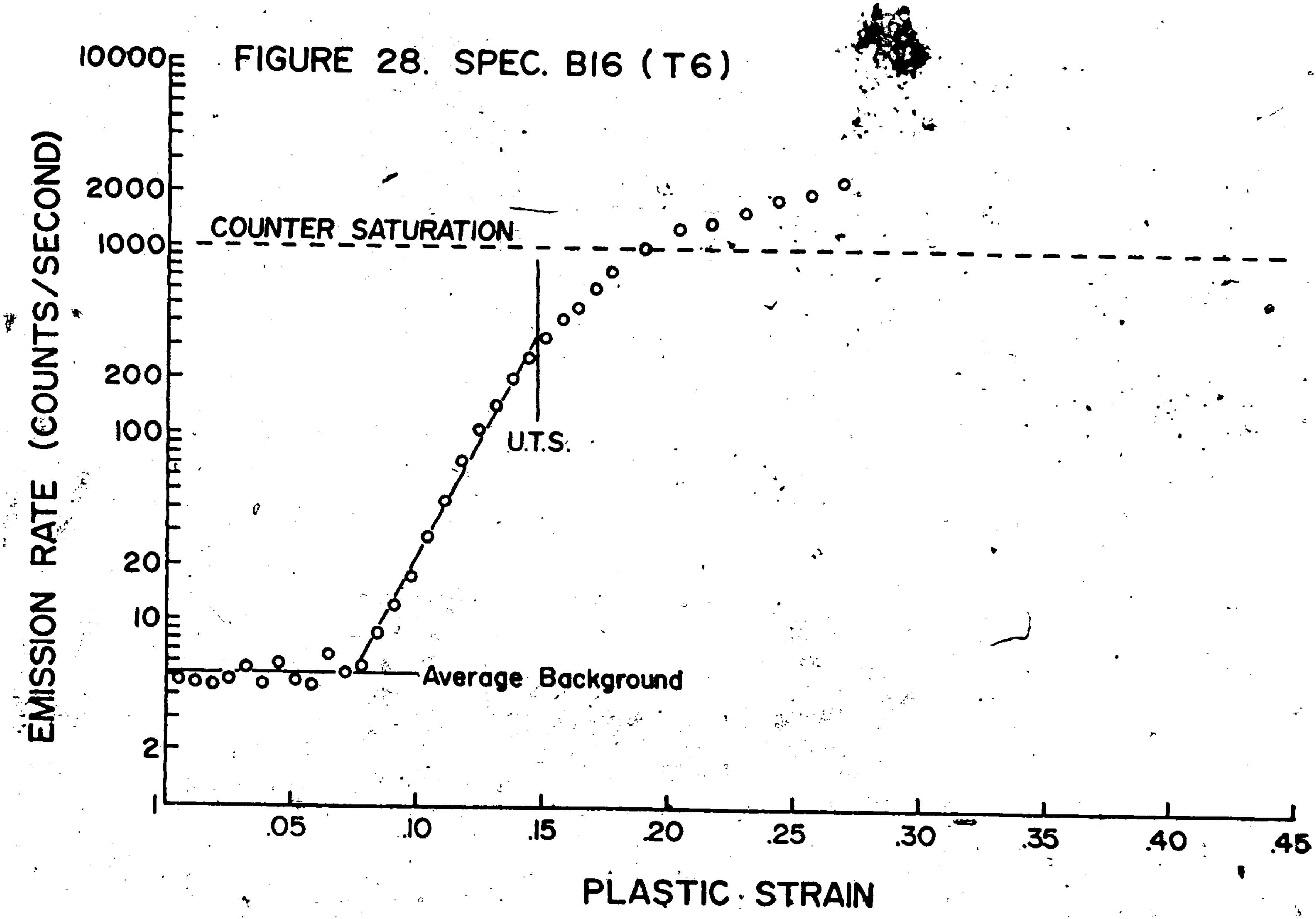
FIGURE 28. SPEC. B16 (T6)

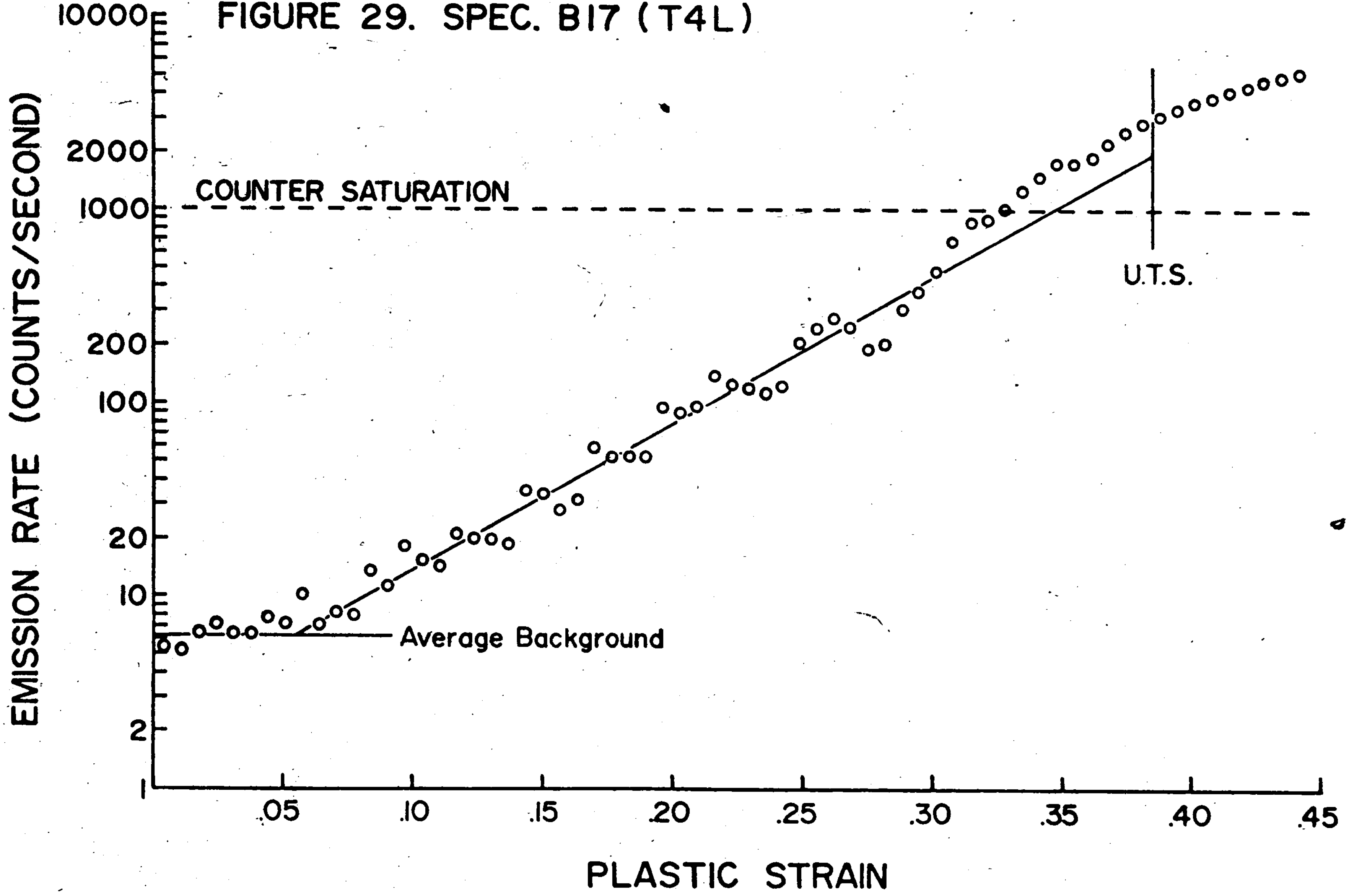

FIGURE 29. SPEC. B17 (T4L)

FIGURE 30. SPEC. B18 (T4S)

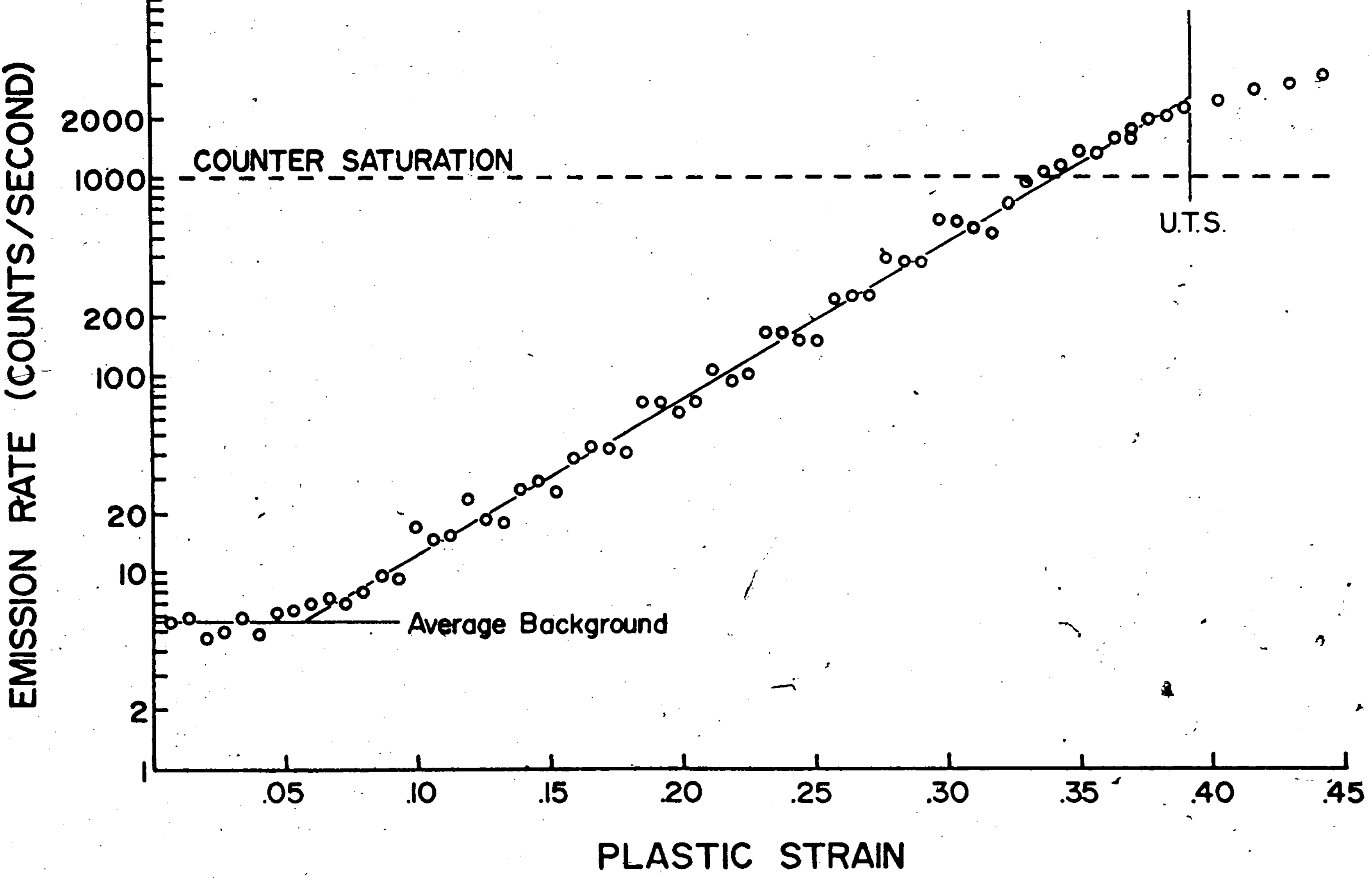

FIGURE 31. GROUP I SPECIMENS

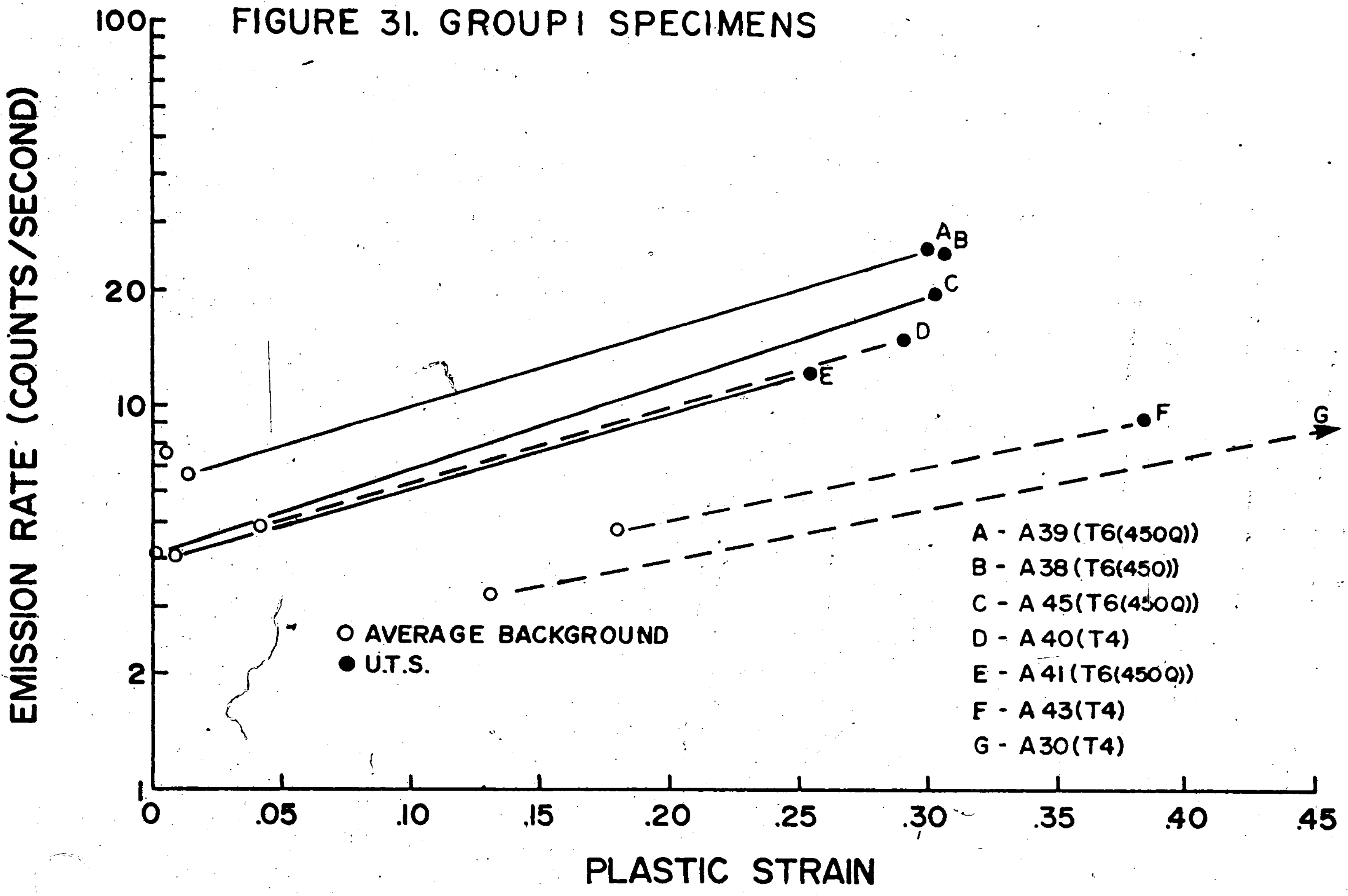

FIGURE 32. GROUP 2 SPECIMENS

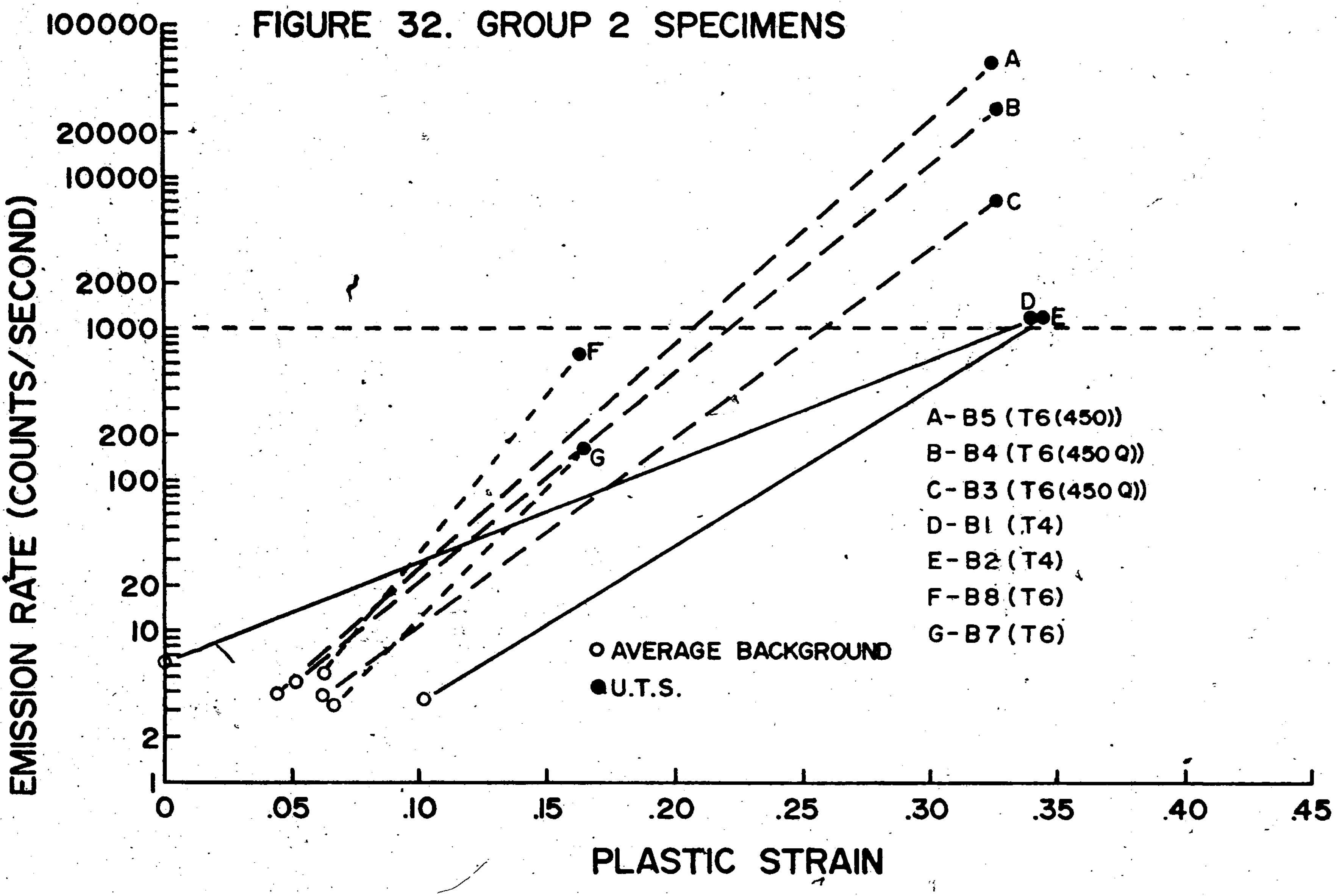

FIGURE 33. GROUP 3 SPECIMENS

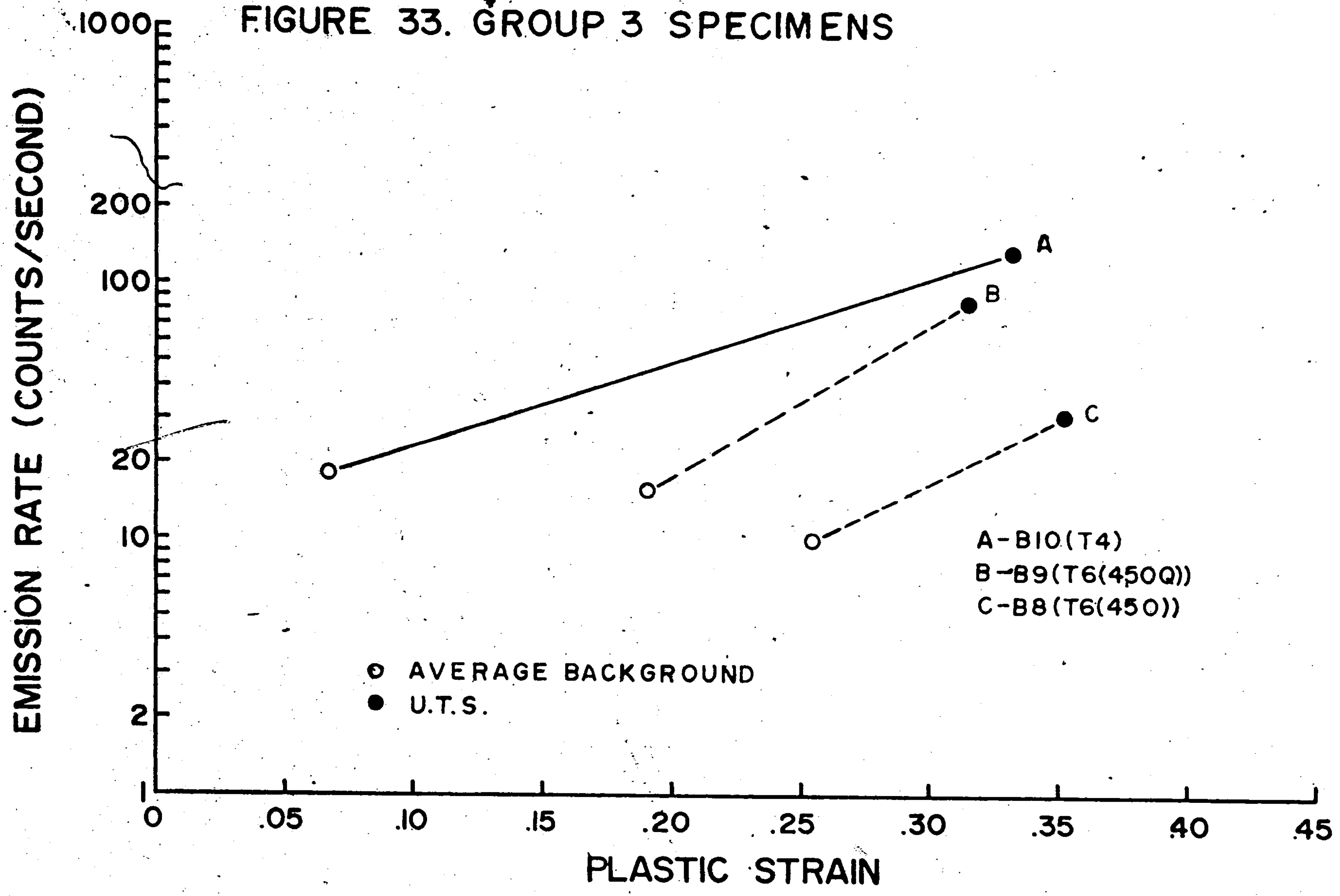

FIGURE 34. GROUP 4 SPECIMENS

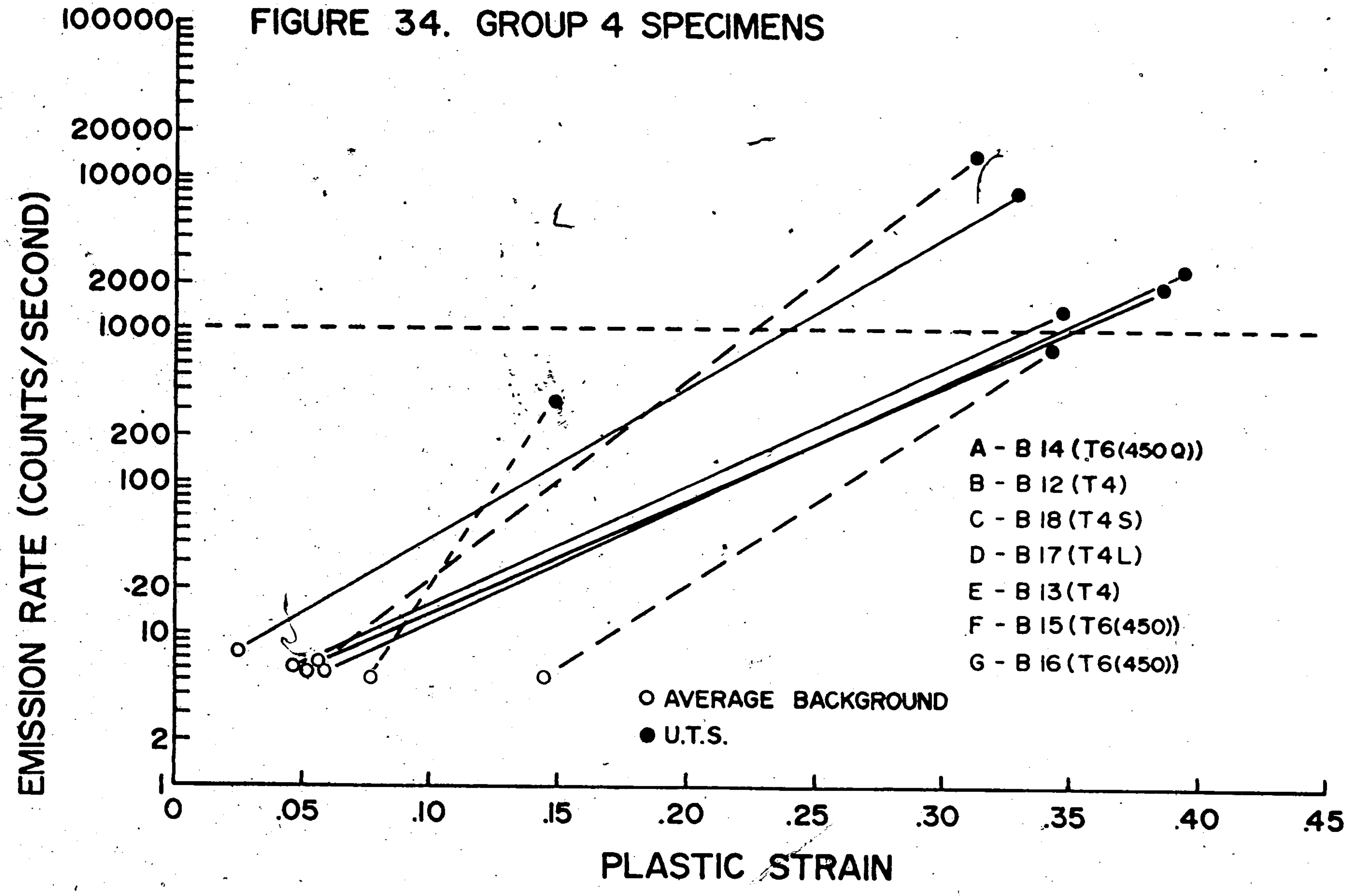

FIGURE 35. B 11 (T6(450)) DECAY

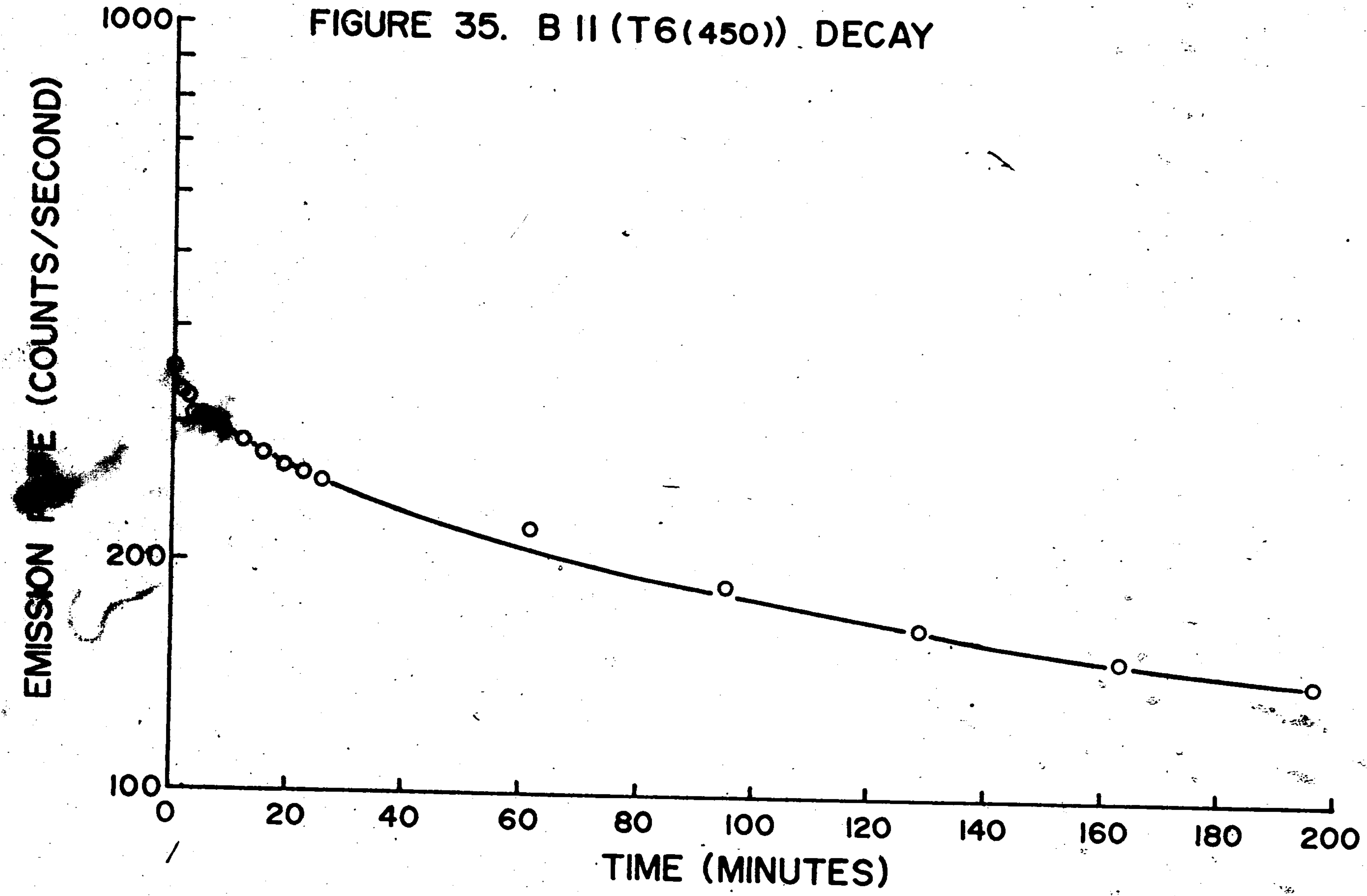

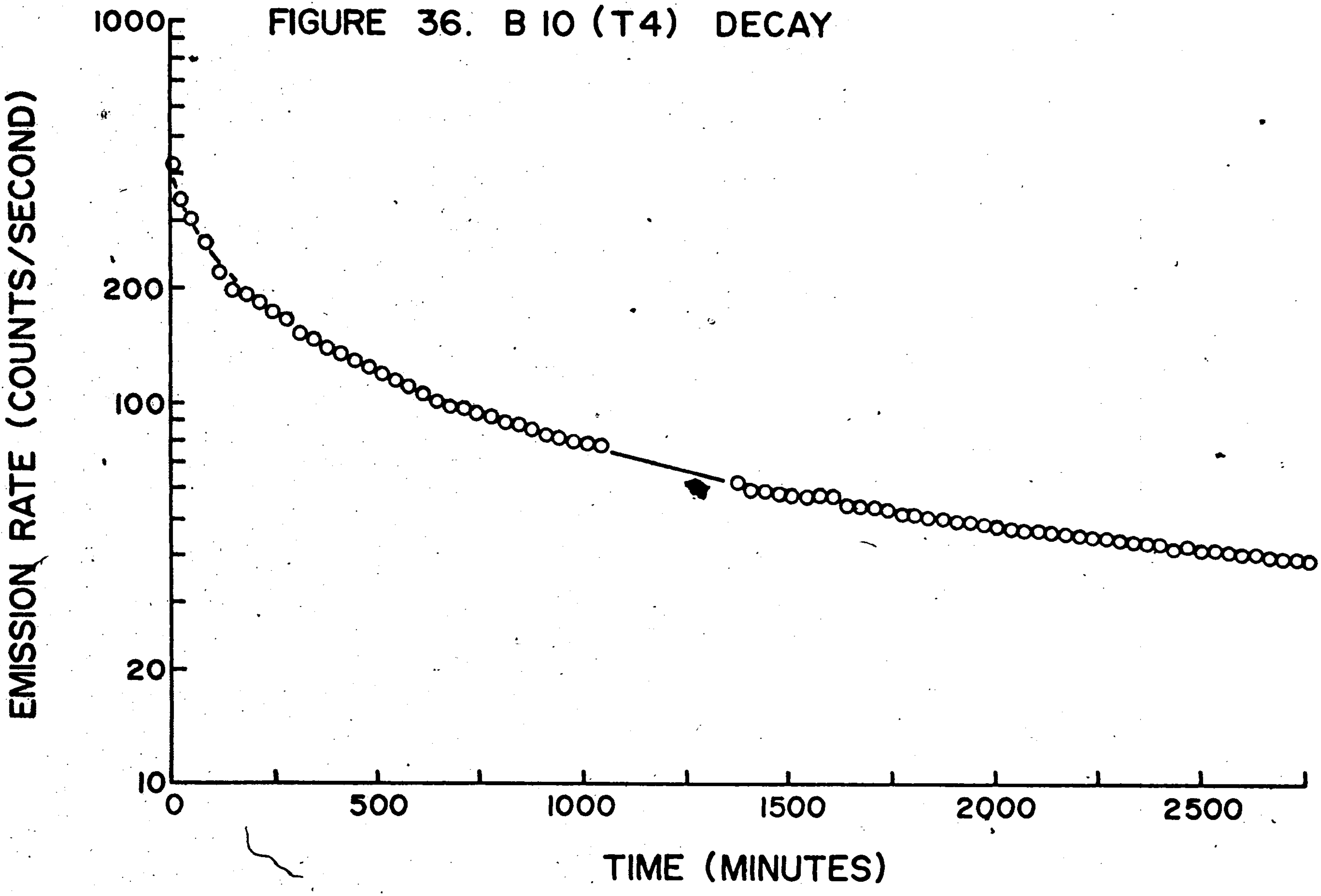

FIGURE 36. B 10 (T4) DECAY

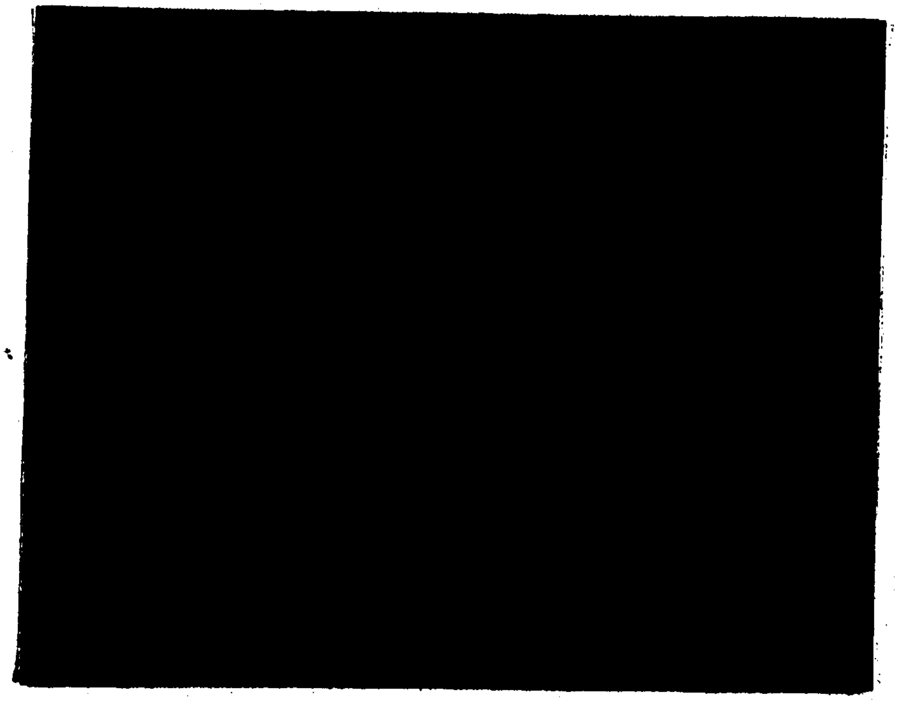

Plate 1 - Specimen configuration II and its appropriate specimen holder.

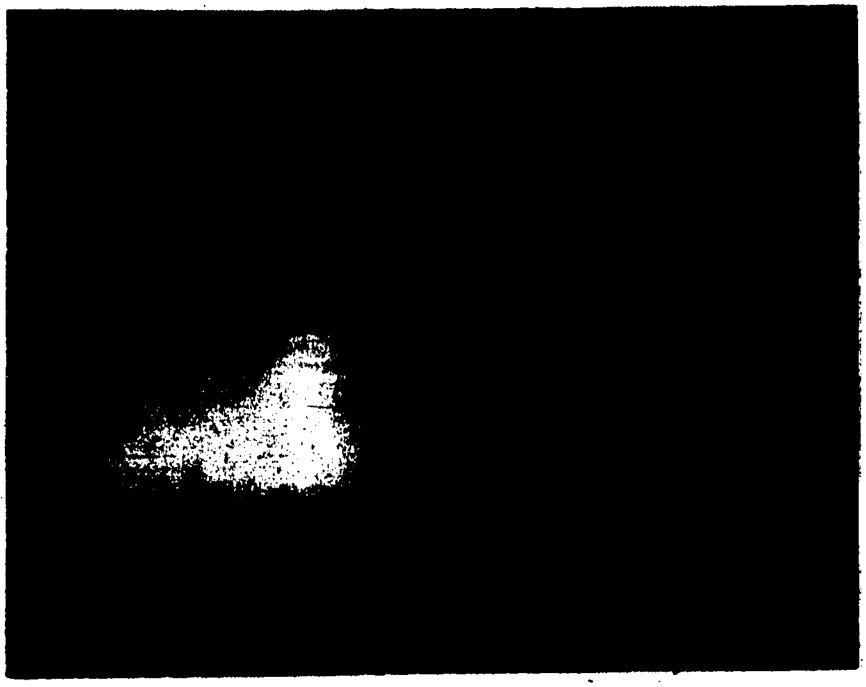

Plate 2 - Specimen configuration III and its appropriate specimen holder.

Plate 3 - Specimens of configurations II and III mounted in their specimen holders, revealing the test areas.

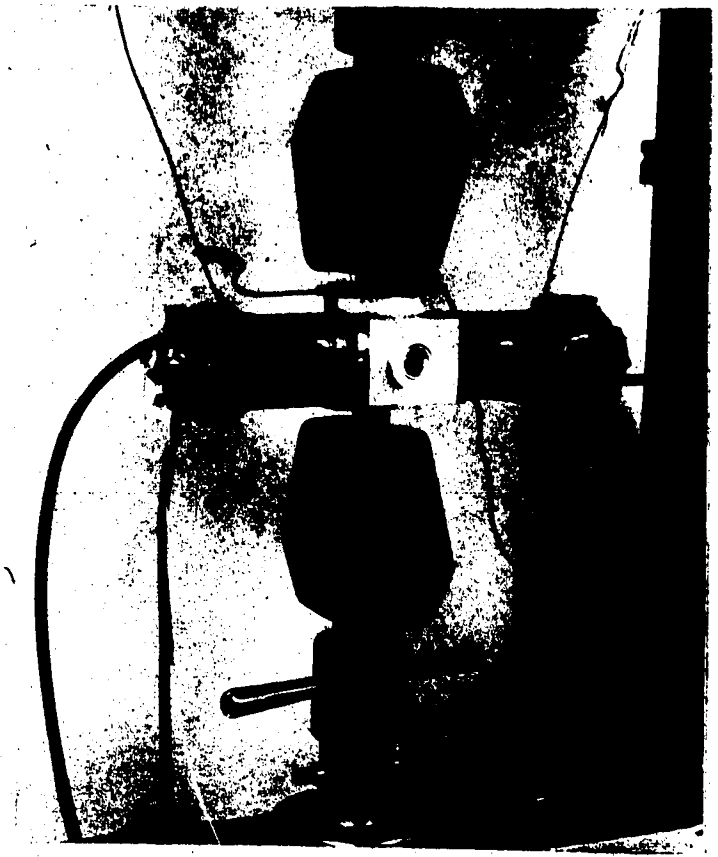

Plate 4 - Side close-up of G-M flow counter in the test position. The specimen is clamped to the counter tube and mounted in the Instron grips. This plate shows the illuminated quartz port, the accellerating grid (through the port) and its voltage source, the assorted electrical connections and gas tubing required for operation of the counter, and the lead foil shielding.

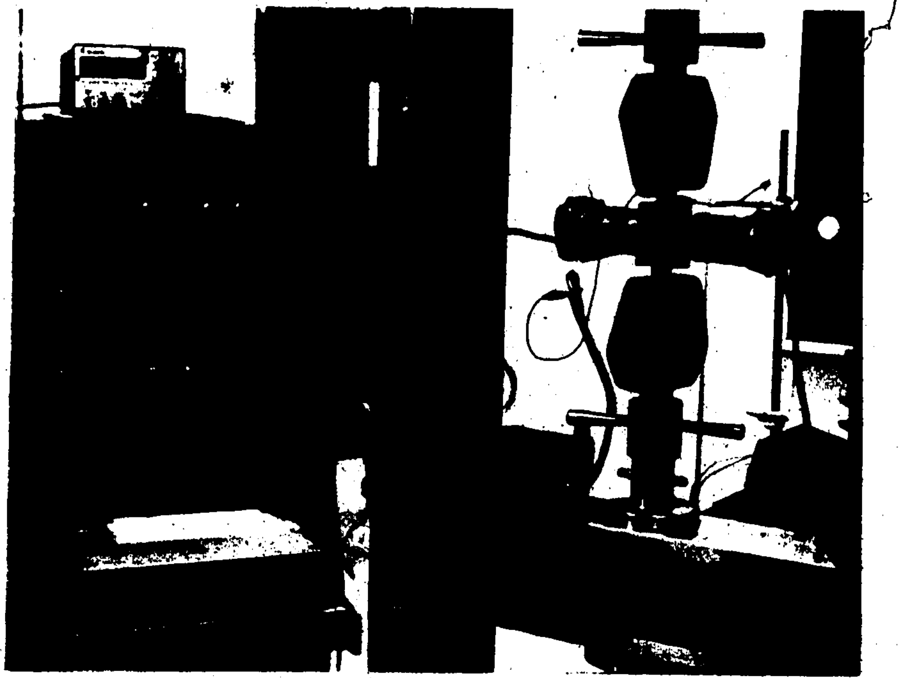

Plate 5 - An overall, rear view of the testing system. This plate shows the Instron testing frame, the Philips electronics and the light source.

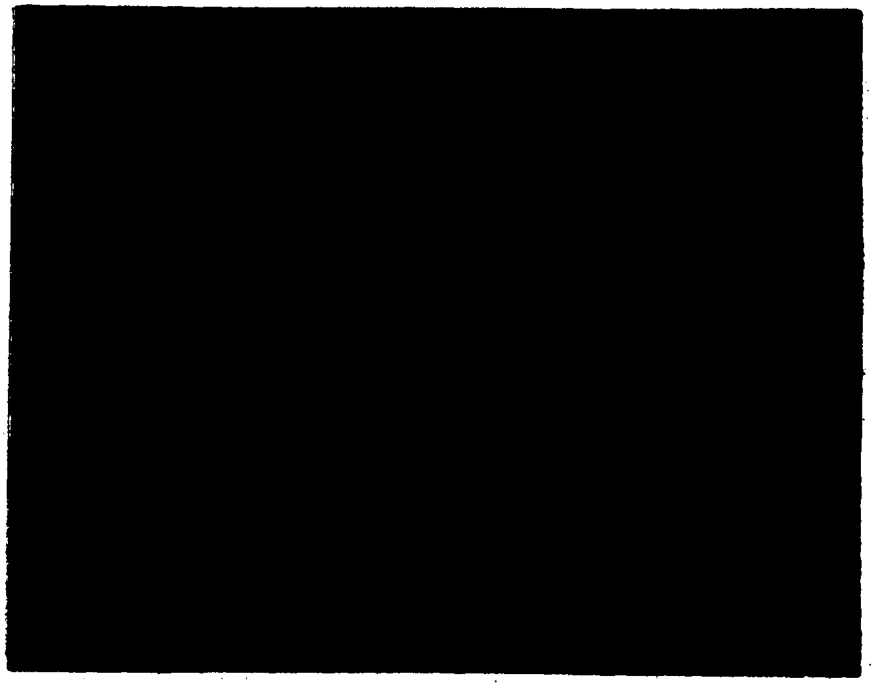

Plate 6 - Slip structure of a T4 specimen, showing distinct, massive planar slip, x 250.

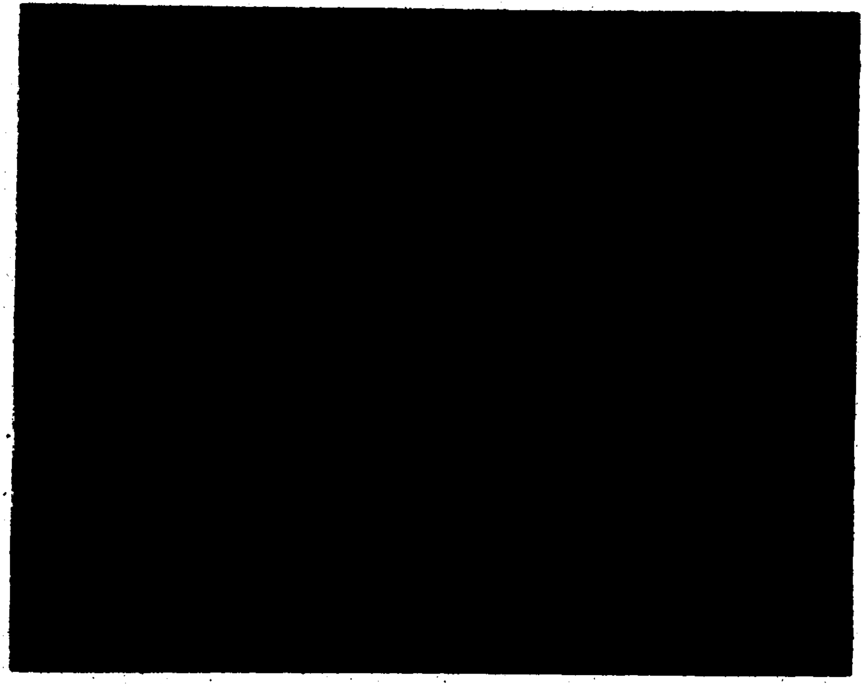

Plate 7 - Slip structure of a T6 specimen, showing indistinct, fine, wavy slip, x 250. (Lines running approximately north-south are polishing scratches.)

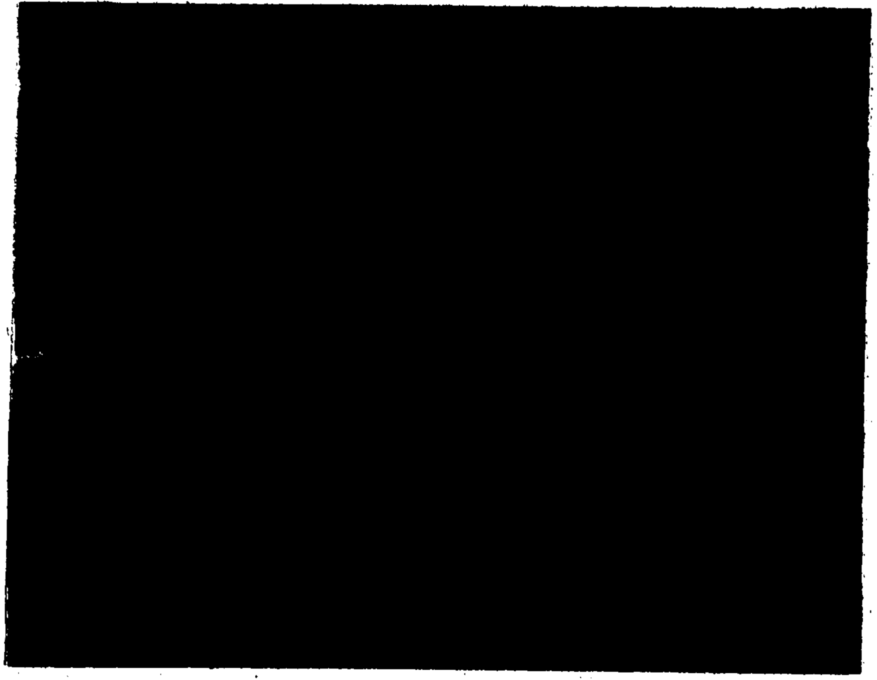

Plate 8 - Slip structure of a T6(450) specimen, showing an intermediate slip (between T4 and T6) which is less indistinct and wavy than T6, x 250.

REFERENCES

1. Kramer, J., *Der Metallische Zustand*, Vandenhoeck and Ruprecht, Goettingen (1950), as reported by [2] and [4].
2. Grundberg, L., *Brit. J. Appl. Phys.*, 9, 85 (1958).
3. Brotzen, F.R., *Phys. Stat. Sol.*, 22, 9 (1967).
4. Vitovec, F.H., Wright Air Development Center, Technical Report 54-200 (1954).
5. Moser, *Pogg. Ann.*, 56, 177 (1842), as reported by [4] and [55].
6. Russel, W.J., *Proc. Roy. Soc.*, A61, 424 (1897), as reported by [4].
7. Oberhofer, M., *Euro-Spectra*, 11, 110 (1972).
8. Scharmann, A., 'Proceedings of the 3rd International Symposium on Exoelectrons', *PTB Mitteilungen*, Brunswick, 318 (1970).
9. Curie, H., *Comptes Rendus*, 129, 714 (1899), as reported by [8].
10. Rutherford, J.W., *Phil. Mag.*, 49, 161 (1900), as reported by [8].
11. van Atta, L.C., Northrup, D.L., van de Graaff, R.J., and van Atta, C.M., *Rev. Sci. Instr.*, 12, 534 (1941).
12. Tanaka, M., *Phys. Rev.*, 48, 916 (1935).
13. Burcham, W.E., and Lewis, W.B., *Proc. Cambridge Phil. Soc.*, 32, 503 (1936).
14. Bathow, G., and Grobrecht, H., *Z. Phys.*, 146, 1 (1956).
15. Haxel, O., Houtermans, F.G., and Seeger, K., *Z. Phys.*, 130, 109 (1951).
16. Seeger, K., *Z. Phys.*, 135, 152 (1953).

REFERENCES (Continued)

17. Grunberg, L., and Wright, K.H.R., *Proc. Roy Sci.*, A232, 423 (1953).

18. Grunberg, L., and Wright, K.H.R., *Acta Phys. Austriaca*, 10, 375 (1957).

19. Seidl, R., *Acta Phys. Austriaca*, 10, 402 (1957).

20. Kramer, J., *Naturwissenschaften*, 41, 160 (1954).

21. Bohun, A., *J. Phys. Radium*, 17, 783 (1956).

22. Hanle, W., *Acta Phys. Austriaca*, 10, 339 (1957)

23. Müller, H. *Acta Phys. Austriaca*, 10, 474 (1957).

24. Lohff, J., *Naturwissenschaften*, 44, 228 (1957).

25. Ku, T.C., and Pimbley, W.T., *J. Appl. Phys.*, 32, 124 (1961).

26. Pimbley, W.T., and Francis, E.E., *J. Appl. Phys.*, 32, 1729 (1961).

27. Doyama, M., and Koehler, J.S., *Phys. Rev.*, 134, A522 (1964).

28. Ramsey, J.A., and Garlick, G.F.J., *Brit. J. Appl. Phys.*, 15, 1353 (1964).

29. Cabrera, N., *Phil. Mag.*, 40, 175 (1949).

30. Elliott, R.B., and O'Neill, F.R., *Surface Sci.*, 21, 189 (1970).

31. Lewowoski, T., *Acta Phys. Polon.*, 20, 161 (1961); *J. Appl. Phys.*, 33, 2393 (1962).

32. Mamose, Y., *J. Appl. Phys.*, 40, 4215 (1969).

33. Langenecker, J.A.M., and Ray, D.B., *J. Appl. Phys.*, 35, 2586 (1964).

34. Craciun, P., *Phys. Stat. Sol. (a)*, 10, 175 (1972).

REFERENCES (Continued)

35. Scharman, A., and Seibert, G., *Z. Phys.*, 183, 249 (1965).

36. Claytor, R.N., Gragg, J.E., and Brotzen, F.R., *J. Appl. Phys.*, 37, 149 (1966).

37. Kurov, J.E., and Sidorova, A.S., *Phys. Metals Metallogr.*, 28, 118 (1969).

38. Meleka, A.H., and Barr, W., *Nature*, 187, 233 (1960).

39. Von Voss, W.D., and Brotzen, F.R., *J. Appl. Phys.*, 30, 1639 (1959).

40. Claytor, R.N., and Brotzen, F.R., *J. Appl. Phys.*, 36, 3549 (1965).

41. Sujak, B., *Acta Phys. Polon.*, 20, 889 (1961).

42. Gieroszynski, A., Mader, J., and Sujak, B., *Acta Phys. Polon.*, 25, 3 (1964).

43. Gieroszynski, A., Mader, J., and Sujak, B., *Acta Phys. Polon.*, 26, 1033 (1965).

44. Sujak, B., Gieroszynski, A., and Pega, E., *Acta Phys. Polon.*, 28, 61 (1965).

45. Sujak, B., and Gieroszynski, A., *Acta Phys. Polon.*, 29, 523 (1966).

46. Gieroszynski, A., and Sujak, B., *Acta Phys. Polon.*, 29, 533 (1966).

47. Gieroszynski, A., and Sujak, B., *Acta Phys. Polon.* 28, 311 (1965).

48. Arnott, D.R., and Ramsey, J.A., *Surface Sci.*, 28, 1, (1971).

49. Mints, R.I., and Kortov, V.S., *Metal Sci. Heat Treat.*, (9-10), 682 (1968).

50. Melekhin, V.P., Mints, R.I., and Kortov, V.S., *Metal Sci. Heat Treat.*, (9-10), 736 (1970).

REFERENCES (Continued)

51. Gel'man, A.G., and Roikl, I.L., *Sov. Phys. Solid State*, 12, 2763 (1971).

52. Gel'man, A.G., and Fainshtein, A.I., *Sov. Phys. Solid State*, 14, 1752 (1973).

53. Shkil'ko, A.M., and Kresnin, A.A., *Sov. Phys. Solid State*, 15, 2048 (1974).

54. Mints, R.I., Kortov, V.S., Aleksandrov, V.L., and Kryuk, V.I., *Phys. Metals Metallogr.*, 26, 100 (1968).

55. Hoenig, S.A., Savitz, C.A., Ott, W.A., Russel, T.A., and Ali, M.T., in *Testing for Prediction of Material Performance in Structure and Components*, ASTM STP 515, American Society for Testing and Materials, p. 107 (1972).

56. Baxter, W.J., *Appl. Phys. Lett.*, 21, 590 (1972).

57. Baxter, W.J., *Vacuum*, 22, 571 (1972).

58. Baxter, W.J., *J. Appl. Phys.*, 44, 608 (1973).

59. Baxter, W.J., *J. Appl. Phys.*, 44, 4400 (1973).

60. Baxter, W.J., *Met. Trans.*, 6A, 749 (1975).

61. Price, W.J., *Nuclear Radiation Detection* , McGraw Hill Book Comp., New York (1958).

62. Metals Handbook, American Society For Metals, vol. 1, p. 946 (1961).

63. Metals Handbook, American Society For Metals, vol. 1, p. 888 (1961).

64. Kortov, V.S., and Mints, R.I., *Metal Sci. Heat Treat.*, (9-10), 682 (1968).

65. Sujak, B., and Gieroszynski, K., *Acta Phys. Polon.*, A39, 137 (1971).

66. Kubaschewski, O., and Hopkins, B.E., *Oxidation of Metals and Alloys*, Butterworths, London (1962).

67. Arnott, D.R., and Ramsey, J.A., *Phys. Stat. Sol. (a)*, 13, K167 (1972).